MCEER
EARTHQUAKE ENGINEERING TO EXTREME EVENTS

ISSN 1520-295X

Response of Steel-plate Concrete (SC) Wall Piers to Combined In-plane and Out-of-plane Seismic Loadings

by

Brian Terranova, Andrew S. Whittaker, Siamak Epackachi and Nebojsa Orbovic

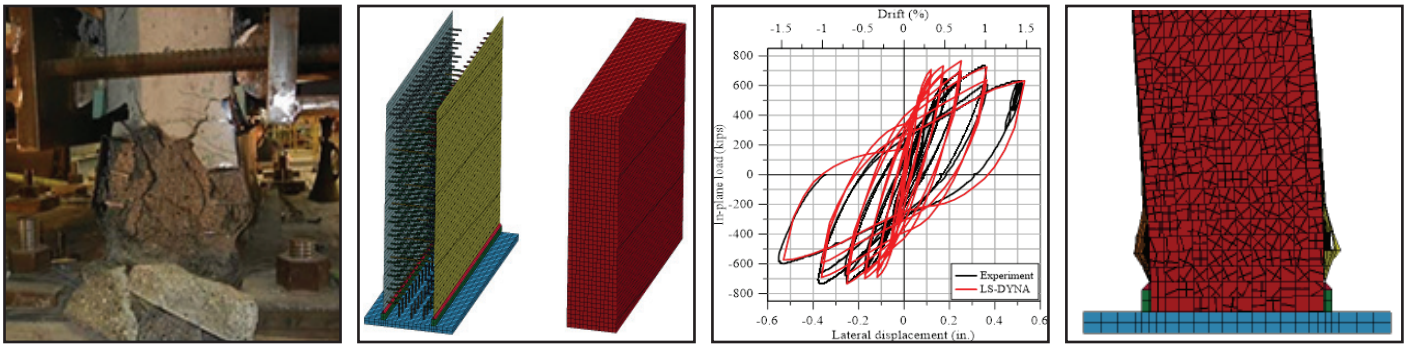

Technical Report MCEER-17-0003

July 17, 2017

This research was conducted at the University at Buffalo, State University of New York, and was supported primarily by MCEER.

NOTICE

This report was prepared by the University at Buffalo, State University of New York, as a result of research sponsored by MCEER. Neither MCEER, associates of MCEER, its sponsors, University at Buffalo, State University of New York, nor any person acting on their behalf:

a. makes any warranty, express or implied, with respect to the use of any information, apparatus, method, or process disclosed in this report or that such use may not infringe upon privately owned rights; or

b. assumes any liabilities of whatsoever kind with respect to the use of, or the damage resulting from the use of, any information, apparatus, method, or process disclosed in this report.

Any opinions, findings, and conclusions or recommendations expressed in this publication are those of the author(s) and do not necessarily reflect the views of MCEER, the National Science Foundation or other sponsors.

Response of Steel-plate Concrete (SC) Wall Piers to Combined In-plane and Out-of-plane Seismic Loadings

by

Brian Terranova,[1] Andrew S. Whittaker,[2] Siamak Epackachi[3] and Nebojsa Orbovic[4]

Publication Date: July 17, 2017
Submittal Date: June 16, 2017

Technical Report MCEER-17-0003

1 Research Engineer and former Graduate Student, Department of Civil, Structural and Environmental Engineering, University at Buffalo, State University of New York
2 Professor and MCEER Director, Department of Civil, Structural and Environmental Engineering, University at Buffalo, State University of New York
3 Teaching Assistant Professor, Department of Civil, Structural and Environmental Engineering, University at Buffalo, State University of New York
4 Technical Specialist, Canadian Nuclear Safety Commission

MCEER
University at Buffalo, State University of New York
212 Ketter Hall, Buffalo, NY 14260
E-mail: *mceer@buffalo.edu*; Website: *http://mceer.buffalo.edu*

Preface

MCEER is a national center of excellence dedicated to the discovery and development of new knowledge, tools and technologies that equip communities to become more disaster resilient in the face of earthquakes and other extreme events. MCEER accomplishes this through a system of multidisciplinary, multi-hazard research, in tandem with complimentary education and outreach initiatives.

Headquartered at the University at Buffalo, The State University of New York, MCEER was originally established by the National Science Foundation in 1986, as the first National Center for Earthquake Engineering Research (NCEER). In 1998, it became known as the Multidisciplinary Center for Earthquake Engineering Research (MCEER), from which the current name, MCEER, evolved.

Comprising a consortium of researchers and industry partners from numerous disciplines and institutions throughout the United States, MCEER's mission has expanded from its original focus on earthquake engineering to one which addresses the technical and socio-economic impacts of a variety of hazards, both natural and man-made, on critical infrastructure, facilities, and society.

The Center derives support from several Federal agencies, including the National Science Foundation, Federal Highway Administration, Department of Energy, Nuclear Regulatory Commission, and the State of New York, foreign governments and private industry.

This report presents results of experimental and numerical studies on the combined in-plane and out-of-plane behavior of steel-plate concrete (SC) composite shear walls. Three medium-scale rectangular SC wall specimens were tested at the Bowen Laboratory at Purdue University. The effects of out-of-plane loading and tie bar spacing on in-plane capacity of SC walls were the primary foci of the investigation. The results of the experiments indicate that the out-of-plane load has a significant effect on the in-plane behavior of SC walls and the effects become very significant as the out-of-plane load develops an average shear stress that is greater than the inclined cracking load of the concrete. Finite element models of the test specimens were developed in LS-DYNA. The LS-DYNA model was used in a parametric study to formulate design guidance for SC walls subjected to combined in-plane and out-of-plane loading.

ABSTRACT

This report investigates the seismic response of components of nuclear power plants constructed using steel-plate-concrete composite walls, subjected to combined in-plane and out-of-plane loadings. Steel-plate concrete (SC) composite shear walls are composed of steel faceplates, infill concrete, shear studs bonding the faceplate to the infill, and tie rods linking the faceplates. To date, a significant amount of studies have focused on the in-plane (IP) response of SC walls, but the effect of out-of-plane (OOP) loading on the IP response has not been addressed in great detail. Three medium-scale rectangular SC wall specimens were built and tested under force-controlled monotonic OOP loading and displacement-controlled cyclic IP loading at the Bowen Laboratory at Purdue University. The magnitude of OOP load and its effects on the IP capacity of SC walls were the focus of this investigation; the effect of tie bar spacing was also investigated. Finite element models of the test specimens were developed in LS-DYNA to investigate the effect of OOP loading (magnitude and location) on the IP response of SC wall piers. The baseline DYNA model was validated for IP behavior using data from the tests of medium-scale rectangular SC wall piers and for OOP behavior using data from these tests. The results of the simulations showed that OOP loading has a significant effect on the IP capacity of SC wall piers; the effects become more significant as the shear span-to-depth ratio and magnitude of the OOP load are increased. The validated model was used in a parametric study to investigate the effect of OOP loading (magnitude and location) on IP response, to formulate design guidance for SC walls subjected to combined IP and OOP loading. The ductility of a wall pier under IP loading is small because damage accumulates over a short height near the bottom of the wall pier. Ductility under IP loading is effectively zero under high OOP loads. These outcomes should be taken into account for both seismic design and for seismic probabilistic risk assessment, which addresses loadings more intense than design basis.

ACKNOWLEDGEMENTS

The Canadian Nuclear Safety Commission funded the research described in this report and this support is gratefully acknowledged. The experiments were executed in the Bowen Laboratory at Purdue University under the leadership of Professor Amit Varma, with important contributions from Mr. Saahas Bhardwaj and Dr. Efe Kurt, and the technicians and staff of the Laboratory. The authors acknowledge and thank their Purdue colleagues for their efforts on the project.

TABLE OF CONTENTS

TABLE OF CONTENTS (CONTD.)

LIST OF FIGURES

LIST OF FIGURES (CONTD.)

LIST OF FIGURES (CONTD.)

LIST OF FIGURES (CONTD.)

LIST OF TABLES

SECTION 1
INTRODUCTION

1.1 Introduction

Steel-plate concrete (SC) composite walls consisting of steel faceplates, infill concrete, and connectors used to anchor the steel faceplates together to the infill concrete may be a viable construction alternative to reinforced concrete (RC) and steel plate shear walls. Double skin SC wall shells can be fabricated offsite, assembled and filled on-site with concrete to create a monolithic wall. The use of steel faceplates by-and-large eliminates the need for formwork, and the plates serve as primary reinforcement. The challenges associated with SC wall construction include joining the shells in the field, splicing SC walls to reinforced concrete walls and foundations, and field inspection of the concrete behind the faceplates.

Challenges remain with the analysis of SC walls for design basis and beyond design basis loadings, including characterization of the effects of interaction of co-existing in-plane (IP) and out-of-plane (OOP) loadings moments and shears. This report addresses such interactions of moments and shears under IP and OOP loadings.

1.2 Literature Review

Varma and his co-workers (Varma et al., 2011; Kurt et al., 2013; Seo et al., 2016), Epackachi et al. (2014a; 2014b; 2015), and others have studied the IP behavior of SC walls, numerically and experimentally. Epackachi et al. present a detailed review of the literature on IP behavior and so those materials are not reported on here.

The OOP behavior of slices of SC walls has been studied, albeit to a lesser degree than IP behavior. Sener et al. (2014; 2015) conducted one-way bending tests on SC beams, representative of vertical strips in SC walls, to investigate OOP behaviors in shear and flexure. They compiled a database of test results and used it to evaluate the utility of design codes. They concluded that the ACI 349-06 (ACI, 2006) equations for RC beams and slabs could be used to predict OOP shear strength of SC walls (for shear span-to-depth ratios larger than 3) and the OOP flexural capacity of SC walls (for any shear span-to-depth ratios). Bhardwaj et al. (2015) investigated the effects of OOP forces on the IP capacity of SC walls using numerical tools developed in LS-DYNA by Kurt et al. (2013) for IP behavior. The results of a limited number of

numerical simulations indicated that the shear span-to-depth ratio and the magnitude of the OOP load significantly affect the IP capacity of SC wall piers. Yang et al. (2016) executed three full-scale experiments investigating the OOP cyclic behavior of SC walls. The parameters considered in that study included shear span-to-depth ratio and thickness of the steel faceplates.

Analysis of nuclear structures predicts large OOP moments and shears in walls at locations of load and stiffness discontinuities, where the walls are also subjected to large IP forces. To the knowledge of the authors, there existed no data on the response of SC walls to combinations of IP and OOP loadings. The lack of data and design guidance on response of SC walls to combined IP and OOP loading prompted the Canadian Nuclear Safety Commission (CNSC) to fund a study, which is the subject of this report. The scope of the CNSC project is presented in the next section.

1.3 Project Scope

This report summarizes work on the CNSC project, entitled "Testing and Development of Regulatory Requirements for Steel Plate Concrete (SC) Structures." The CNSC project was awarded to the University at Buffalo (UB); Purdue University was a subcontractor to UB.

The project described in Chapters 2, 3, 4, and 5 of this report included physical and numerical simulations of the response of SC wall piers subjected to simultaneous in-plane and out-of-plane loadings. The physical simulations were performed in the Bowen Laboratory at Purdue University under the direction of Professor Amit Varma, with assistance from graduate student Mr. Saahas Bhardwaj. The authors assisted with the testing program, and performed all of the data reduction and numerical simulations reported in the following chapters.

1.4 Organization of this Report

This report is organized into four chapters. Chapter 2 describes the physical testing of SC wall piers subjected to IP and OOP loadings, including the test fixture, instrumentation, loading protocol, and results of the experiments.

Numerical modeling of SC wall piers subjected to combined IP and OOP loadings is described in Chapter 3. The physical tests of the SC wall piers are simulated using LS-DYNA (LSTC, 2012). Chapter 4 presents parametric studies conducted to investigate the effects of OOP loading on the

IP behavior of SC walls. The results of these studies are used to provide draft technical guidance for the performance assessment of SC wall piers subjected to combined loadings.

Chapter 5 summarizes the studies presented in Chapters 2 through 4, and provides the key conclusions and findings.

A list of references is presented in Chapter 6.

SECTION 2
PHYSICAL TESTING OF SC WALL PIERS

2.1 Introduction

This chapter presents details and results of the physical tests on the SC wall piers conducted at Purdue University. The test matrix and test fixture are discussed in Section 2.2. Instrumentation of the test specimens is presented in Section 2.3. Results and discussion of the tests of CNSC1, CNSC2, and CNSC3 are presented in Sections 2.4, 2.5, 2.6, respectively.

2.2 Test Matrix and Test Fixture

The matrix of tests is presented in Table 2-1, wherein f_c' is concrete compressive strength and A_c is the plan area of the infill concrete. This matrix was reviewed and accepted by CNSC in 2014. The specimens are labeled CNSC1, -2 and -3. Each specimen was 12 in. thick, which includes the two 3/16-inch steel faceplates. The resultant faceplate reinforcement ratio (total area of faceplates divided by total area of wall) is 0.031, which is significant by comparison with reinforced concrete shear walls. The faceplates were constructed with ASTM Grade A36 steel, with a minimum specified yield strength of 36 ksi and a minimum specified tensile strength of 58 ksi. Based on tension coupon tests, the yield strength and tensile strength of the steel faceplate material were 47 ksi and 80 ksi, respectively.

Table 2-1: CNSC test matrix

Specimen	Height (in.)	Length (in.)	Tie spacing (in.)	Stud spacing (in.)	Target out-of-plane force
CNSC0	36	60	12	4	N.A.
CNSC1	36	60	12	3	$2\sqrt{f_c'}A_c$
CNSC2	36	60	6	3	Cracking
CNSC3	36	60	12	3	Cracking

Each specimen had an aspect (height-to-length) ratio of 0.6. An additional (control) specimen was constructed and tested in advance of CNSC1: tagged as CNSC0 in Table 2-1. The concrete compressive strength of the infill concrete and faceplate yield strength of CNSC0 were 5800 psi and 57 ksi, respectively. The aspect ratio and reinforcement ratio of CNSC0 were 0.6 and 0.031

(a 12 in. thick wall with two 3/16-inch steel faceplates), respectively. Additional information on CNSC0 is presented in Kurt et al. (2015).

The shear studs and tie bars were fabricated from carbon steel with nominal yield and ultimate stress of 50 and 75 ksi, respectively. The 3/8 inch diameter tie bars were spaced at a distance equal to the wall thickness (=12 in.) in CNSC0, CNSC1, and CNSC3 and one-half the wall thickness (= 6 in.) in CNSC2. The spacing of the shear studs (connectors) is presented in Table 2-1. The faceplate slenderness ratio ($= s_s / t_p$, where s_s is the spacing of the connectors [shear studs and cross ties], and t_p is the faceplate thickness) was 16 for CNSC1, CNSC2 and CNSC3, and 21 for CNSC0, noting that the limiting value specified in Supplement No. 1 to AISC N690s1 (AISC, 2015) for steel with yield strength of 36 ksi is 28.

Figure 2-1 is a cross-section through the connection of a faceplate to the baseplate. This detail, which was developed by Purdue University to enable re-use of a foundation for testing SC walls, effectively strengthens the faceplate at its connection to the baseplate and forces buckling, fracture and tearing of the faceplate away from the baseplate.

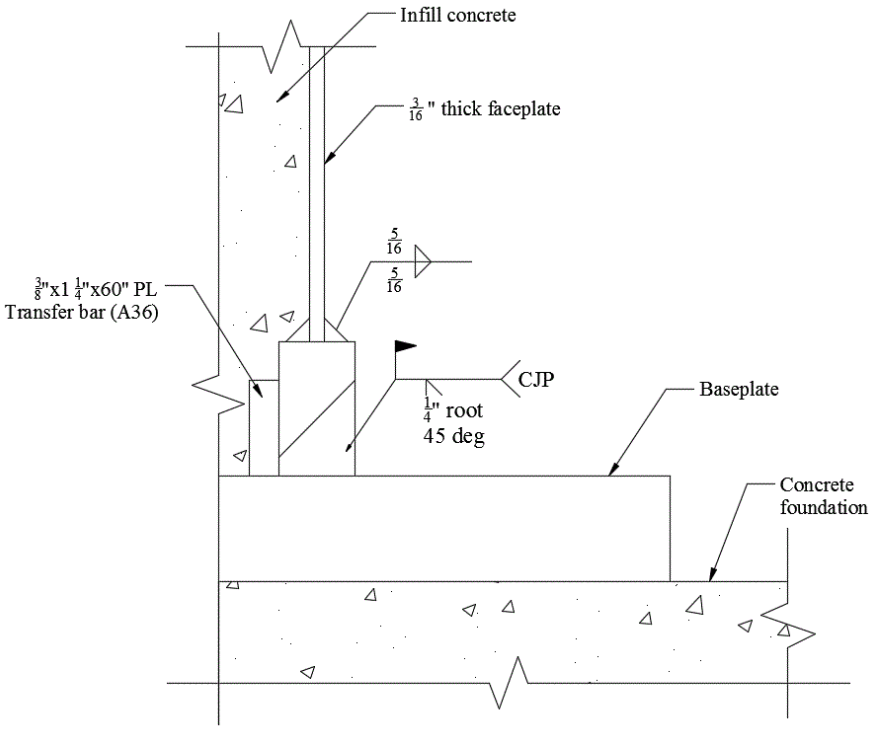

Figure 2-1: Faceplate-to-baseplate connection (courtesy of Purdue University)

Each wall was founded on a large re-usable foundation designed and constructed by Purdue University. The connection of the foundation to the wall was designed to develop the capacity of the faceplates, with the goal of forcing inelastic action into the walls above the foundation.

The last column in Table 2-1 identifies the target out-of-plane (OOP) force to be imposed prior to in-plane loading. An out-of-plane load was not applied to the control specimen, CNSC0. The amplitude of the out-of-plane (OOP) loadings for CNSC1, CNSC2 and CNSC3 were tied to equations derived in the early 1960s for shear resistance of plain concrete beams reinforced for flexure only. The concrete contribution to shear strength of $2\sqrt{f_c'}A_c$ is traditionally used for reinforced concrete design in the United States, although it has limited technical basis. (Wight (2015) shows that this empirical equation is unconservative for low longitudinal reinforcement ratios and conservative for high reinforcement ratios: for shallow specimens subjected to monotonic loading to failure in the absence of co-existing in-plane loadings. The effect of section depth (= wall thickness in this case), for which an increase in depth results in a decrease in shear strength of plain concrete, could not be investigated given the specimen dimensions studied here. Cracking denotes imposing an OOP loading sufficient to introduce a diagonal crack in the concrete, which was estimated for preliminary calculations using equation 22.5.5.1 in ACI 318-14 (2014). The OOP loading was imposed statically and not cycled during the IP loading to failure.

A photograph of the test fixture and a 3D rendering of the fixture are shown in Figure 2-2a and Figure 2-2b, respectively. The OOP setup consisted of one 660-kip dual action actuator and beams to apply the OOP load to the specimen. The OOP load was applied 18 inches above the foundation, and the resulting ratio of shear span-to-depth was 1.5. In-plane loading was imposed on the specimen via loading beams and two 660-kip dual action actuators. The actuator clevises were detailed to accommodate the rotations associated with the IP and OOP loadings.

2.3 Instrumentation of the Test Specimens

Traditional transducers were used to monitor the response of each test specimen: strain gages, strain rosettes, string potentiometers, and linear variable differential transducers (LVDTs).

The locations of strain gages on the inner face, outer East face, and outer West face, near the base of the wall for CNSC1 and CNSC3 are identified in Figure 2-3a, Figure 2-3b, and Figure

2-3c, respectively. Strain rosettes on the exterior faces of the plates were used to estimate shear strain. Figure 2-3 shows the locations of the tie bars and shear studs near the base of the wall; a legend is presented in Figure 2-3a. Companion information for CNSC2 is presented in Figure 2-4. The scale in these figures can be determined by the distance between the shear studs: 3

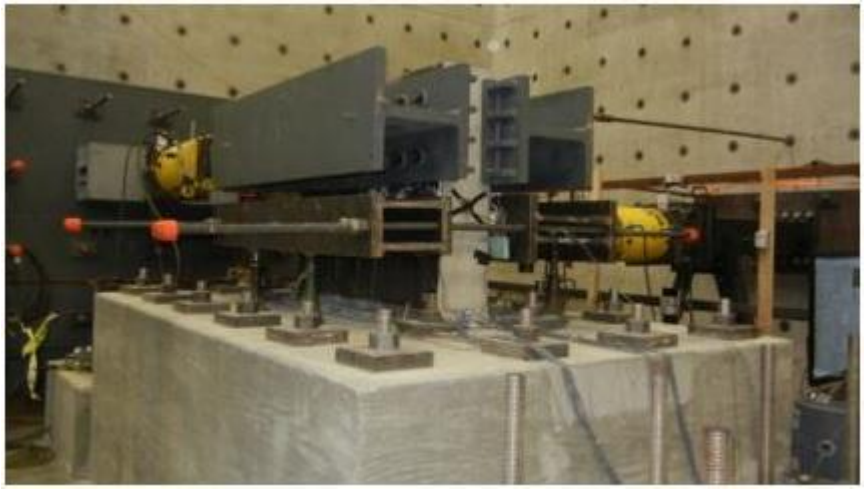

(a) photograph of the test fixture

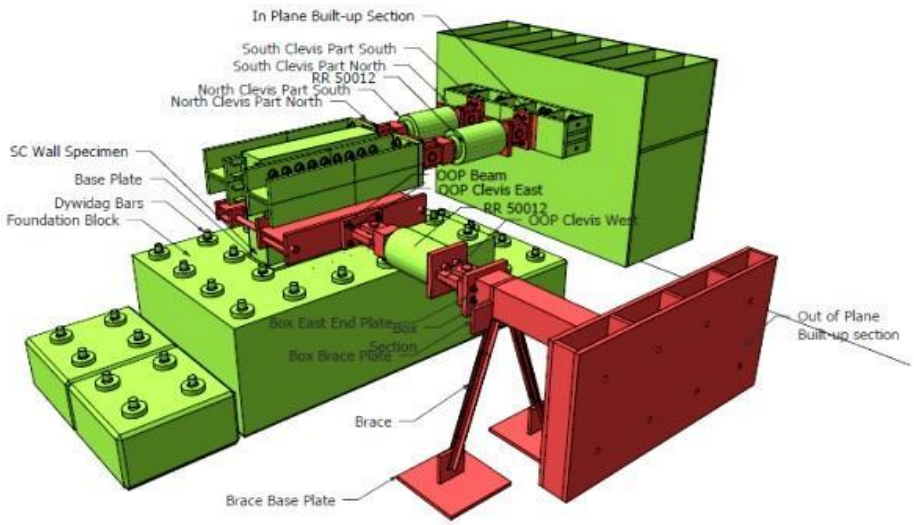

(b) 3D rendering of the test fixture

Figure 2-2: CNSC test setup (courtesy of Purdue University)

inches. The solid black shaded zone identifies the baseplate; the hatched zone identifies the depth of the welded connection joining the faceplate to the baseplate.

The locations of the string potentiometers used to measure the in-plane and out-of-plane movement of a specimen are presented in Figure 2-5a and Figure 2-5b, respectively. Three

inclinometers were mounted on a specimen to measure rotation; two for in-plane movement (CM2, CM3) and one for out-of-plane movement (CM1). The locations of the inclinometers are identified in Figure 2-5. Eight LVDTs were attached to a specimen: four to measure in-plane movement of the foundation block with respect to the strong floor, and four to measure vertical movement of the base plate with respect to the foundation block.

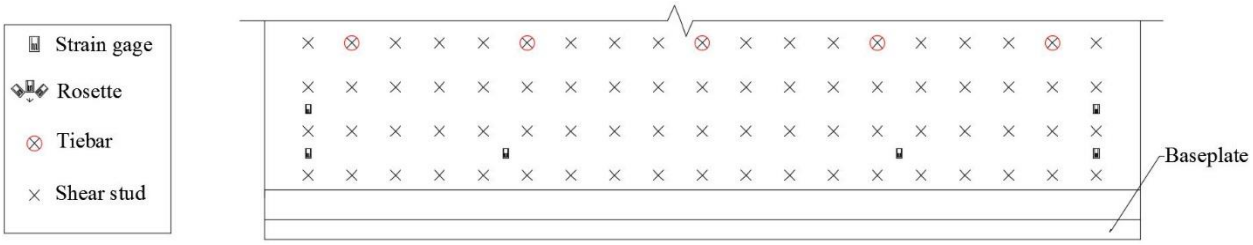

(a) Typical faceplate, inner face

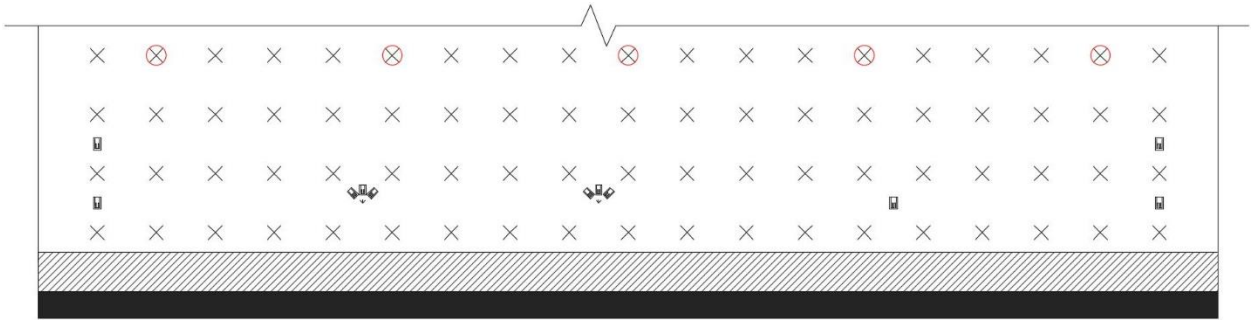

(b) East faceplate, outer face

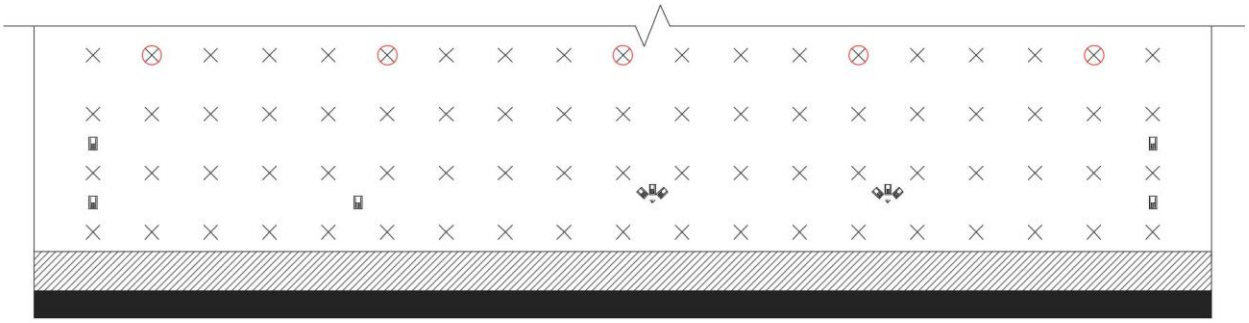

(c) West faceplate, outer face

Figure 2-3: Layout of strain gages, tie bars, and shear studs, CNSC1, CNSC3 (adapted from Purdue University drawings)

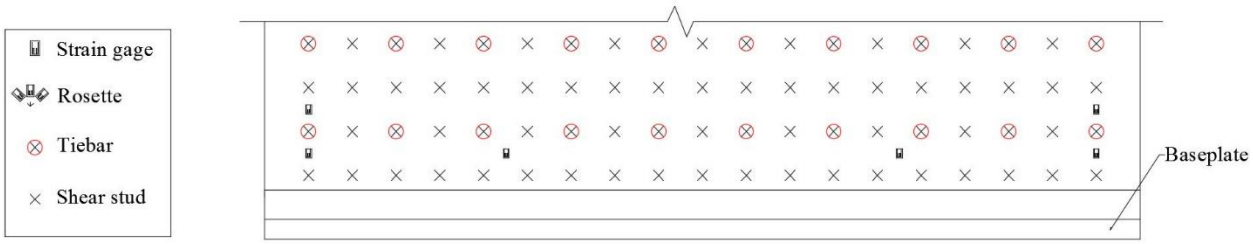

(a) Typical faceplate, inner face

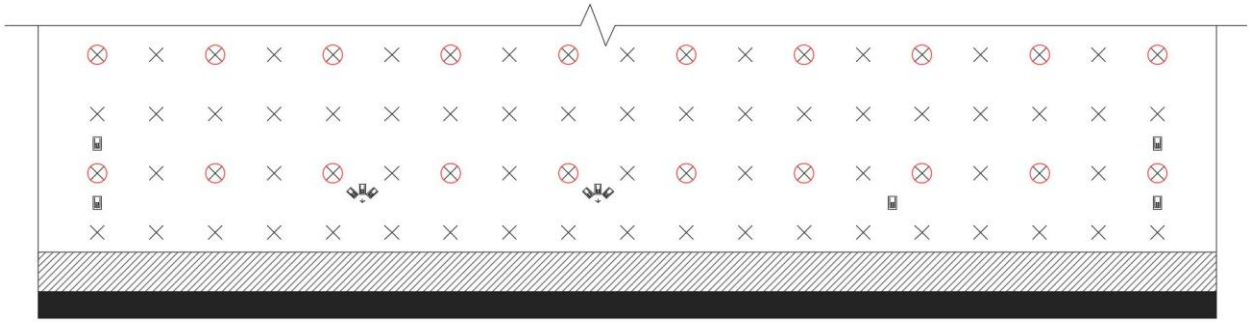

(b) East faceplate, outer face

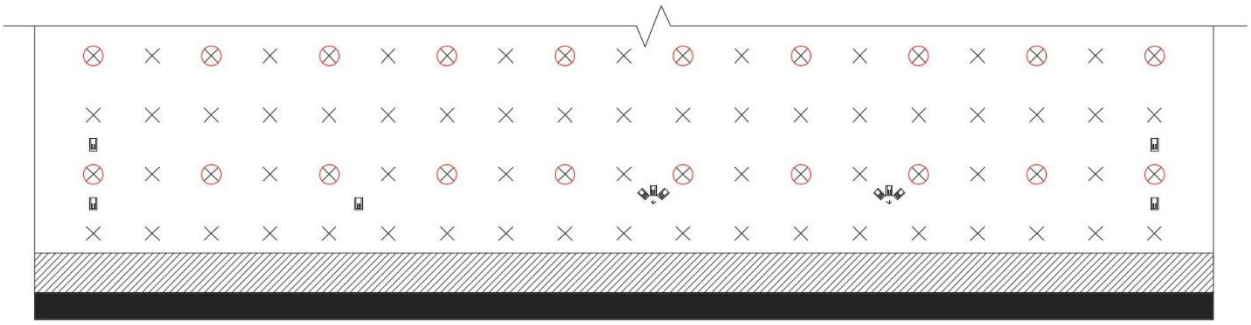

(c) West faceplate, outer face

Figure 2-4: Layout of strain gages, tie bars, and shear studs, CNSC2 (adapted from Purdue University drawings)

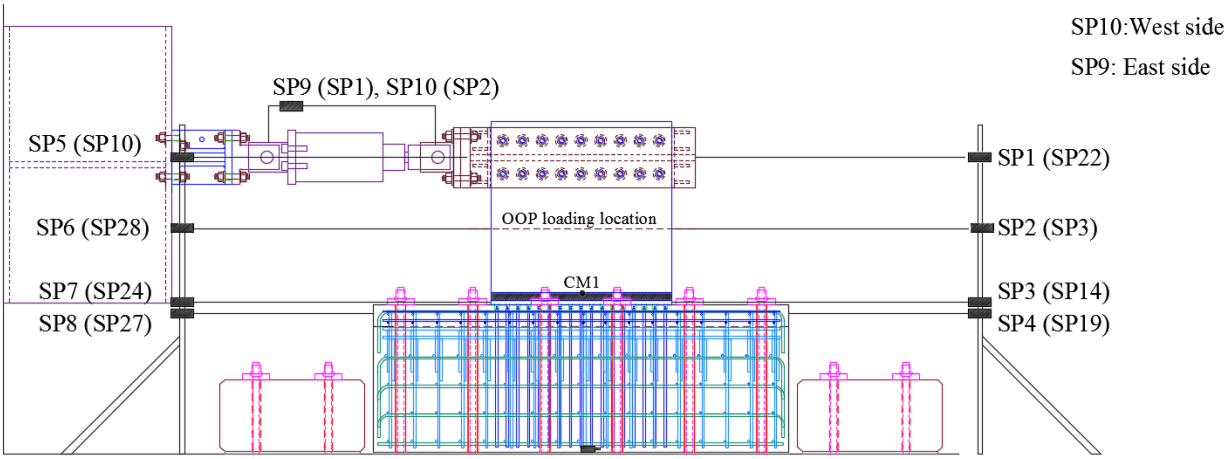

(a) in-plane

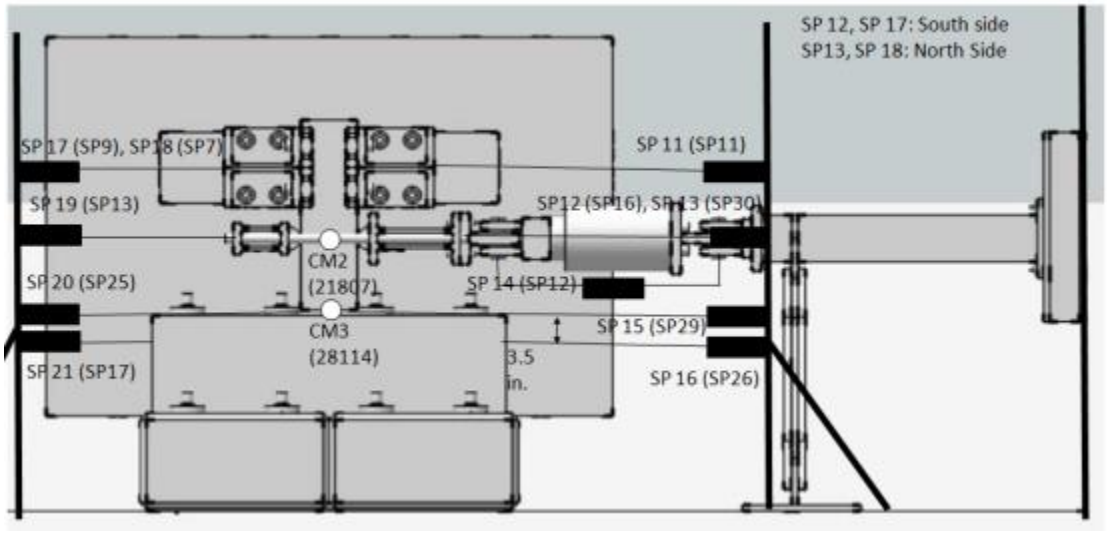

(b) out-of-plane

Figure 2-5: Locations of string potentiometers (courtesy of Purdue University)

2.4 CNSC1 Test Protocol, Results, and Discussion

2.4.1 CNSC1 Test Protocol

Specimen CNSC1 was tested between 06/01/15 and 06/04/15. The concrete compressive strength on the first day of testing was 7700 psi, as determined by cylinder breaks. The specimen was initially subjected to four cycles of OOP loading, at magnitudes of 30, 60, 90, and 120 kips, respectively, to verify the test setup was functioning as intended. The OOP load was then maintained at a constant value of 120 kips (=$1.96\sqrt{f_c'}A_c$)[1] and incremental cyclic IP loading imposed. The loading protocol for CNSC1 is presented in Table 2-2, where P_y and Δ_y are the yield load (=650 kips) and yield displacement of the specimen, respectively, calculated by pre-test analysis. The cycles are fully reversed loading, namely, one cycle is a push half cycle followed by a pull half cycle.

Table 2-2: Loading protocol for CNSC1

Cycle	IP loading	Control	OOP loading
1-2	$0.25\,P_y$	Force	120 kips
3-4	$0.50\,P_y$	Force	
5-6	$0.75\,P_y$	Force	
7-8	$1.0\,P_y$	Displacement	
9-10	$1.5\,\Delta_y$	Displacement	
11-12	$2.1\,\Delta_y$	Displacement	
13	$3.0\,\Delta_y$	Displacement	

2.4.2 CNSC1 Test Results

The OOP cyclic force-displacement relationship for CNSC1 is presented in Figure 2-6, where the OOP displacement was measured at the top of the wall, at the level where IP loading was applied later, as an average of the SP displacements at the ends of the wall. Data from OOP cycles at loads of 30 and 90 kips were lost and are not reported here. The IP cyclic force-displacement

[1] The concrete area is the product of the length of the pier (60 in.) and the thickness of the concrete (11.625 in.).

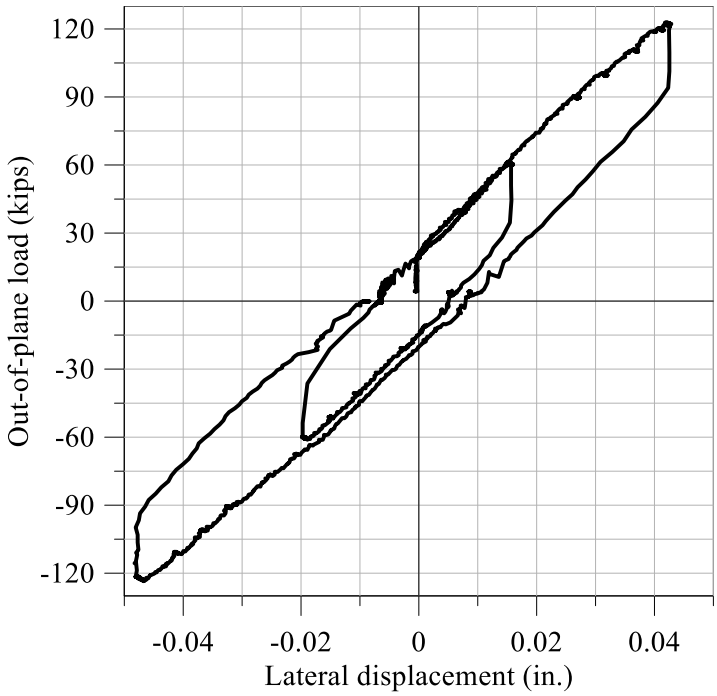

Figure 2-6: Out-of-plane force-displacement relationship, CNSC1

relationship for CNSC1 is presented in Figure 2-7. The post-yield displacement cycles (9 to 13) are presented in Figure 2-8. The loss of IP capacity with increasing cycles can be identified using the data presented in Table 2-3. Significant reductions in IP resistance were observed at large displacements. The IP displacement is the relative horizontal displacement between the level of the IP loading and the bottom of the wall (or top of footing).

The IP load-displacement relationship and backbone curve are presented in Figure 2-9. Points A, B, C, and D in the figure represent the onset of concrete cracking, yielding of steel faceplates, buckling of steel faceplates, and concrete crushing, respectively. The test was terminated at the displacement × shown on the plot. The sequence of damage to CNSC1 is presented in Table 2-4. Concrete cracking at the open ends of the wall, steel faceplate yielding, steel face plate buckling, and concrete crushing in the SC wall occurred at drift ratios of 0.23%, 0.38%, 0.70%, and 1.0%, respectively, and these points were identified by visual inspection (i.e., cracking and crushing of concrete, faceplate buckling) and review of strain gage data (faceplate yielding).

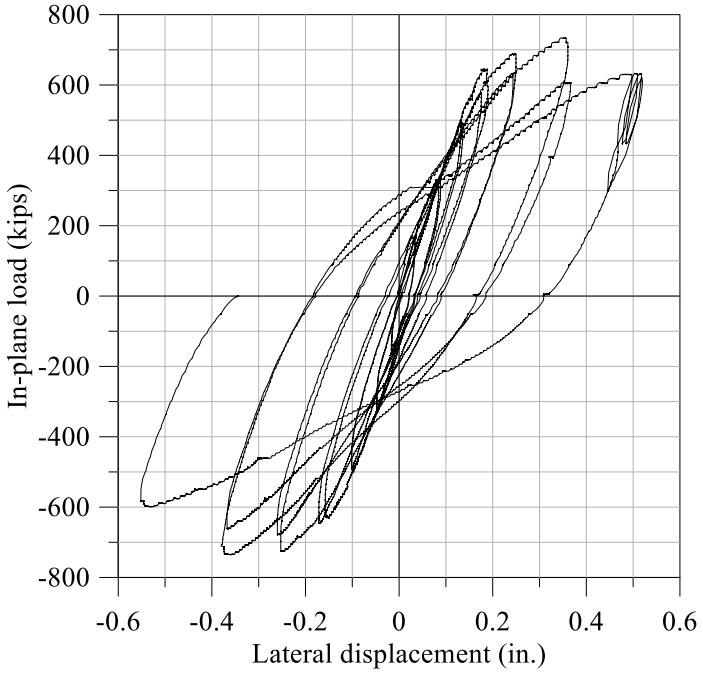

Figure 2-7: In-plane force-displacement relationship, CNSC1

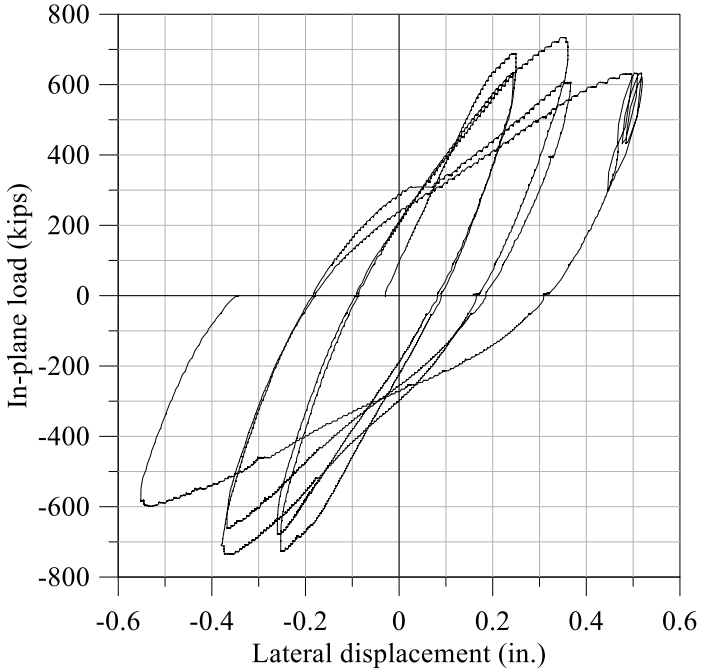

Figure 2-8: In-plane force-displacement relationship for post-yield cycles, CNSC1

Table 2-3: Loss of IP shear capacity, CNSC1

Cycle	IP resistance at IP displacement (kips)							
	Δ_y		$1.5\Delta_y$		$2.1\Delta_y$		$3\Delta_y$	
	Push	Pull	Push	Pull	Push	Pull	Push	Pull
7	630	625	-	-	-	-	-	-
8	575	645	-	-	-	-	-	-
9	570	632	687	726	-	-	-	-
10	515	532	630	675	-	-	-	-
11	500	518	630	610	730	735	-	-
12	400	432	496	552	606	661	-	-
13	375	376	456	445	544	515	630	600

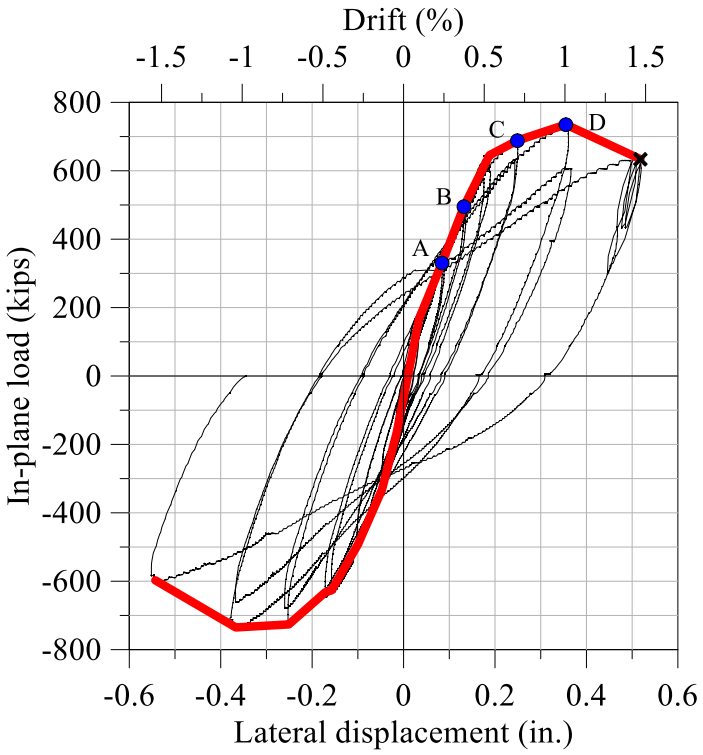

Figure 2-9: In-plane force-displacement relationship and backbone curve, CNSC1

Key results are presented in Table 2-5. The initial stiffness of the SC wall, calculated at a drift ratio less than 0.02%, is presented in the first column for the push and pull directions. The values of load and drift ratio at the onset of steel plate yielding are presented in columns two and three. The fourth and fifth column present the load and drift ratio at the onset of steel faceplate

buckling. The peak loads and their corresponding drift ratios for the push and pull directions are presented in columns six and seven. The maximum drift ratios for the experiment and their corresponding loads in the push and pull directions are presented in columns eight and nine. Note that the maximum drift ratio does not correspond to failure of the CNSC1.

Table 2-4: Sequence of damage, CNSC1

Cycle	Drift ratio (%) Push/Pull	Damage/Observations
3	0.23/0.13	Cracks on the North and South faces of the wall; specimen twisting
5	0.38/0.28	Yielding of steel faceplates, diagonal cracking at the base of the South wall; new cracks on the North face of the wall
6	0.38/0.28	New cracks; residual OOP drift
7	0.51/0.45	Large residual strains develop in the steel faceplates, initial separation of the faceplates from the infill concrete; new cracks formed
9	0.70/0.70	Buckling of the steel faceplate in the northwest and southwest corners of the wall; diagonal cracking on the South face; new diagonal cracks on the South face of the wall
10	0.70/0.70	Severe buckling of the steel faceplate in the northwest corner of the wall; buckling of the steel faceplate in the southeast corner of the wall; new diagonal cracks on the South face
11	1.00/1.01	Propagation of faceplate buckling from the southeast corner towards the mid-length of the wall; extensive cracking on the South face
12	1.00/1.01	Concrete crushing and spalling at the toes of the wall (North and South faces)
13	1.43/1.52	Propagation of faceplate buckling from the Northeast corner towards the mid-length of the wall

Table 2-5: Summary results for CNSC1

Initial stiffness (kip/in.)	Onset of steel plate yielding		Onset of steel plate buckling		Peak load		Maximum drift	
Push/Pull	Load (kips)	Drift (%)	Load (kips)	Drift (%)	Load (kips) Push/Pull	Drift (%) Push/Pull	Load (kips) Push/Pull	Drift (%) Push/Pull
5139/4966	493	0.38	689	0.70	735/735	0.99/1.01	634/597	1.44/1.51

The accumulated damage to the wall pier on its South and North faces from cycles 1 through 12 is shown in Figure 2-10 and Figure 2-11, respectively. The text on the red fill in the figures identifies the forces at which the related cracks formed. Damage to the South and North faces of

CNSC1 after cycle 13 are presented in Figure 2-12 and Figure 2-13, respectively. Local buckling of the steel faceplates and concrete cracking and spalling are clearly visible. The wall twisted in the latter stages of the test and there was considerable OOP residual drift.

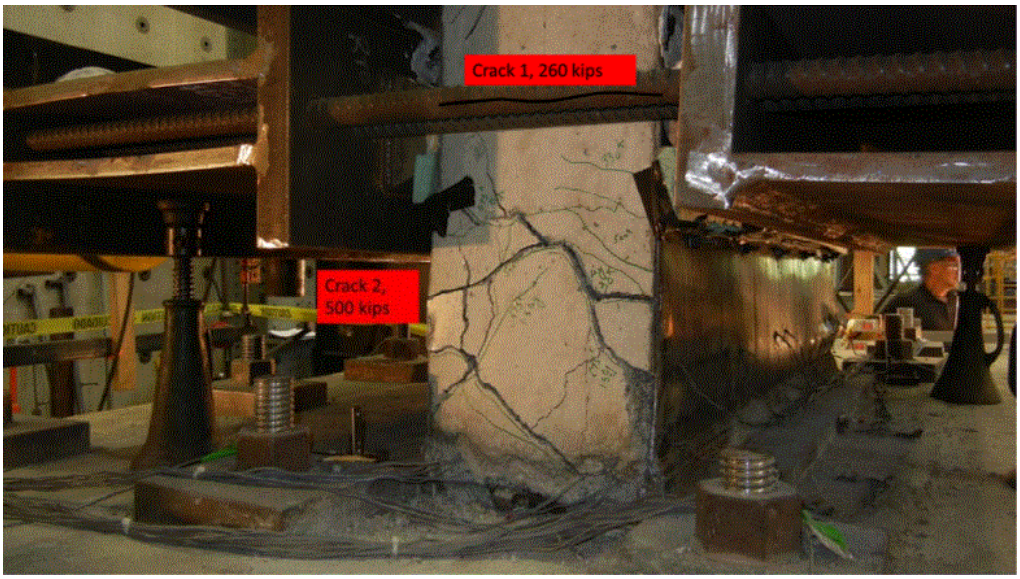

Figure 2-10: Accumulated damage on South face, cycles 1-12, CNSC1 (UB and Purdue)

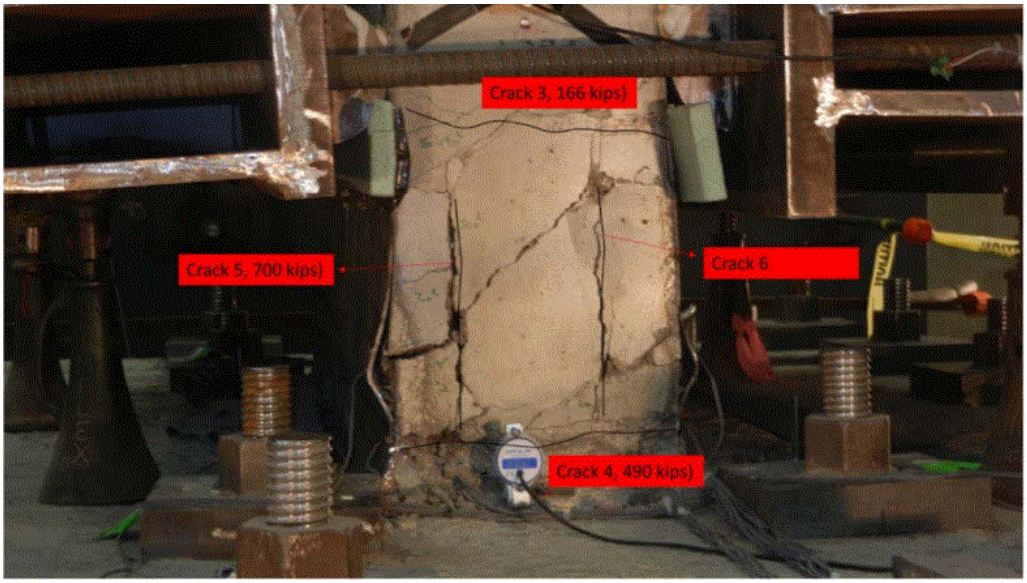

Figure 2-11: Accumulated damage on the North face, cycles 1-12, CNSC1 (UB and Purdue)

Figure 2-12: Damage on South face of CNSC1 after cycle 13 (UB and Purdue)

Figure 2-13: Damage on North face of CNSC1 after cycle 13 (UB and Purdue)

The cumulative energy dissipation in CNSC1 is presented in Figure 2-14. The energy dissipated in each cycle (*EDC*) is presented in Table 2-6.

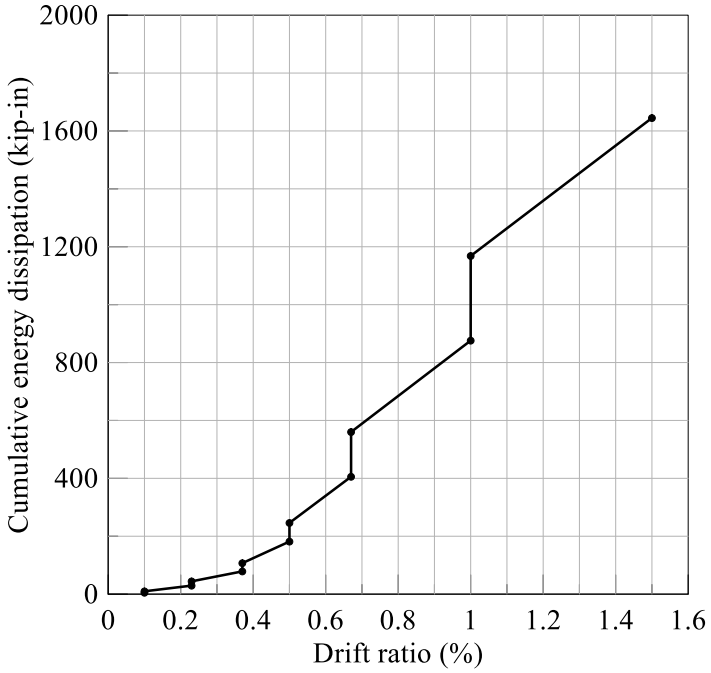

Figure 2-14: Cumulative energy dissipation, CNSC1

Table 2-6: Energy dissipated per cycle, CNSC1

Cycle	5	6	7	8	9	10	11	12	13
EDC (kip-in)	34.4	28.5	74.5	64.4	159	154	315	292	476

Equivalent viscous damping (*EVD*) data are presented in Figure 2-15 and Table 2-7, where *EVD* is computed using equation (2-1) (Chopra, 2011).

$$EVD = \frac{1}{4\pi}\frac{EDC}{E_{So}} \tag{2-1}$$

where *EDC* is the energy dissipated per cycle (area under the force-displacement relationship) and E_{So} is the strain energy (defined as $ku_o^2/2$, where k is the secant stiffness to maximum displacement u_o).

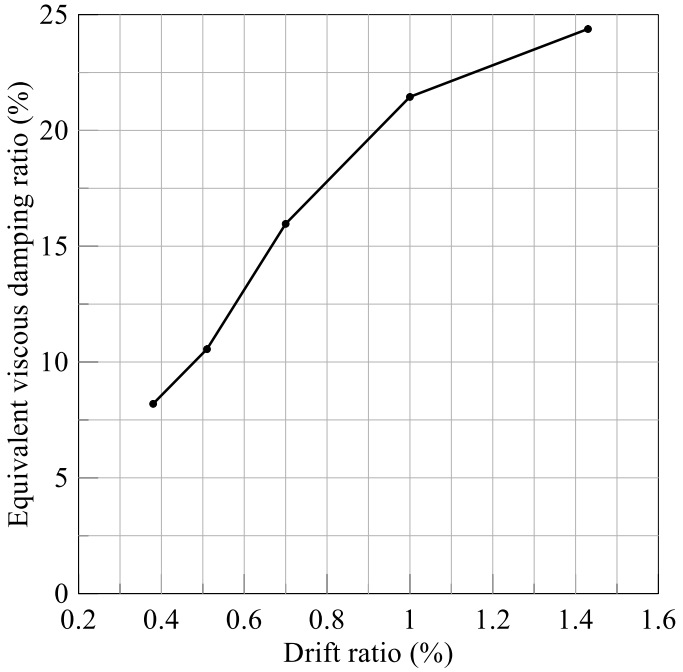

Figure 2-15: Equivalent viscous damping ratio, CNSC1

Table 2-7: Equivalent viscous damping, CNSC1

Drift ratio (%)	0.38	0.51	0.70	1.00	1.43
EVD (%)	8.2	10.6	16.0	21.4	24.4

2.4.3 Behaviors of CNSC1 and CNSC0

Figure 2-16 presents the in-plane force-displacement responses of the control specimen (CNSC0) and CNSC1. The uniaxial compressive strengths of the concrete for CNSC0 and CNSC1 were 5800 psi and 7700 psi, respectively. The yield strengths of the steel faceplates (slenderness ratios) in CNSC0 and CNSC1 were 57 ksi (21) and 47 ksi (16), respectively. These differences in material strengths and slenderness ratios make a direct comparison of the responses of the CNSC0 and CNSC1 impossible because both the steel faceplates and infill concrete contribute to the in-plane strength of SC wall piers. Both specimens were pushed to a drift ratio (lateral displacement divided by the distance between the point of in-plane loading) of approximately 1.5%. The control specimen failed due to cyclic yielding of the steel faceplates, leading to fracture of the base metal close to the weld (Kurt et al., 2015). The test of CNSC1 was terminated after cyclic yielding of the steel faceplates, leading to compression failure and spalling of infill concrete.

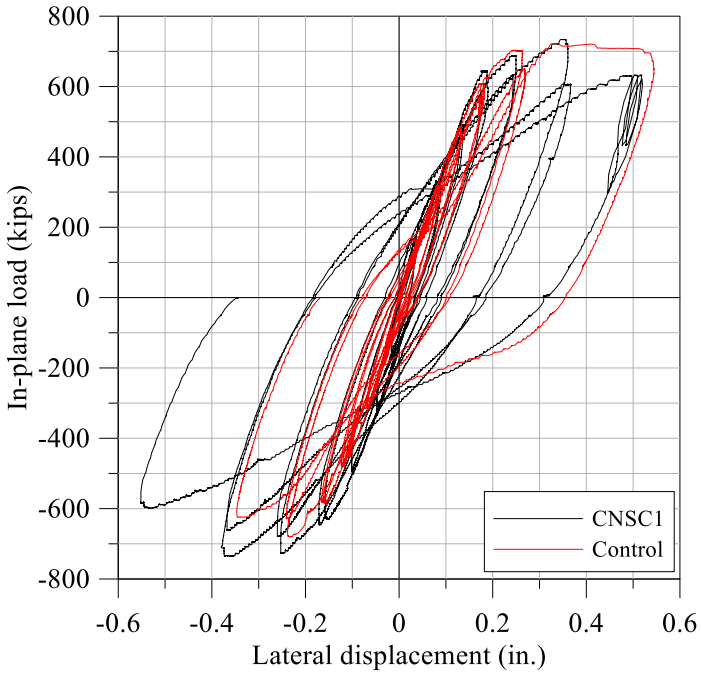

Figure 2-16: In-plane force-displacement responses of CNSC0 and CNSC1

2.5 CNSC2 Test Protocol, Results, and Discussion

2.5.1 CNSC2 Test Protocol

Specimen CNSC2 was tested on 11/11/15 and 11/12/15. The concrete compressive strength on the first day of testing was 5300 psi. The specimen was initially subjected to five cycles of OOP loading, at magnitudes of 30, 60, 90, 120 and 240 kips, respectively, to verify the test setup was functioning as intended, and to crack the wall due to OOP shear. Cracking of the specimen due to OOP load was first observed at 220 kips. The OOP load was then maintained at 240 kips ($=4.73\sqrt{f_c'}A_c = 1.2*(2\sqrt{f_c'}A_c + A_s f_y d/s)$, where f_c' is concrete compressive strength, A_c is plan area of infill concrete, A_s, f_y, and s are the area, tensile yield strength, and spacing of the shear reinforcement, respectively, and d is the effective depth of the cross section) and then incremental cyclic IP loading imposed. The loading protocol for CNSC2 is presented in Table 2-8, where P_y and Δ_y are the yield load (=504 kips) and yield displacement (=0.19 in.) of the specimen, respectively, calculated by pre-test analysis considering in-plane and out-of-plane loading. The cycles were fully reversed: a push half cycle followed by a pull half cycle.

Table 2-8: Loading protocol for CNSC2

Cycle	IP loading	Control	OOP loading
1-2	$0.25\,P_y$	Force	240 kips
3-4	$0.50\,P_y$	Force	
5-6	$0.75\,P_y$	Force	
7-8	$1.00\,P_y$	Displacement	
9-10	$1.50\,\Delta_y$	Displacement	
11-12	$2.00\,\Delta_y$	Displacement	
13	$3.00\,\Delta_y$	Displacement	

2.5.2 CNSC2 Test Results

The OOP cyclic force-displacement relationship for CNSC2 is presented in Figure 2-17, where the OOP displacement was measured at the top of the wall, at the level where the IP loading was later applied. Cracking was first observed at an OOP load of approximately 220 kips. The cyclic loading of the wall in the OOP direction resulted in diagonal cracks on its exposed North and South faces as presented in Figure 2-18. The long diagonal crack on the North face was produced by OOP loading before the application of IP loads. The short diagonal cracks on the South face near the base of the wall resulted from OOP loading; the longer diagonal crack propagating from the point of application of the OOP load formed after the first IP cycle of loading.

The IP cyclic force-displacement relationship for CNSC2 is presented in Figure 2-19. The post-yield displacement cycles (9 to 13) are presented in Figure 2-20. The loss of IP capacity with increasing cycles can be identified using the data presented in Table 2-9. Data from cycle 10 was lost. Significant reductions in IP resistance were observed at large displacements.

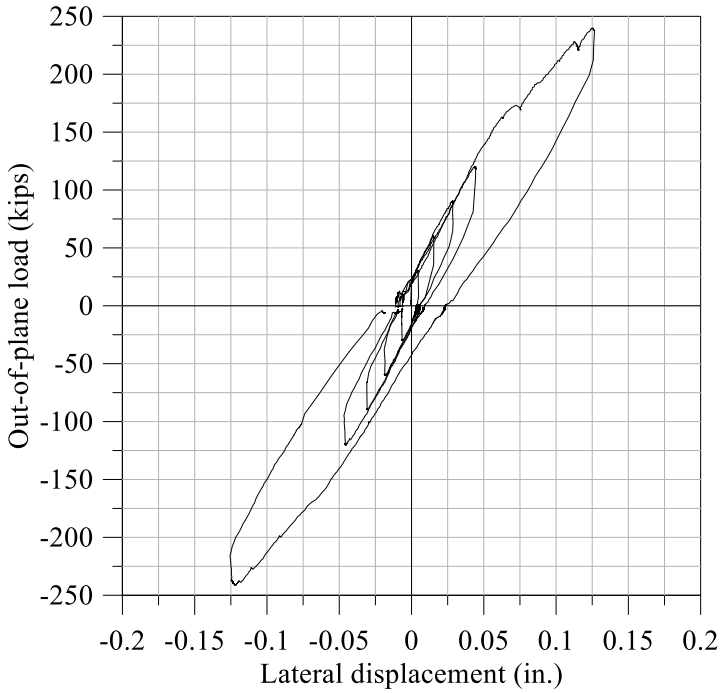

Figure 2-17: Out-of-plane force-displacement relationship, CNSC2

(a) North face (b) South face

Figure 2-18: Diagonal cracking caused by OOP loading, CNSC2 (UB and Purdue)

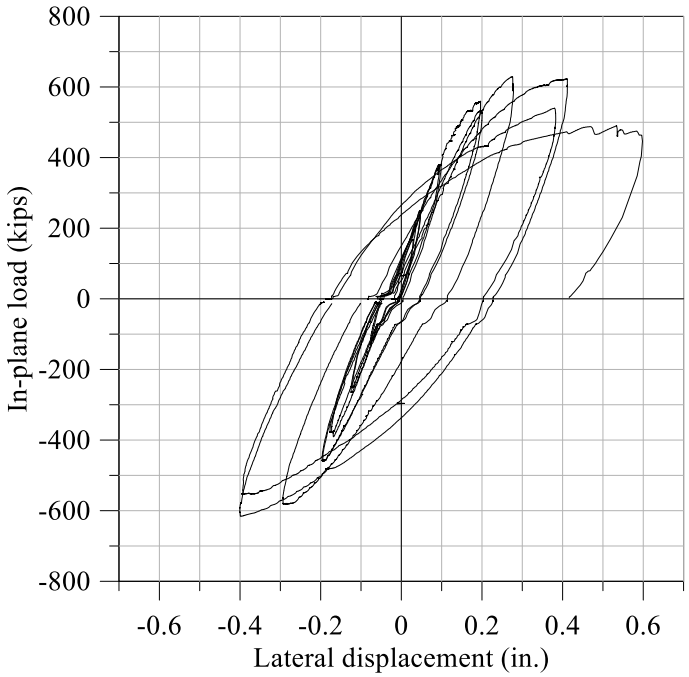

Figure 2-19: In-plane force-displacement relationship, CNSC2

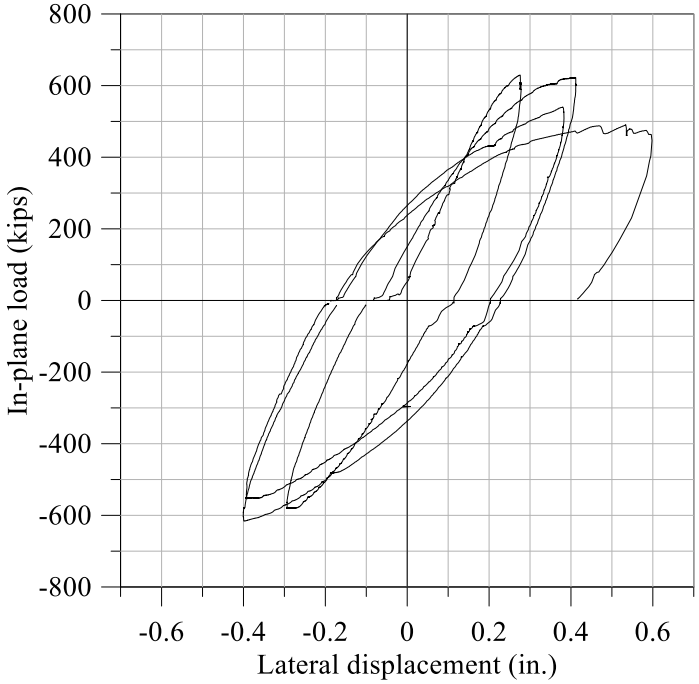

Figure 2-20: In-plane force-displacement relationship for post yield cycles, CNSC2

Table 2-9: Loss of IP capacity, CNSC2

Cycle	IP resistance at IP displacement (kips)							
	Δ_y		$1.5\Delta_y$		$2.0\Delta_y$		$3\Delta_y$	
	Push	Pull	Push	Pull	Push	Pull	Push	Pull
7	558	458	-	-	-	-	-	-
8	530	457	-	-	-	-	-	-
9	536	493	630	580	-	-	-	-
10	-	-	-	-	-	-	-	-
11	471	496	568	565	623	616	-	-
12	430	455	493	510	539	551	-	-
13	387	-	435	-	466	-	463	-

The IP load-displacement relationship and backbone curve are presented in Figure 2-21; the hysteresis loops are offset approximately 0.03 inch from the origin due to twisting of the SC wall pier caused by the applied OOP load. Points A, B, C, and D in the figure represent the onset of concrete cracking under IP loading, yielding of steel faceplates, buckling of steel faceplates, and concrete crushing, respectively. The test was terminated at the displacement × shown on the plot. The sequence of damage to CNSC2 is presented in Table 2-10. Concrete cracking under IP loading, steel faceplate yielding, steel face plate buckling, and concrete crushing in the SC wall occurred at drift ratios of 0.15%, 0.37%, 0.76%[2], and 1.14%, respectively. The tie bar on the North end of the wall ruptured in cycle 13; the approximate point of its rupture on the IP force-displacement relationship is identified in Figure 2-21 by point E.

Key results are presented in Table 2-11. The initial stiffness of the SC wall, calculated at a drift ratio less than 0.02%, is presented in the first column for the push and pull directions. The values of load and drift ratio at the onset of steel plate yielding are presented in columns two and three. The fourth and fifth column present the load and drift ratio at the onset of steel faceplate buckling. The peak loads and their corresponding drift ratios for the push and pull directions are presented in columns six and seven. The maximum drift ratios for the experiment and their corresponding loads in the push and pull directions are presented in columns eight and nine. The maximum drift ratio does not correspond to failure (loss of gravity load resistance) of CNSC2.

[2] Steel faceplate buckling occurred in cycle 10; the drift in cycle 9 is presented here and used in Figure 2-21.

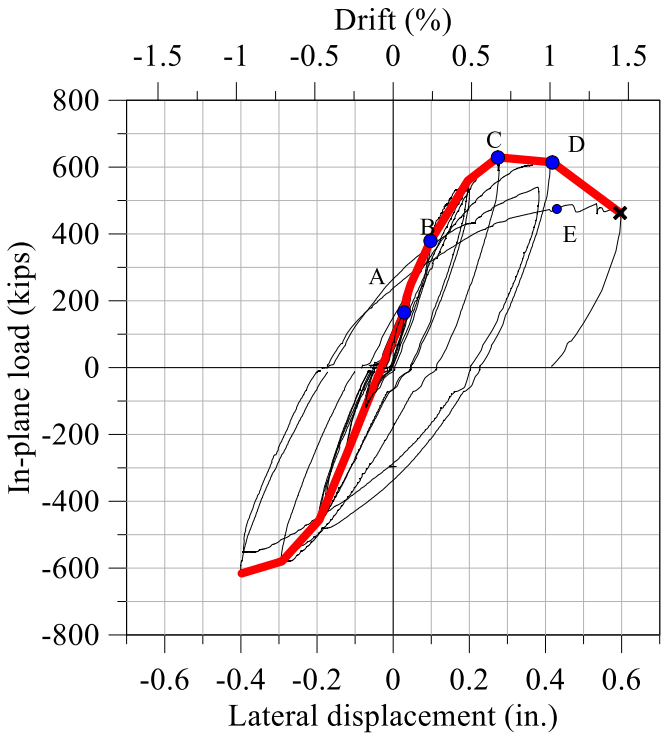

Figure 2-21: In-plane force-displacement relationship and backbone curve, CNSC2

The accumulated damage to the wall pier on the South and North faces from cycles 1 through 12 is shown in Figure 2-22. The accumulated damage to the South and North faces of CNSC2 after cycle 13 is presented in Figure 2-23. Local buckling of the steel faceplates and concrete cracking and spalling are clearly visible. The wall twisted in the latter stages of the test and there was considerable OOP residual drift. A tie bar ruptured on the North end of the wall in cycle 13, as described previously and shown in Figure 2-24.

The cumulative energy dissipation in CNSC2 is presented in Figure 2-25. The energy dissipated in each cycle (*EDC*) is presented in Table 2-12. Equivalent viscous damping (*EVD*) data are presented in Figure 2-26 and Table 2-13, where *EVD* is calculated per equation (2-1).

Table 2-10: Sequence of damage, CNSC2

Cycle	Drift ratio (%) Push/Pull	Damage/Observations
OOP 240 kips	-	Diagonal crack on the North face propagating from the point of application of OOP load; short diagonal cracks near the base of the wall on the South face
1	0.15/0.15	Diagonal crack on the South face propagating from the point of application of OOP load
2	0.17/0.15	Propagation of cracks on the South face; new diagonal cracks on the North face at the top and bottom of the wall
3	0.23/0.24	New diagonal cracks on North and South face at the point of OOP loading
4	0.23/0.24	Specimen twisting
5	0.37/0.39	Yielding of the steel faceplate on the West (tension) side of the wall; new cracking observed on the North and South faces of the wall
6	0.35/0.38	New cracks form on the South face of the wall at the point of OOP loading
7	0.54/0.55	Yielding of the steel faceplate on the East (compression) side of the wall; additional cracking on the South face at top and bottom of wall and IP loading location
8	0.56/0.55	Additional cracking observed on South wall at IP loading location; OOP residual displacement approximately 0.4 inch
9	0.76/0.81	Drifting of wall in OOP direction; difficult to maintain OOP load; cracks propagate on South and North faces
10	- / -[1]	Buckling of steel faceplate in the northwest, southeast and southwest corners of the wall; OOP residual displacement approximately 0.8 inch
11	1.14/1.11	Buckling of steel faceplate in the Northeast corner of the wall; cracks propagating; concrete crushing and spalling at the toes of the wall; OOP and IP residual drifts are 1.6 and 0.17 inch, respectively
12	1.06/1.08[2]	Extensive cracking on the South and North faces of the wall; additional spalling of concrete; shear studs visible on the South face of the wall; severe buckling of face plates in the North and South East corners of the wall; propagation of faceplate buckling towards the mid-point of the wall
13	1.7/ -	Tie bar rupture on the North side of the wall

1. The data from cycle 10 was not recovered from the test; description based on visual observation.
2. The drift ratios of cycle 12 are slightly smaller than cycle 11 due to uncertainty in the stability of the wall during this cycle.

Table 2-11: Summary results for CNSC2

Initial stiffness (kip/in.)	Onset of steel plate yielding		Onset of steel plate buckling		Peak load		Maximum drift	
Push/Pull	Load (kips)	Drift (%)	Load (kips)	Drift (%)	Load (kips) Push/Pull	Drift (%) Push/Pull	Load (kips) Push/Pull	Drift (%) Push/Pull
2658/3051	380	0.37	629	0.76	629/616	0.76/1.11[1]	464/616	1.70/1.11[2]

1. Peak load in the push (pull) direction occurred in cycle 9 (11)
2. Maximum drift occurred in cycle 13 (11) for the push (pull) direction; drifts in cycle 12 are slightly smaller due to concerns regarding the stability of the wall; pull cycle 13 not conducted

(a) South face (b) North face

Figure 2-22: Accumulated damage, cycles 1-12, CNSC2 (UB and Purdue)

(a) South face (b) North face

Figure 2-23: Accumulated damage to CNSC2 after cycle 13 (UB and Purdue)

Figure 2-24: Tie bar rupture at North end of wall, CNSC2 (UB and Purdue)

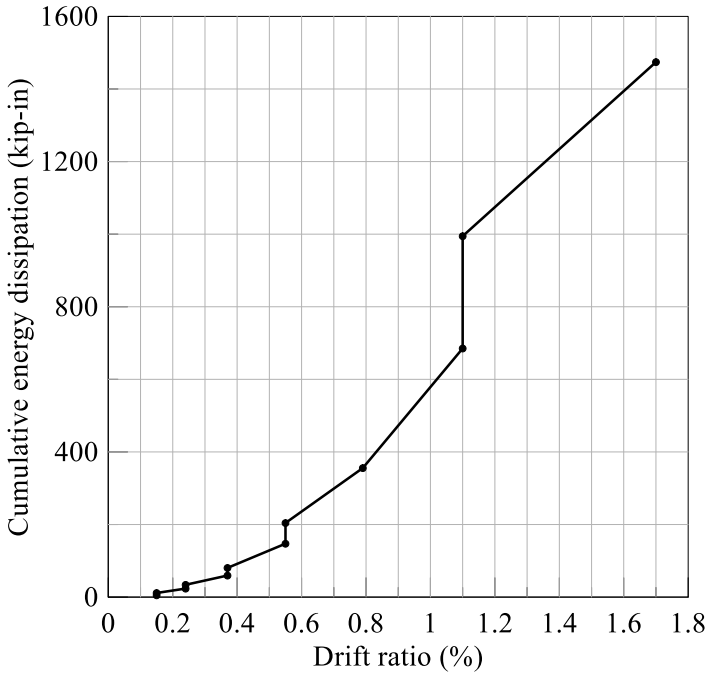

Figure 2-25: Cumulative energy dissipation, CNSC2

Table 2-12: Energy dissipated per cycle, CNSC2

Cycle	5	6	7	8	9	10	11	12	13
EDC (kip-in)	25.5	21.0	66.7	57.0	151	-	330	309	480

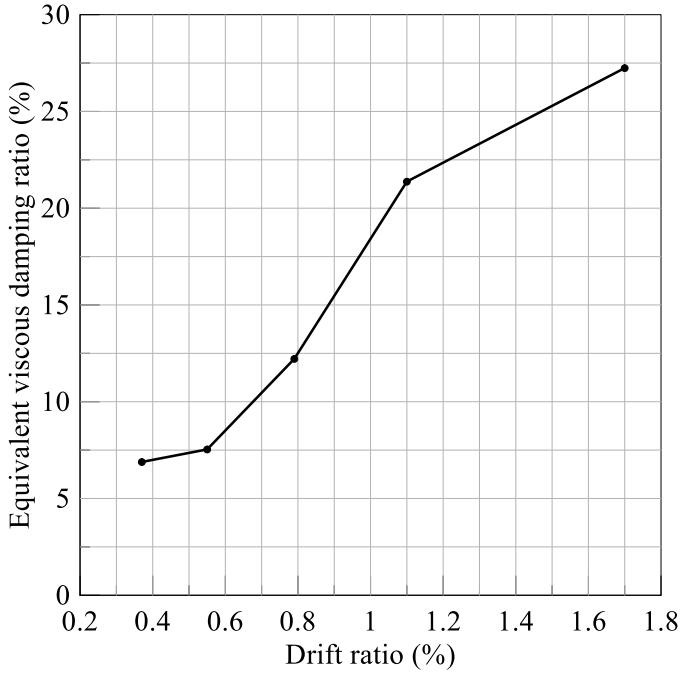

Figure 2-26: Equivalent viscous damping ratio, CNSC2

Table 2-13: Equivalent viscous damping, CNSC2

Drift ratio (%)	0.37	0.55	0.79	1.10	1.70
EVD (%)	6.9	7.5	12.2	21.4	27.2

2.5.3 Behaviors of CNSC2 and CNSC0

Figure 2-27 presents the in-plane force-displacement responses of CNSC0 and CNSC2. The uniaxial compressive strengths of the concrete (slenderness ratio) for CNSC0 and CNSC2 were 5800 psi (21) and 5300 psi (16), respectively. The faceplate yield strengths of CNSC0 and CNSC2 were 57 ksi and 47 ksi, respectively. These differences in faceplate slenderness and material strengths make it difficult to quantify the effects of the OOP load on the IP response by comparing specimen responses. The control specimen and CNSC2 were pushed to a drift ratio of 1.5% and 1.7%, respectively. CNSC0 failed due to cyclic yielding of the steel faceplates, leading to fracture of the base metal close to the weld (Kurt et al., 2015). The test of CNSC2 was terminated after cyclic yielding of the steel faceplates leading to spalling of the infill concrete and tie bar rupture.

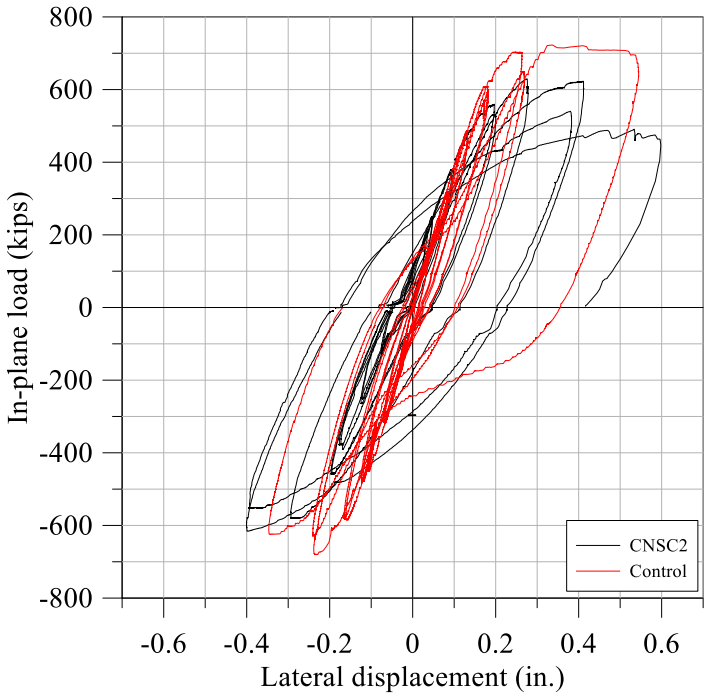

Figure 2-27: In-plane force-displacement responses of CNSC0 and CNSC2

2.6 CNSC3 Test Protocol, Results, and Discussion

2.6.1 CNSC3 Test Protocol

Specimen CNSC3 was tested on 02/09/16 and 02/10/16. The concrete compressive strength on the first day of testing was 5300 psi. Cracks formed on the exposed North and South faces of the wall (see Figure 2-28) due to the post-tensioning of the beams to the specimen (see Figure 2-2) for the application of OOP loads. The specimen was subjected to five cycles of OOP loading, at magnitudes of 50, 100, 150, 200 and 250 kips, respectively, to verify the test setup was functioning as intended, and to crack the infill concrete due to OOP shear. The OOP load was then maintained at 250 kips ($=4.92\sqrt{f_c'}A_c$) and incremental cyclic IP loading imposed. The loading protocol for CNSC3 is presented in Table 2-14, where P_y and Δ_y are the in-plane yield load (=505 kips) and yield displacement (=0.175 in.) of the specimen, respectively, calculated by pre-test analysis.

(a) North face

(b) South face

Figure 2-28: Initial cracking of specimen before OOP load application, CNSC3 (UB and Purdue)

Table 2-14: Loading protocol for CNSC3

Cycle	IP loading[1]	Control	OOP loading
1-2	$0.25\,P_y$	Force	250 kips
3-4	$0.50\,P_y$	Force	
5-6	$0.75\,P_y$	Force	
7-8	$1.00\,P_y$	Displacement	

1. P_y is the estimated in-plane yield strength

2.6.2 CNSC3 Test Results

The OOP cyclic force-displacement relationship for CNSC3 is presented in Figure 2-29, where the OOP displacement was measured at the top of the wall, at the level where the IP loading was later applied. The OOP cyclic loading resulted in diagonal cracks in both the push and pull directions, on the exposed North and South faces of the wall, as presented in Figure 2-30. The cracks propagated diagonally downwards from the level of application of the OOP load.

The IP cyclic force-displacement relationship for CNSC3 is presented in Figure 2-31. Significant reductions in IP resistance were observed in cycle 8. The significant drop in the in-plane load in cycle 8, at a displacement of 0.18 inch, resulted from the operator trying to avoid overshooting the target displacement.

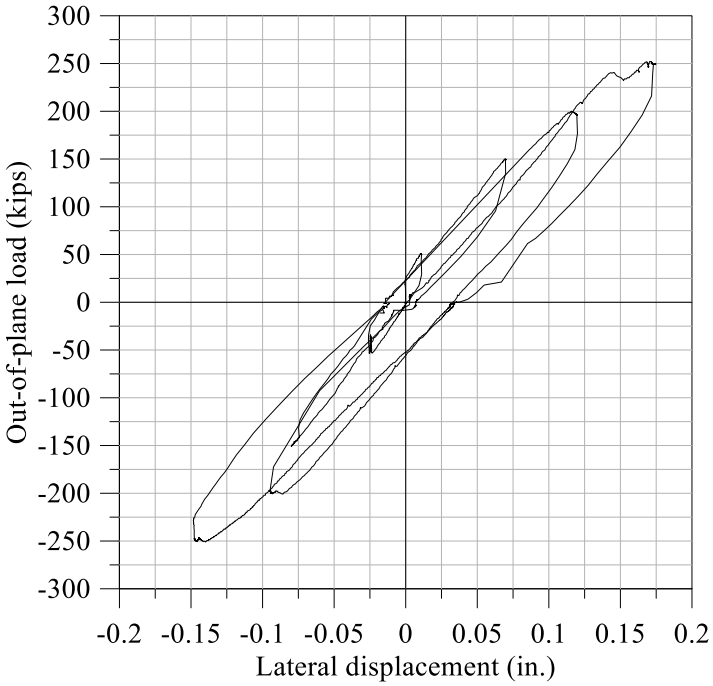

Figure 2-29: Out-of-plane force-displacement relationship, CNSC3

(a) North face (b) South face

Figure 2-30: Additional diagonal cracking caused by OOP loading, CNSC3 (UB and Purdue)

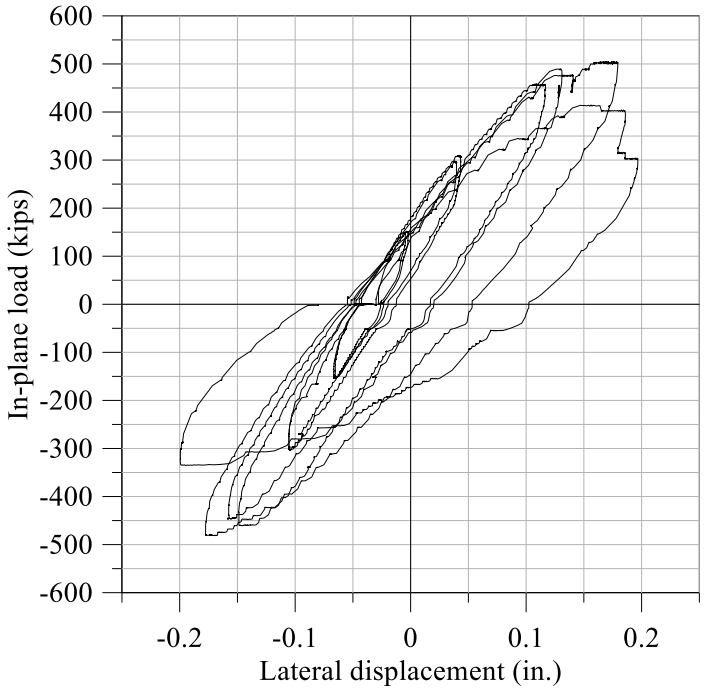

Figure 2-31: In-plane force-displacement relationship, CNSC3

The IP load-displacement relationship and backbone curve are presented together in Figure 2-32; the hysteresis loops are offset from the origin by approximately 0.035 inch due to twisting of the SC wall pier caused by the applied OOP load. Points A, B, C, and D in the figure represent the onset of concrete cracking under IP loading, yielding of steel faceplates, buckling of steel faceplates, and concrete crushing, respectively. The test was terminated at the displacement × shown on the plot (displayed at point D). The sequence of damage to CNSC3 is presented in Table 2-15. Concrete cracking under IP loading, steel faceplate yielding, steel face plate buckling, and concrete crushing in the SC wall occurred at drift ratios of 0.09%, 0.19%, 0.50%, and 0.56%, respectively.

Key results are presented in Table 2-16. The initial stiffness of the SC wall, calculated at a drift ratio less than 0.02%, is presented in the first column for the push and pull directions. The values of load and drift ratio at the onset of steel plate yielding are presented in columns two and three. The fourth and fifth column present the load and drift ratio at the onset of steel faceplate buckling. The peak loads and their corresponding drift ratios for the push and pull directions are presented in columns six and seven. The maximum drift ratios for the experiment and their

corresponding loads in the push and pull directions are presented in columns eight and nine. The maximum drift ratio does not correspond to gravity load failure of CNSC3.

Table 2-15: Sequence of damage, CNSC3

Cycle	Drift ratio (%) Push/Pull	Damage/Observations
Pre-test	-/-	Diagonal cracks on the North and South faces propagating from the point of application of OOP load on the East face to the base plate on the West face; diagonal cracks on the North face propagating from the West face: cracks above the point of OOP load application; small diagonal cracks on the South face located mid-depth of the cross section and above point of OOP load application
OOP 100 kips	-	Short diagonal cracks on the North face propagating from the East face towards the base plate on the West face below the point of OOP load application; short diagonal cracks on the South face at the mid-depth of the cross section, propagating from East to West
OOP 150 kips	-	Diagonal cracks on the North face propagating from the point of OOP load application on the East face towards the base plate on the West face
OOP 200 kips	-	Diagonal cracks on the South face from the point of OOP load application to the mid-depth of the cross section from the East face towards the West face
OOP 250 kips	-	Diagonal cracks on the North face propagating from the point of OOP load application on the West face to the East face towards the base plate; short diagonal cracks on the South face propagating from the West face to the East face
1	0.09/0.08	Propagation of diagonal cracks on the North and South faces; new diagonal cracks on the South face
2	0.08/0.09	New diagonal cracks on the South face
3	0.19/0.21	Yielding of the steel faceplate on the West (tension) side of the wall; new diagonal cracks on the North face at the point of OOP loading
4	0.20/0.21	Propagation of diagonal cracks on the South face; new diagonal cracks on the North face near the base of the wall
5	0.35/0.36	New horizontal cracks located at the mid-depth of the cross section on the South face
6	0.39/0.41	Significant growth of cracks on the North and South faces; yielding of the steel faceplate on the East (compression) side of the wall
7	0.50/0.49	Buckling of the steel faceplate in the northeast corner of the wall; significant opening of cracks on the North and South faces
8	0.56/0.56	Concrete crushing and spalling at the toes of the wall; significant movement of wall in the OOP direction; difficult to maintain OOP load; buckling of the East faceplate along the length of the wall, 2 inches above the baseplate; deformation of the steel faceplate at the point of OOP load application on the West face; OOP and IP residual drifts are 1.0 and 0.07 inch, respectively

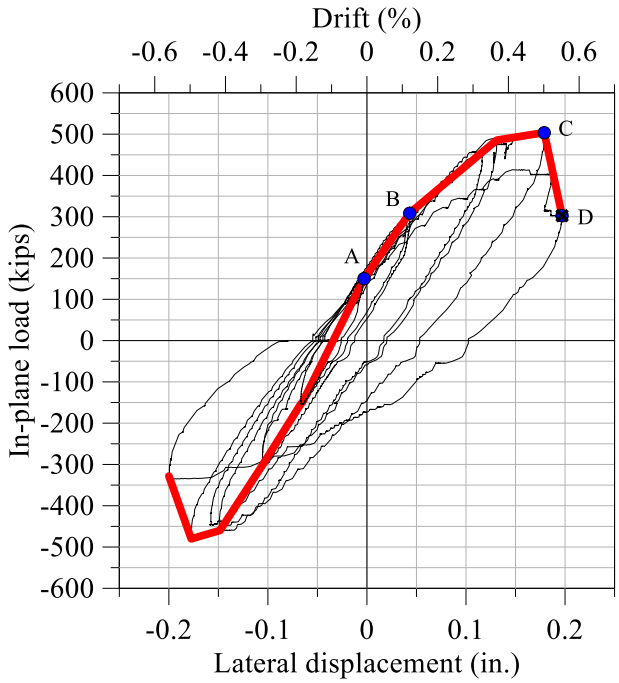

Figure 2-32: In-plane force-displacement relationship and backbone curve, CNSC3

Table 2-16: Summary results for CNSC3

Initial stiffness (kip/in.)	Onset of steel plate yielding		Onset of steel plate buckling		Peak load		Maximum drift	
Push/Pull	Load (kips)	Drift (%)	Load (kips)	Drift (%)	Load (kips) Push/Pull	Drift (%) Push/Pull	Load (kips) Push/Pull	Drift (%) Push/Pull
3500/3576	309	0.19	504	0.50	504/481	0.50/0.49	303/328	0.56/0.56

The accumulated damage to the wall pier on the exposed South and North faces of the wall after cycle 8 is shown in Figure 2-33. Local buckling of the steel faceplates and concrete cracking and spalling are clearly visible. Figure 2-34 presents additional photographs of damage including faceplate buckling and OOP residual drift.

The cumulative energy dissipation in CNSC3 is presented in Figure 2-35. The energy dissipated in each cycle (*EDC*) is presented in Table 2-17. Equivalent viscous damping (*EVD*) data are presented in Figure 2-36 and Table 2-18, where *EVD* is computed using equation (2-1).

(a) South face

(b) North face

Figure 2-33: Accumulated damage after cycle 8, CNSC3 (UB and Purdue)

(a) Faceplate buckling

(b) OOP residual drift

Figure 2-34: Additional photographs of damage after cycle 8, CNSC3 (UB and Purdue)

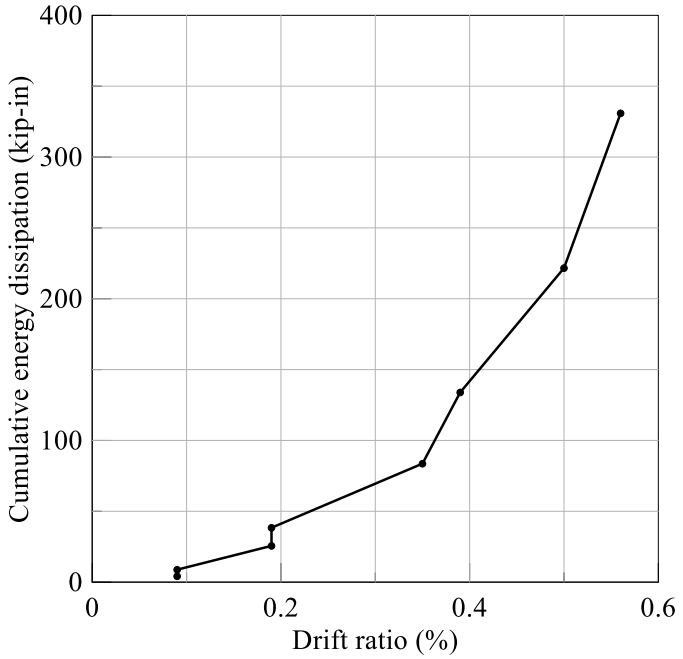

Figure 2-35: Cumulative energy dissipation, CNSC3

Table 2-17: Energy dissipated per cycle, CNSC3

Cycle	6	7	8
EDC (kip-in)	50.3	87.7	109

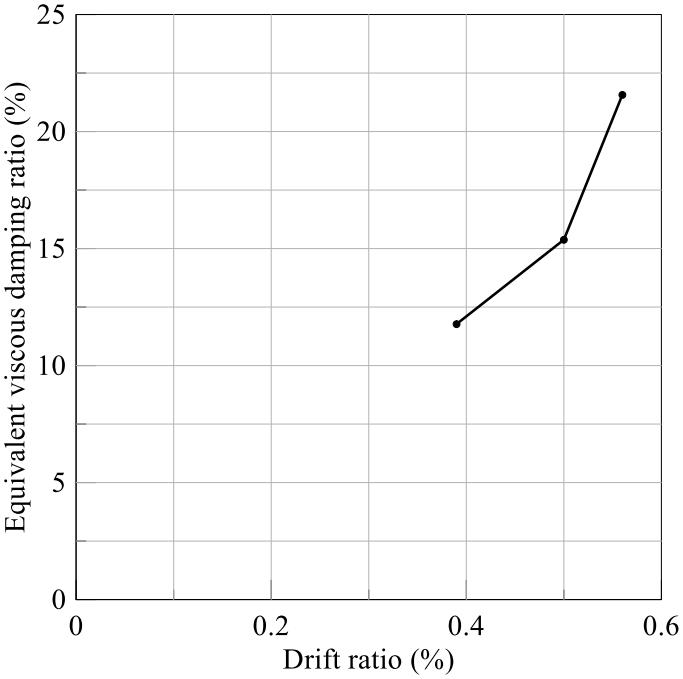

Figure 2-36: Equivalent viscous damping ratio, CNSC3

Table 2-18: Equivalent viscous damping, CNSC3

Drift ratio (%)	0.39	0.50	0.56
EVD (%)	11.8	15.4	21.6

2.6.3 Behaviors of CNSC3 and CNSC0

Figure 2-37 presents the in-plane force-displacement responses of CNSC0 and CNSC3. The uniaxial compressive strengths of the concrete (slenderness ratio) for CNSC0 and CNSC3 were 5800 psi (21) and 5300 psi (16), respectively. The faceplate yield strengths of CNSC0 and CNSC3 were 57 ksi and 47 ksi, respectively. These differences between CNSC0 and CNSC3 make it impossible to directly compare the experimental results. CNSC0 and CNSC3 were pushed to a drift ratio of 1.50% and 0.56%, respectively. CNSC0 failed due to cyclic yielding of the steel faceplates, leading to fracture of the base metal close to the weld. The test of CNSC3 was terminated after significant buckling of the steel faceplate on the Northeast corner of the wall and spalling of the infill concrete.

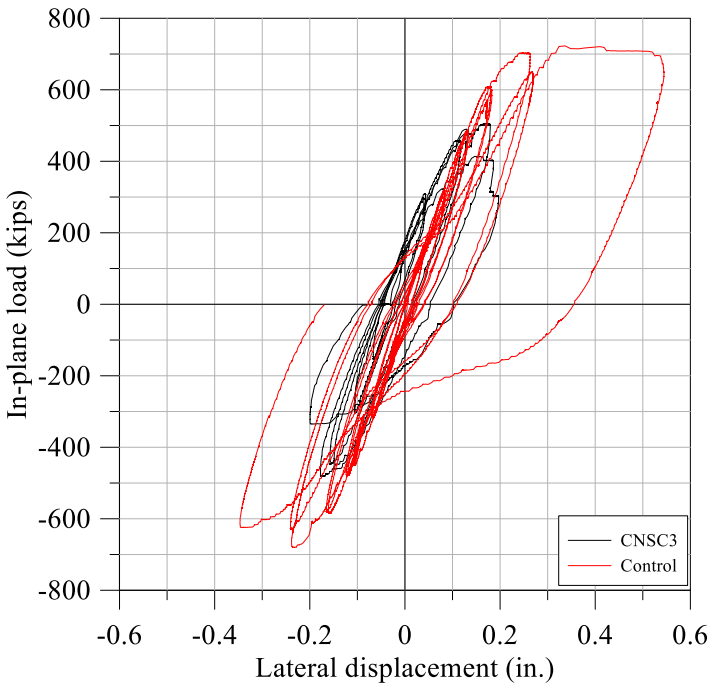

Figure 2-37: In-plane force-displacement responses of control specimen and CNSC3

SECTION 3
NUMERICAL SIMULATION OF THE SEISMIC RESPONSE OF SC WALL PIERS

3.1 Introduction

This chapter describes numerical simulations performed to support the physical tests of Chapter 2, namely, the simultaneous in-plane (IP) and out-of-plane (OOP) loading of SC wall piers. The simulations described here utilized, as a starting point, validated numerical models developed in LS-DYNA (LSTC, 2012) by Epackachi et al. (2014b, 2015) for calculating the IP response of SC wall piers. The validated model developed by Epackachi et al. for the IP response of SC walls used:

- The smeared crack Winfrith model for infill concrete, MAT085, using concrete material properties including the nominal compressive and tensile strengths, elastic modulus, Poisson's ratio of 0.18, specific fracture energy, and aggregate size. In the absence of experimental data, the specific fracture energy can be estimated for a given aggregate size using CEB (1993).

- The plastic-damage model for the steel faceplates, MAT081, using steel material properties including the nominal yield and ultimate strengths, elastic modulus, Poisson's ratio, and plastic strain thresholds corresponding to the beginning of the softening and rupture as established using coupon test results.

- Beam, shell, and solid elements to model connectors, steel faceplates, and infill concrete, respectively, and a mesh size of 1 in for the solids and shells

- Tie constraint to attach the studs and tie rods to the steel faceplates (and the baseplate if provided) and LAGRANGE-IN-SOLID constraint available in LS-DYNA to attach the connectors to the infill concrete elements.

The IP response of SC wall piers is dominated by the behavior of the steel faceplates. Given that the OOP response of an SC wall will be strongly influenced by the behavior of the concrete, it was prudent to first exercise the IP model described above using data from tests of singly reinforced concrete (RC) specimens that were not reinforced for shear. The RC beam simulations

are presented in Section 3.2. Section 3.3 presents numerical simulations of the physical tests described in Chapter 2.

3.2 RC Beam Simulations

Data from tests of RC beams performed by Bresler et al. (1963) and Mphonde et al. (1984) were used to validate the Winfrith (MAT085) concrete model. The corresponding LS-DYNA simulations are summarized in Table 3-1, where w is the width of the beam, h is the height of the beam, l is the length of the beam, f_c' is the unconfined uniaxial compressive strength of concrete, f_t' is the tensile strength of the concrete (taken as $0.1 f_c'$ unless specified in the experiment), ρ is the longitudinal reinforcement ratio, E is Young's modulus for concrete, calculated as $E = 57000\sqrt{f_c'}$ per ACI 318-14 (ACI, 2014), G is fracture energy calculated using Equation 2.1-7 or Table 2.1.4 of CEB-FIP Model Code (CEB, 1993), and w_c is crack width, calculated as $w_c = 2G / f_t'$ per Figure 3 of Wittmann et al. (1988). Test 1 was performed by Bresler et al. and Tests 2 through 6 were performed by Mphonde et al. (1984). In these experiments, the shear span-to-depth ratio, a/d, was varied from 1.5 to 4 and the concrete compressive strength varied between 3200 and 10634 psi. The longitudinal reinforcement ratios in these beams are high, and especially so for specimens 2 through 6. Additional simulations were then performed for $a/d = 1.5$: the ratio chosen for the testing of the SC wall panels, as described in Chapter 2.

Table 3-1: Summary of LS-DYNA simulations of plain RC specimens

Test	Beam dimensions $w \times h \times l$ (in)	a/d	f_c' (psi)	f_t' (psi)	ρ (%)	E (psi)	G (lb-in/in^2)	w_c (in)
1	12.2 × 21.9 × 144	4	3,270	575	1.8	3.26E6	0.371	0.0013
2	6 × 13.25 × 96	3.6	3,273	327	3.4	3.26E6	0.371	0.0023
3	6 × 13.25 × 96	2.5	3,246	325	3.4	3.25E6	0.371	0.0023
4	6 × 13.25 × 96	1.5	3,637	364	3.4	3.44E6	0.399	0.0022
5	6 × 13.25 × 96	1.5	6,593	659	3.4	4.63E6	0.548	0.0017
6	6 × 13.25 × 96	1.5	10,364	1036	3.4	5.88E6	0.714	0.0014

Figure 3-1 describes the Bresler et al. experiment. The corresponding LS-DYNA model is presented in Figure 3-2. One-inch long beam elements were used to model the longitudinal reinforcement (4 #9 bars with a 1-inch cover, corresponding to a reinforcement ratio of 1.8%). Eight-node solid elements were used to model the concrete. The concrete was modeled with 1 × 1 × 1 in. elements. The rebar was embedded into the concrete using node sharing. The constant

stress formulation (ELFORM=1 in LS-DYNA) and cross section integrated beam element (Hughes-Liu beam in LS-DYNA) were used for the solid and beam elements, respectively. The Winfrith concrete model was used to model the concrete in the beam. The d3crack database was activated to visualize the crack pattern during loading. The PIECEWISE_LINEAR_PLASTICITY (MAT024) material model was used to model the Grade 60 reinforcement. The pin and roller boundary conditions were applied by constraining the displacements of three rows of nodes in the (Y and Z) and (Z) directions, respectively. A displacement was imposed at the center of the beam (1495 nodes) using a PRESCRIBED_MOTION_SET. Figure 3-3 shows the boundary conditions and the applied load.

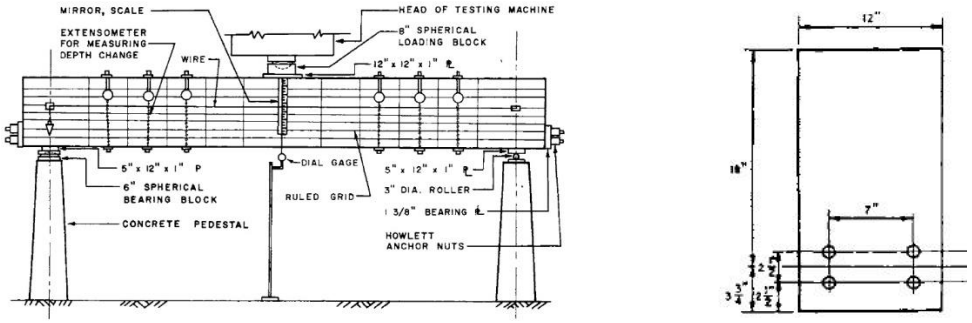

Figure 3-1: Experimental setup (Bresler et al., 1963)

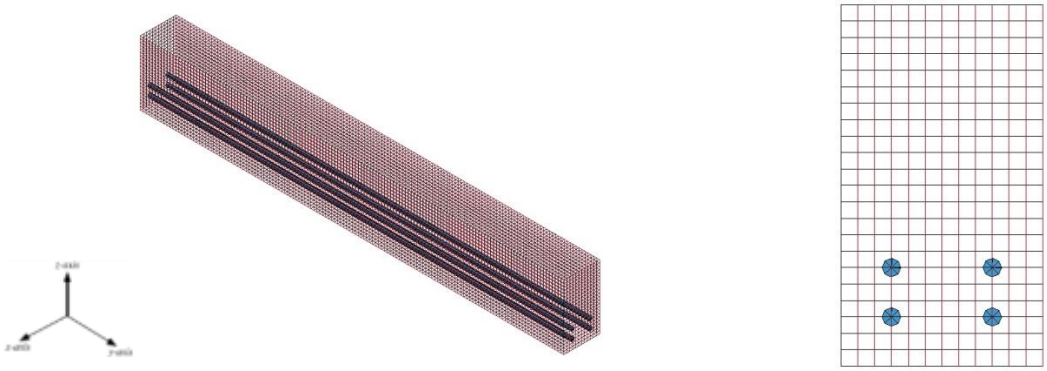

(a) Isometric view (b) Cross section view (XZ plane)

Figure 3-2: LS-DYNA model of the Bresler et al. (1963) experiment

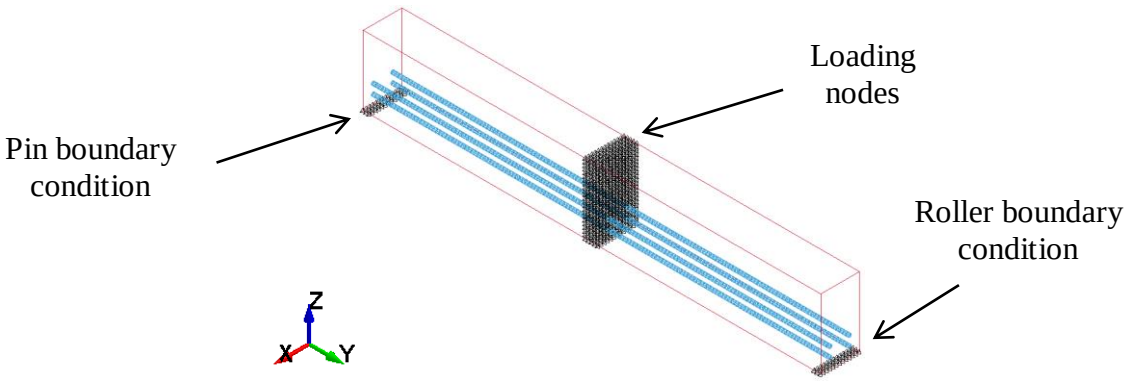

Figure 3-3: LS-DYNA loading and boundary conditions

Figure 3-4a and Figure 3-4b present the final crack pattern of the beam from the LS-DYNA simulation and the experiment, respectively. The crack pattern from the simulation is in reasonably good agreement with the experiments. Cracking at the support caused by slippage of the longitudinal reinforcement was not observed in the simulation because perfect bond was assumed. Figure 3-4c presents the force-displacement relationship at the center of the beam for the experiment and the simulation. The peak force observed in the simulation and experiment are 70 and 75 kips, respectively. The simulation is in good agreement with the experiment.

An illustration of the beam used in the Mphonde et al. (1984) experiments is presented in Figure 3-5. The input for the simulations is presented in Table 3-1 as Tests 2 through 6. The LS-DYNA model to simulate the Mphonde experiments is presented in Figure 3-6. One-inch beam elements were used to model the longitudinal reinforcement (3 #8 bars with a 1-inch cover corresponding to a reinforcement ratio of 3.36%). Eight-node solid elements were used to model the concrete. The concrete was modeled with $1 \times 1 \times 1$ in. elements. The rebar was embedded into the concrete using node sharing. The constant stress formulation (ELFORM=1 in LS-DYNA) and cross section integrated beam element (Hughes-Liu beam in LS-DYNA) were used for the solid and beam elements, respectively. The Winfrith concrete model was used to model the concrete in the beam. Material constants are presented in Table 3-1. The d3crack database was activated to visualize the crack pattern during loading. The PIECEWISE_LINEAR_PLASTICITY (MAT024) material model was used to model the Grade 60 reinforcement. The pin and roller boundary conditions were applied by constraining the displacements of one row of nodes in the (Y and Z) and (Z) directions, respectively. The location of the constraints was moved to simulate the different span lengths (i.e., 35.25, 58.75, and 84 in). A displacement was imposed at the center of the beam (505 nodes) using a PRESCRIBED_MOTION_SET.

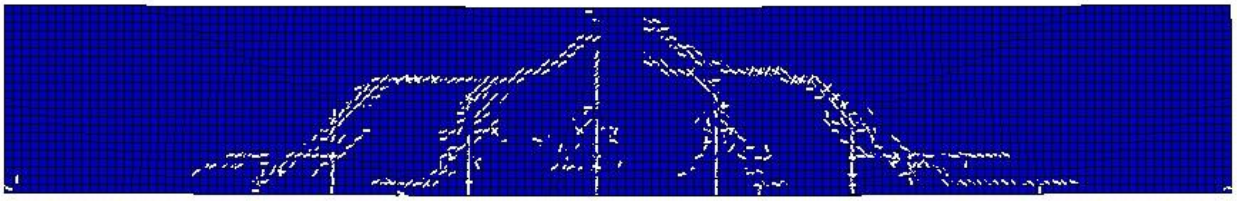

(a) Simulation

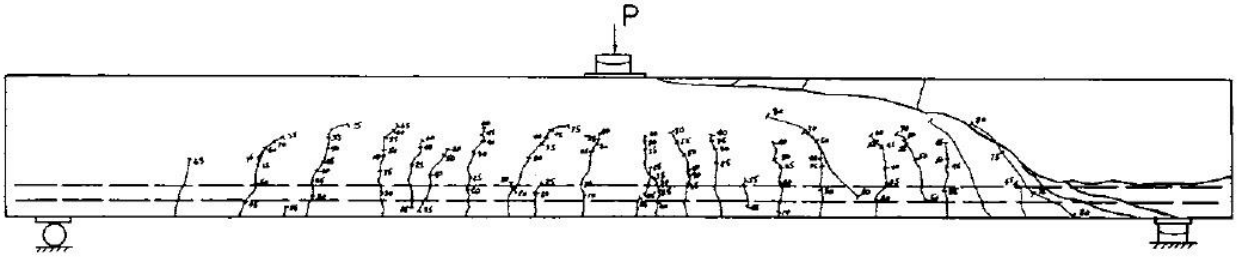

(b) Experiment

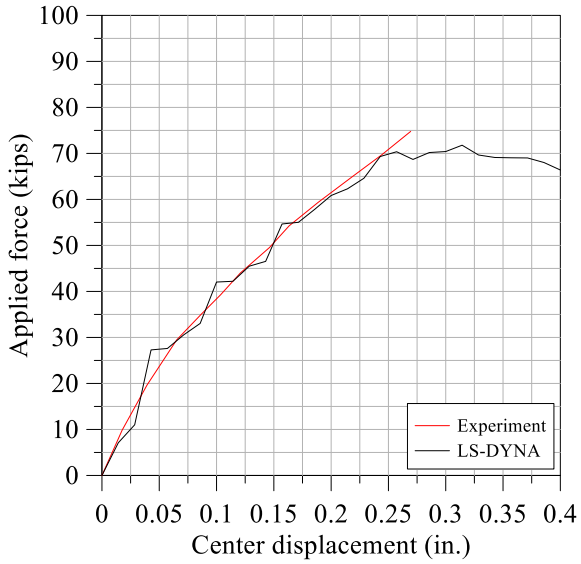

(c) Force-displacement relationships

Figure 3-4: Experimental (Bresler) and LS-DYNA results

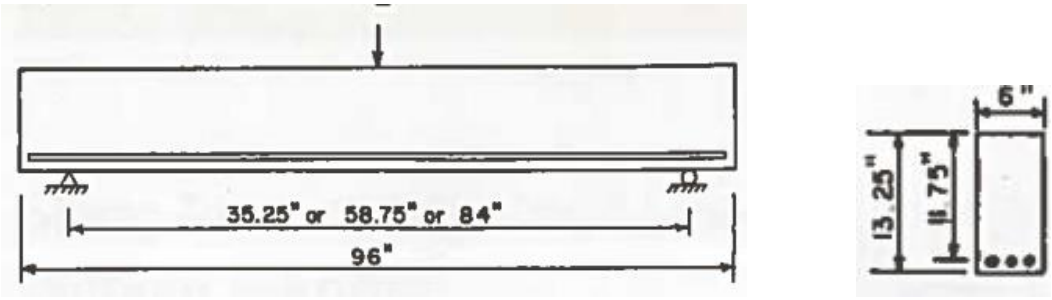

Figure 3-5: Experimental setup (Mphonde et al., (1984))

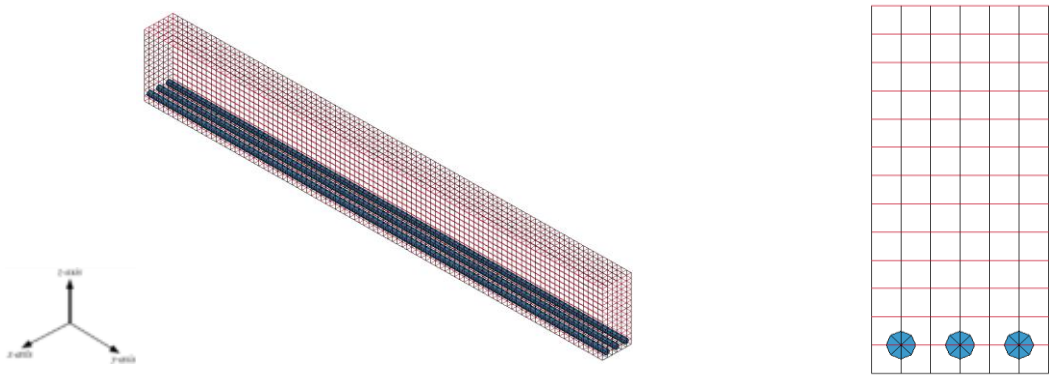

Figure 3-6: LS-DYNA model of the Mphonde et al. (1984) experiment

Table 3-2 summarizes the simulations of the Mphonde experiments using average shear stress at maximum resistance, calculated here as peak load divided by the product of the section width and total depth. The simulations reasonably recover the maximum shear stress calculated from the experimental results for different values of a/d. Not shown here, because the experimental data are not available, is the post-peak shear force response, which will affect the IP behavior of SC walls. The Winfrith concrete model reasonably captures the OOP peak shear strength of plain reinforced concrete beams (i.e., no shear reinforcement) under *monotonic* loading, and is used hereafter to simulate the *cyclic* OOP and combined IP and OOP response of SC walls. Note that the normalized maximum shear stresses for Tests 2 through 6 are much greater than the value of 2.0 routinely used for the shear design of reinforced concrete beams and slabs in the United States for two reasons: 1) the longitudinal reinforcement ratios are high for all specimens (which increases monotonic shear capacity of plain reinforced concrete), and 2) the ratio of *a* to *d* is 1.5 for Tests 4, 5 and 6, which alters the shear-force-resisting mechanism from that of a slender beam to a deep beam (i.e., strut joining the point of load application to the point of reaction).

Table 3-2: Summary of RC beam simulation results

Test	a/d	Maximum shear stress (psi)		Maximum shear stress normalized by $\sqrt{f_c'}$		Difference (%)
		Experiment	LS-DYNA	Experiment	LS-DYNA	
2	3.6	183	198	3.19	3.46	8
3	2.5	220	302	3.86	5.30	37
4	1.5	328	379	5.44	6.28	16
5	1.5	881	974	10.85	12.0	11
6	1.5	1223	1371	11.86	13.3	12

3.3 Simulation of CNSC Experiments

A model of the CNSC experiments was prepared in LS-DYNA using the approach described in Section 3.1. The model, shown in Figure 3-7, is composed of infill concrete, baseplate, steel faceplates, tie bars, and shear studs. The foundation was not included in the model: the bottom nodes of the baseplate were fixed. The element types, sizes, and formulations, and material models used for each part of the model are summarized in Table 3-3.

In experiments CNSC1 and CNSC3, the tie bars were spaced at 12 inches on center along the height and length of the wall, with the first tie bar located 12 inches above the baseplate and 6 inches from the edge of the wall (see Figure 3-8); the tie bar is shown in yellow. In CNSC2, the tie bars were spaced at 6 inches on center along the height and length of the wall, with the first tie bar located 6 inches above the baseplate and 3 inches from the edge of the wall (see Figure 3-9). The shear studs on the faceplates were spaced at 3 inches on center along the height and length of the wall. The total wall thickness was 12 inches. The yield strength and tensile strengths of the steel faceplate material were 47 ksi and 80 ksi, respectively. The OOP loading was simulated by applying nodal forces to the steel and concrete elements at a height of 18 inches above the base of the wall. Once the wall was cycled OOP and the desired OOP load was reached, the OOP load was held constant, and the wall was then subjected to displacement-controlled cyclic IP loading at its top. The follow subsections present results of the LS-DYNA simulations. Comparisons are made between the results of the experiments and the LS-DYNA simulations.

Table 3-3: Summary of the LS-DYNA models of the CNSC specimens

Component	Element			Material model
	Type	Size	Formulation	
Infill concrete	Solid	1 × 1 × 1 in	Constant stress solid	Winfrith (MAT085)
Faceplate	Shell	1 × 1 in	Belytschko-Tsay	Plasticity_with_Damage (MAT081)
Shear studs	Beam	1 in	Hughes-Liu with cross section integration	Piecewise_Linear_Plasticity (MAT024)
Tie bars	Beam	1 in	Hughes-Liu with cross section integration	Piecewise_Linear_Plasticity (MAT024)
Baseplate	Solid	1 × 1 × 1 in	Constant stress solid	Elastic (MAT003)
Welds	Solid	1 × 1 × 1 in	Constant stress solid	Elastic (MAT003)

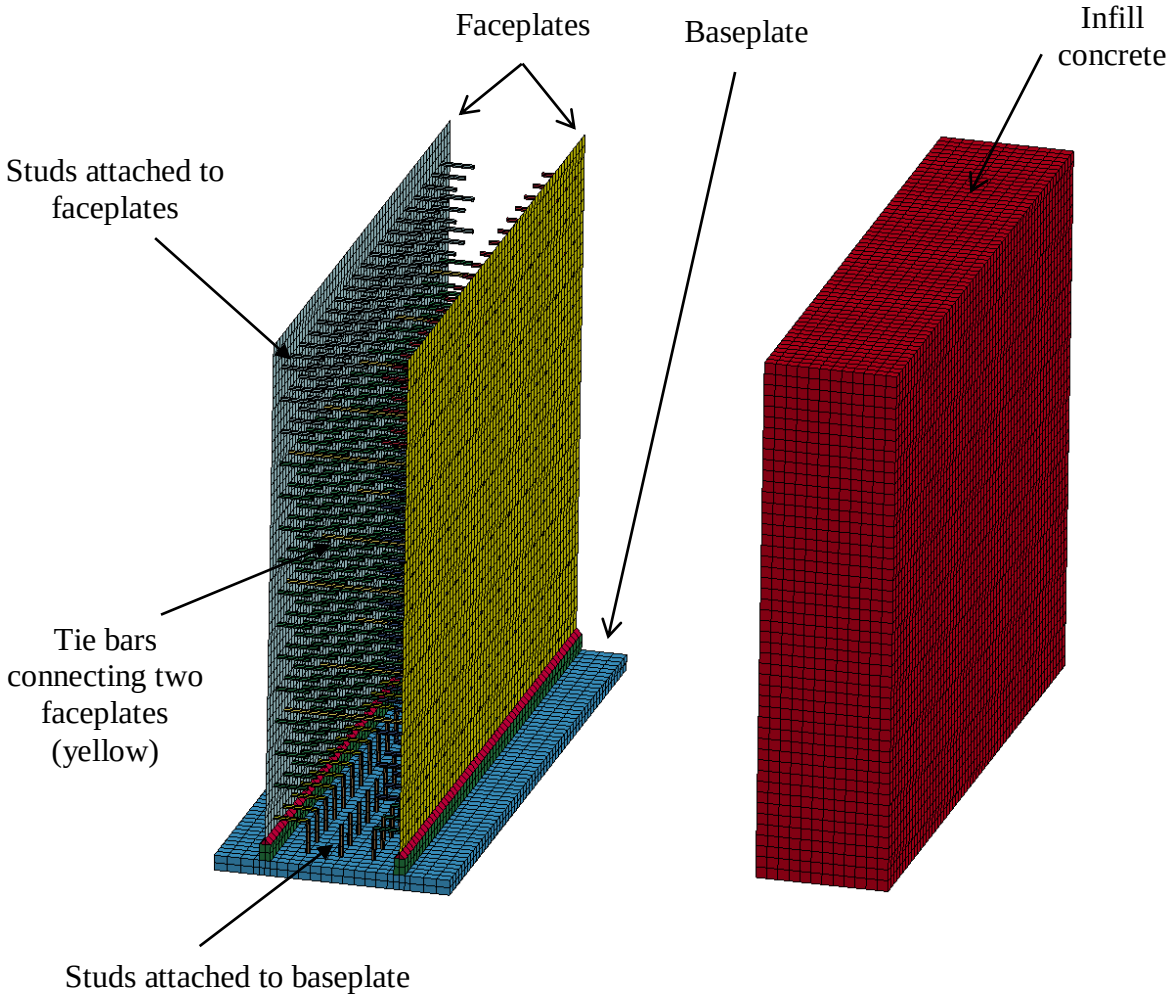

Figure 3-7: LS-DYNA model of the CNSC experiments

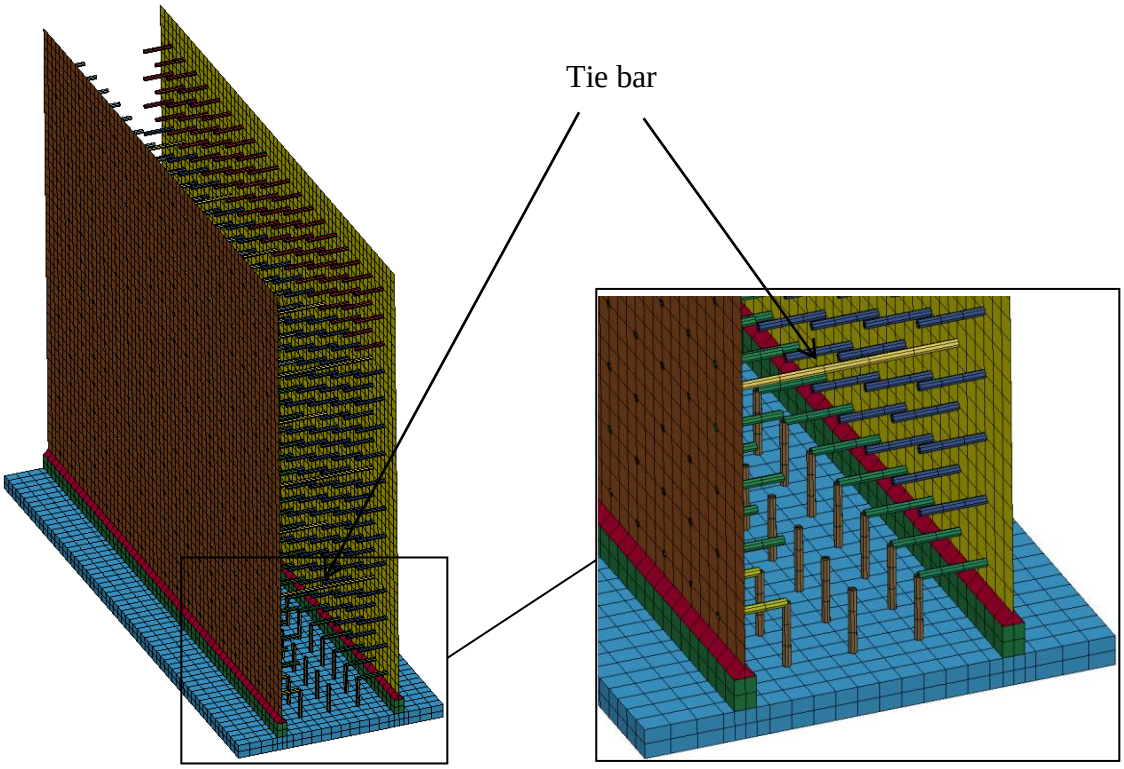

Figure 3-8: CNSC1 and CNSC3 tie bar details

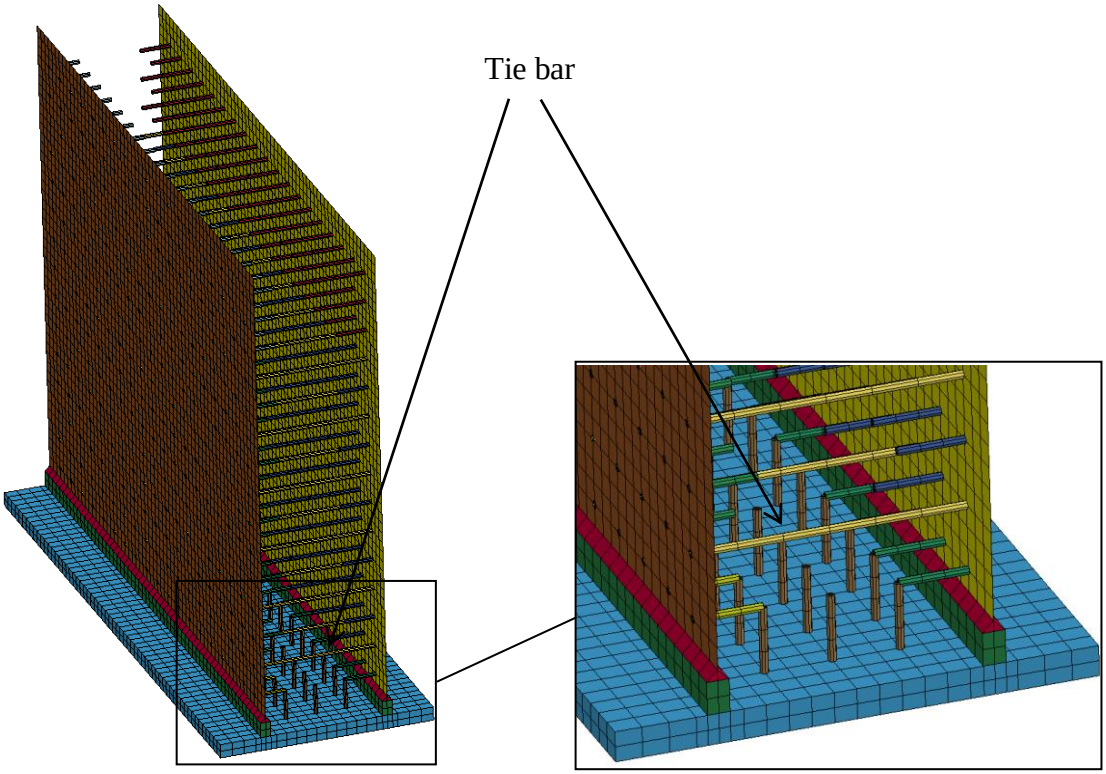

Figure 3-9: CNSC2 tie bar details

3.3.1 CNSC1 Simulations

The uniaxial compressive strength of the infill concrete in CNSC1 on the first day of physical testing was 7700 psi. CNSC1 was initially subjected to four cycles of OOP loading at magnitudes of 30, 60, 90 and 120 kips. The OOP load was maintained at a constant value of 120 kips and incremental cyclic IP loading was then imposed. The IP loading protocol in the simulation and experiment consisted of seven load steps with two cycles per load step and a maximum drift of 1.6%: see Table 2-2.

The OOP force-displacement relationship of the SC panel for the experiment and the simulation are shown in Figure 3-10. The stiffness of the SC panel in the numerical model is slightly greater than that observed in the experiment because the foundation (and its flexibility) was not modeled. A plan view of the wall pier and directions of applied IP and OOP load are presented in Figure 3-11. The configuration presented in Figure 3-11 shows the direction of applied OOP load during IP loading and is denoted as the push direction; the West and East faceplate is in tension and compression due to the OOP load, respectively. The distribution of vertical stress on the tension faceplate (West) at the instant before the IP cyclic loading was imposed for the experiment and the numerical model are presented in Figure 3-12; the stresses are plotted as a function of the distance along the length of the wall from point O (see Figure 3-11). Points P1, P2, P3, P4, and P5 (labeled in Figure 3-11 and Figure 3-12) correspond to distances of 3, 15, 30, 45, and 57 inches from point O at the bottom of the base plate. Points P1, P2, P3, P4, and P5 also correspond to locations of strain gages on the West face (shown in Figure 2-3c). The vertical stresses calculated from the numerical analysis are in reasonably good agreement with the values measured in the experiment. No yielding of the faceplates was observed during OOP loading in either the experiment or the simulation.

The axial stresses in the tie bars at the instant before application of the IP loading is shown in Figure 3-13; the stresses are shown in units of psi. The greatest stresses are observed in the tie bars located below point of application of the OOP load, which is an expected outcome. The maximum axial stress due to the applied OOP load is 6.2 ksi: much less than the yield stress (=50 ksi).

The IP force-displacement relationship of the SC panel for the simulation and the experiment are shown in Figure 3-14. The predictions of peak shear resistance, post-peak strength reductions,

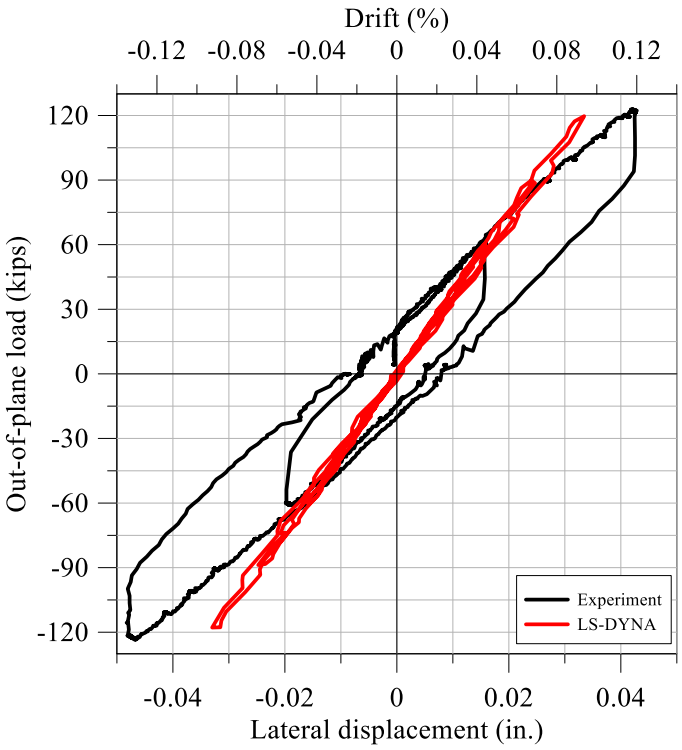

Figure 3-10: OOP force-displacement relationship, LS-DYNA and experiment, CNSC1

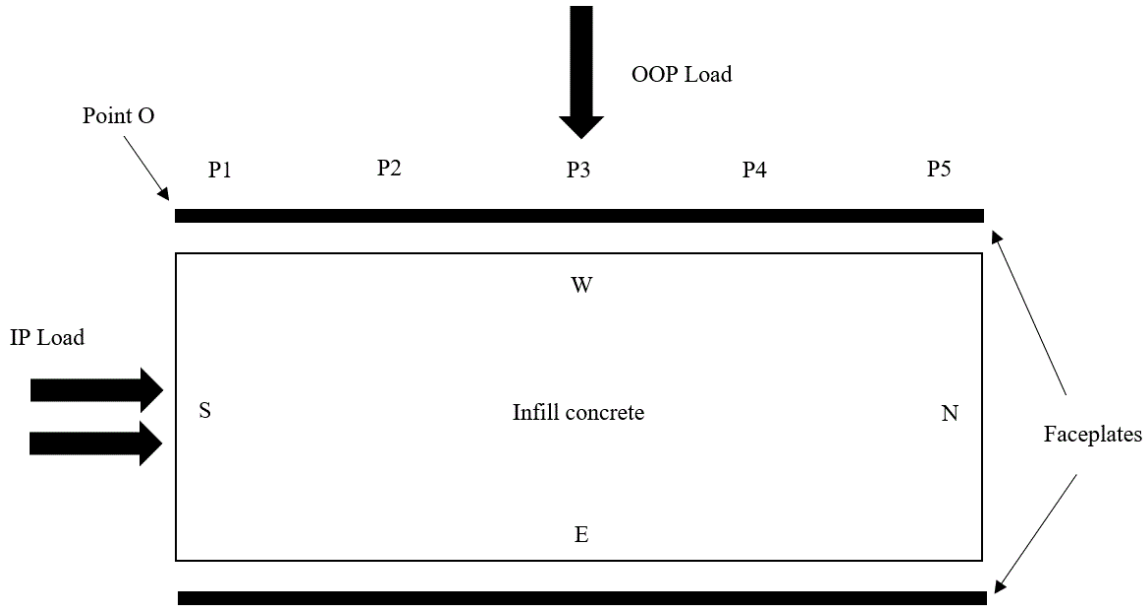

Figure 3-11: Plan view of wall pier and loading

and rate of reloading/unloading stiffness for peak and post-peak IP strength cycles compared favorably with the test results; the initial IP stiffness of the numerical model is significantly larger than that of the experiment because the flexibility of the foundation was not considered in the numerical model.

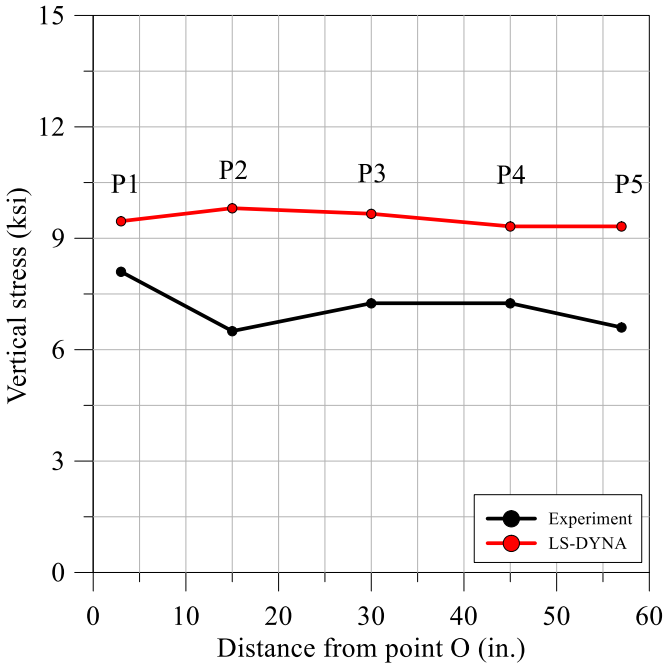

Figure 3-12: Distribution of vertical stresses on tension plate at instant before IP cyclic loading, CNSC1

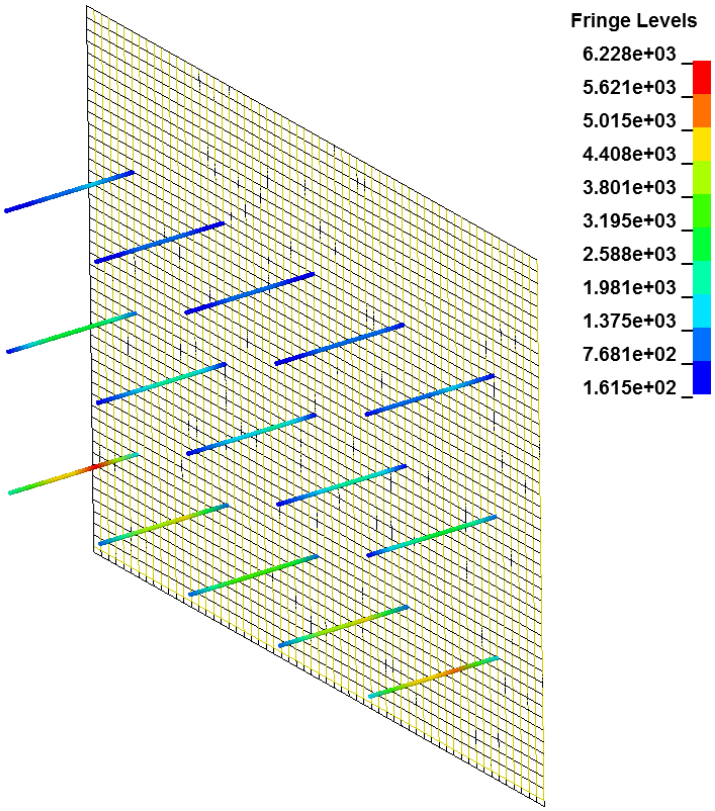

Figure 3-13: Distributions of axial stress in tie bars at instant before IP cyclic loading, CNSC1 (units of psi)

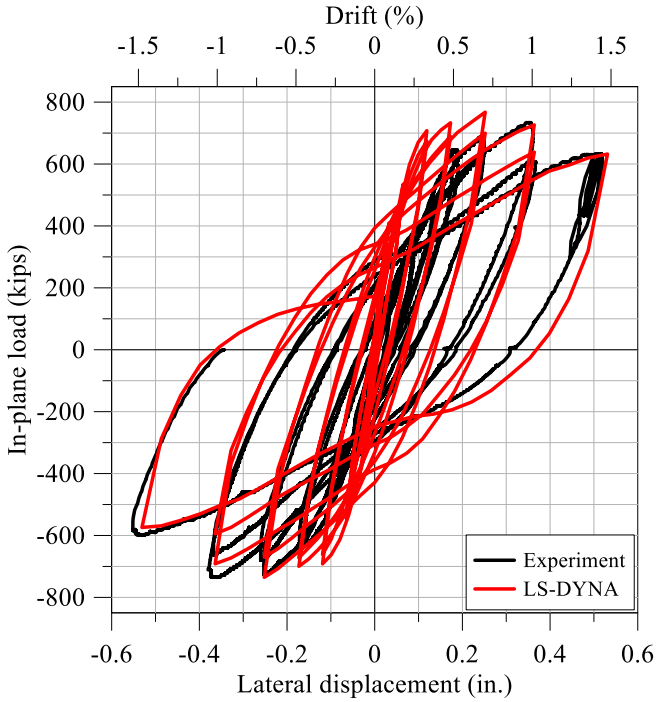

Figure 3-14: IP force-displacement relationship, LS-DYNA and experiment, CNSC1

The IP equivalent viscous damping, EVD, calculated using equation (2-1) at different levels of story drift are presented in Figure 3-15 for both the numerical simulation and the experiment. The calculated damping ratios from the numerical simulation are slightly greater than from the experiment. The IP force-displacement relationships for cycles 8 and 9, which correspond to drift ratios of 0.5 and 0.7%, respectively, are shown in Figure 3-16a and Figure 3-16b, respectively. The numerical model slightly overshoots the peak force and its hysteresis loops are wider, leading to an overprediction of the dissipated energy. Because the secant stiffness to maximum displacement is similar for the numerical solution and the experiment, the overprediction of dissipated energy leads directly to an overprediction of EVD: see Figure 3-15. Figure 3-17 presents the observed and simulated local damage to CNSC1; cracking of the concrete and local buckling of the steel faceplates at the toes of the wall were observed in both the experiment and the numerical simulation. The numerical model cannot predict the crushing (spalling) of infill concrete observed in the experiment.

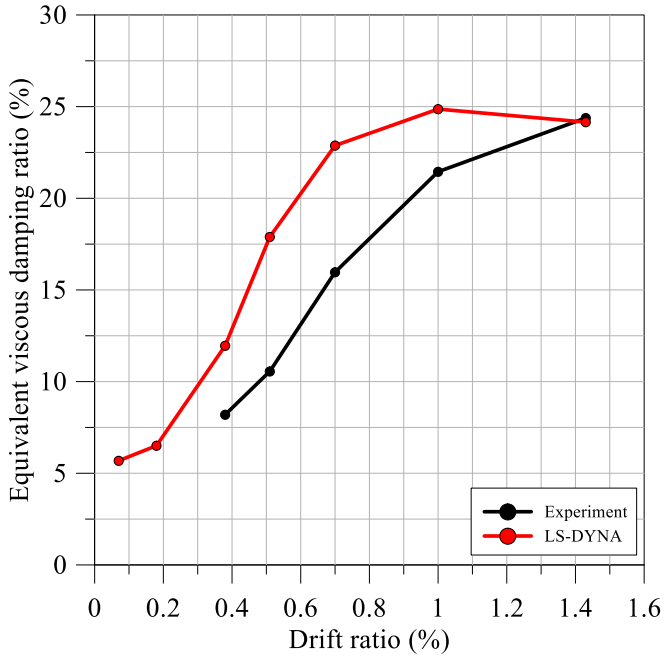

Figure 3-15: Equivalent viscous damping ratio, LS-DYNA and experiment, CNSC1

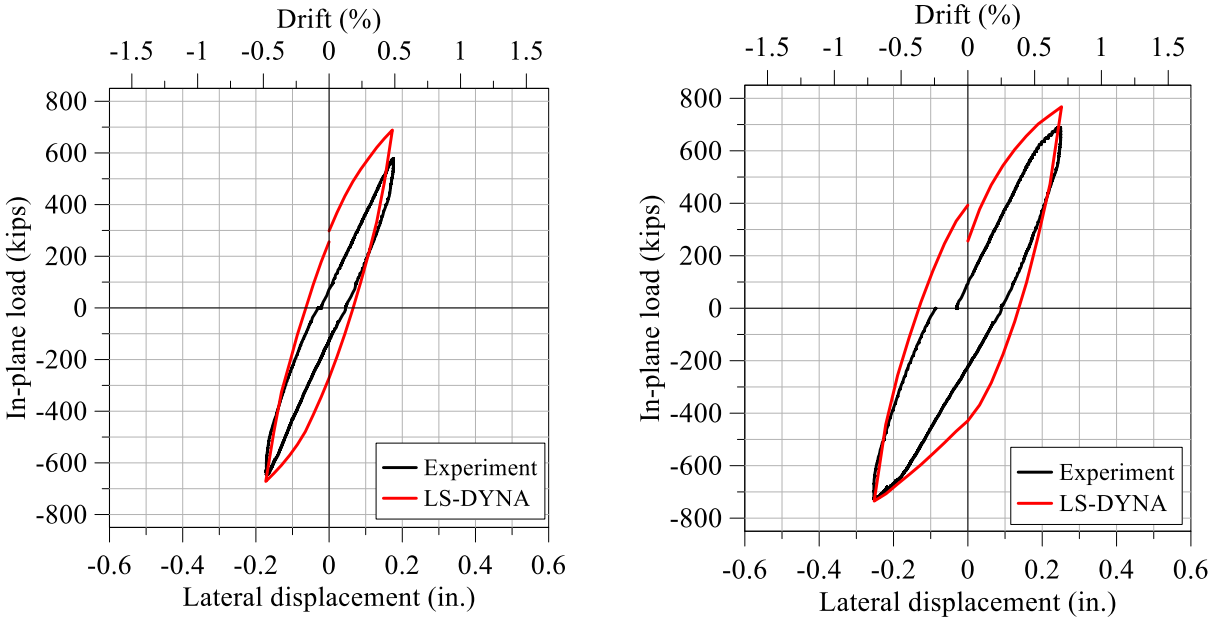

(a) Cycle 8, drift ratio = 0.5% (b) Cycle 9, drift ratio = 0.7%

Figure 3-16: Selected IP force-displacement relationships, LS-DYNA and experiment, CNSC1

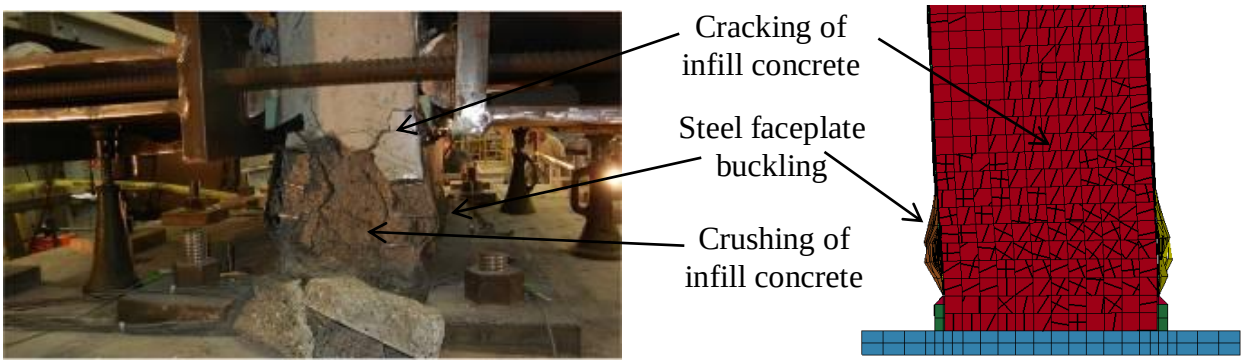

Figure 3-17: Observed and predicted damage to CNSC1

The LS-DYNA-predicted cyclic force-displacement relationships of the infill concrete and steel faceplates are presented in Figure 3-18a and Figure 3-18b, respectively. The IP shear forces in the infill concrete and steel faceplates were calculated at the baseplate using the SPLANE feature in LS-DYNA; the feature allows the user to perform cuts using section planes to aggregate forces. The total IP force-displacement relationship is also presented in Figure 3-18a and Figure 3-18b (in grey), to show the contribution of the infill concrete and steel faceplates to the overall resistance of the wall pier. The steel faceplates dominate the behavior of the SC wall pier in the IP direction, which is an expected result. The pinched hysteresis loops for the infill concrete is associated with damage to the infill concrete (i.e., cracking), as observed in Figure 3-17.

The LS-DYNA-predicted OOP force history of the infill concrete and the steel faceplates is presented in Figure 3-19. The SC wall pier was subjected to four cycles of OOP load at magnitudes of 30, 60, 90, and 120 kips before being held constant (at time=1.7 seconds in Figure 3-19) for the application of the IP loading. The infill concrete dominates the behavior of the SC wall pier in the OOP direction.

Figure 3-20 presents the IP force-displacement relationship for the experiment, and the LS-DYNA simulations with and without the applied OOP load. The initial stiffness, pinching, and rate of reloading/unloading of the numerical model are similar for the numerical model with and without the applied OOP load. The backbone curves for the force-displacement relationships presented in Figure 3-20 are presented in Figure 3-21. The differences in initial stiffness for the experiment and the numerical model are observed clearly using the backbone curves. The OOP load reduces the IP capacity of the LS-DYNA model by approximately 6%.

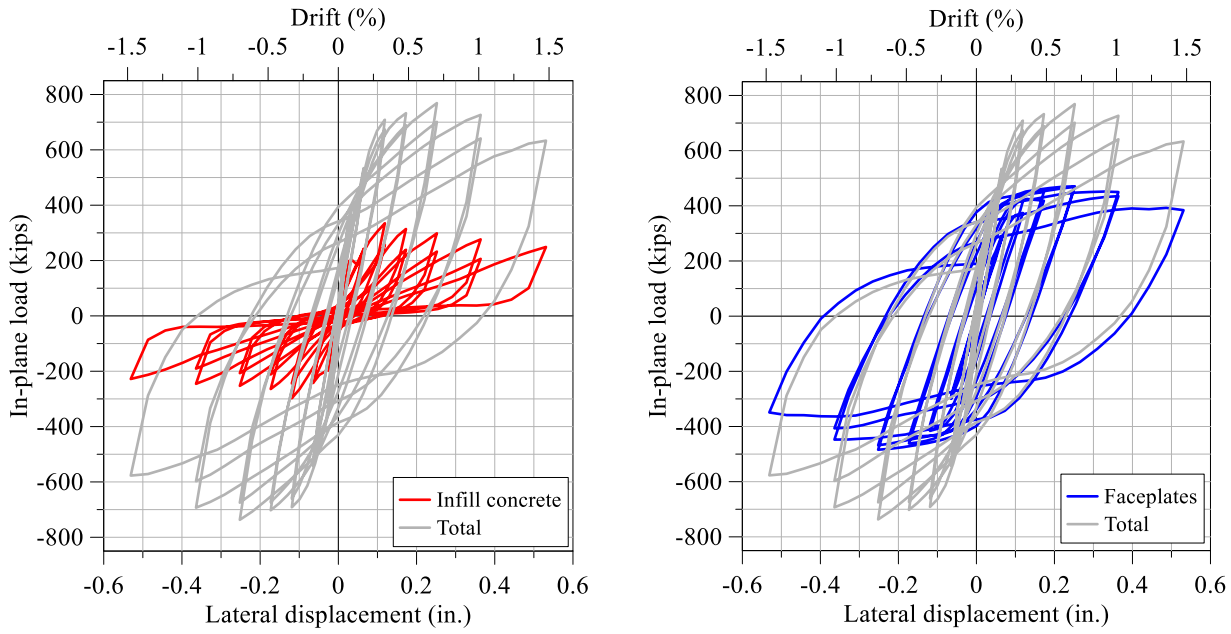

(a) Infill concrete (b) Steel faceplates

Figure 3-18: LS-DYNA-predicted IP cyclic force-displacement relationships, CNSC1

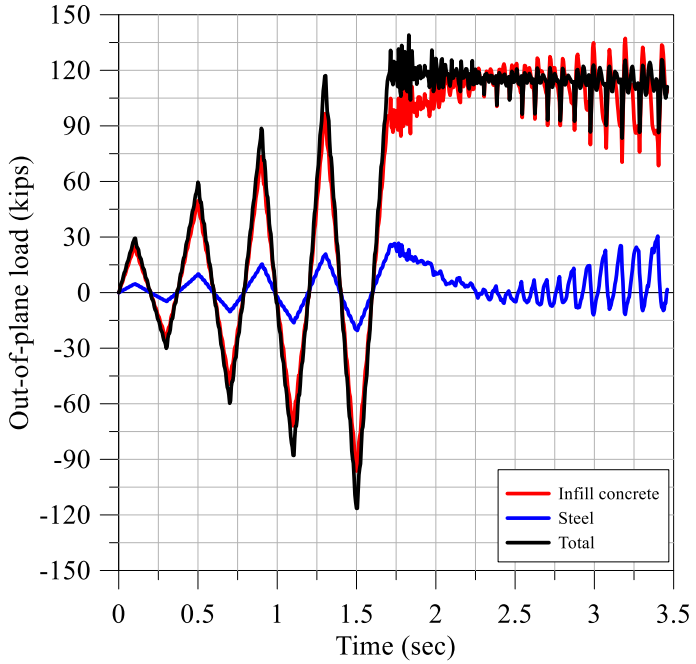

Figure 3-19: LS-DYNA-predicted components of the OOP cyclic force history, CNSC1

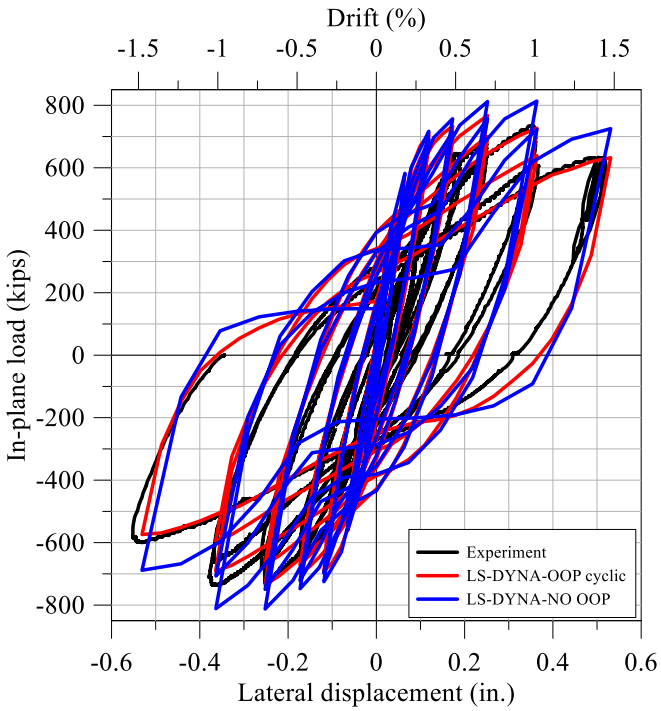

Figure 3-20: IP force-displacement relationships, CNSC1

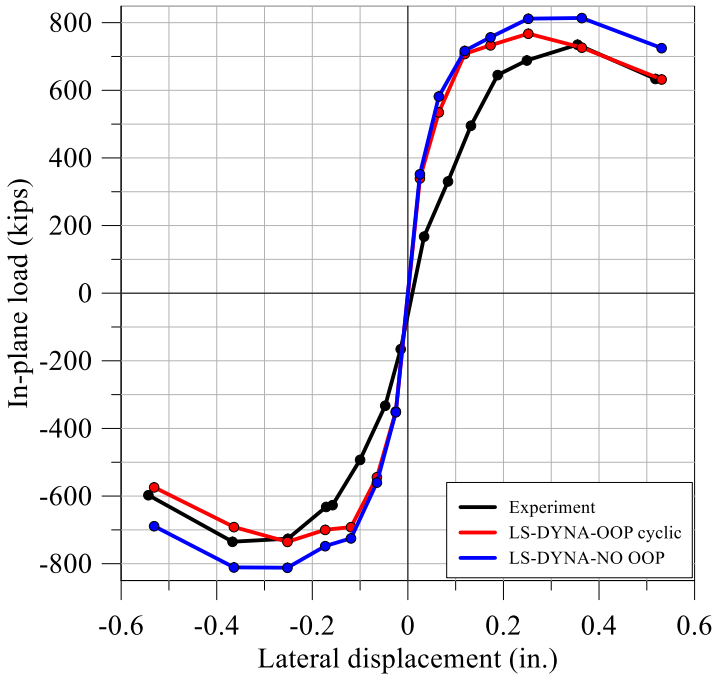

Figure 3-21: Backbone curves, CNSC1

3.3.2 CNSC2 Simulations

The uniaxial concrete compressive strength on the first day of testing was 5300 psi. The SC specimen was initially subjected to five cycles of OOP loading, at magnitudes of 30, 60, 90, 120, and 240 kips, respectively. In both the simulation and the experiment, the OOP load was then maintained at 240 kips and incremental cyclic IP loading was imposed. The loading protocol in the experiment and the simulation consisted of seven load steps with two cycles per load step and a maximum drift of 1.7%: see Table 2-8.

Figure 3-22 presents the OOP force-displacement relationship for the experiment and the simulation. The stiffness of the numerical model is in relatively good agreement with that of the experiment. The distributions of vertical stress on the tension faceplate (West side) in the push configuration at OOP loads of 60, 90, 120, and 240 kips are presented in Figure 3-23a, Figure 3-23b, Figure 3-23c , and Figure 3-23d, respectively; the stresses are plotted as a function of the distance along the length of the wall from point O (see Figure 3-11). The distances of 3, 15, 30, 45, and 57 inches from Point O correspond to points P1, P2, P3, P4, and P5, respectively. The predicted stresses are in relatively good agreement with the stresses measured in the experiment. The faceplates did not yield during cyclic OOP loading in either the experiment or the numerical simulation.

Figure 3-24 presents the distributions of axial stress in the tie bars at the instant before application of the IP load; the magnitude of the OOP load was 240 kips. The maximum axial stress was observed in the tie bars near the base of the wall: an expected result. The predicted maximum axial stress was 37 ksi, and less than the yield value (=50 ksi).

The IP force-displacement relationship for the simulation and the experiment are presented in Figure 3-25. The numerical model predicted the peak shear resistance and rates of reloading/unloading with reasonable accuracy. The OOP load in cycles 12 and 13 of the experiment was not maintained at 240 kips: it gradually decreased as the IP capacity of the wall diminished. To account for this in the numerical simulation, the OOP load in the numerical model decayed linearly from 240 kips at the start of cycle 12 to a value of 0 kips at the end of cycle 13.

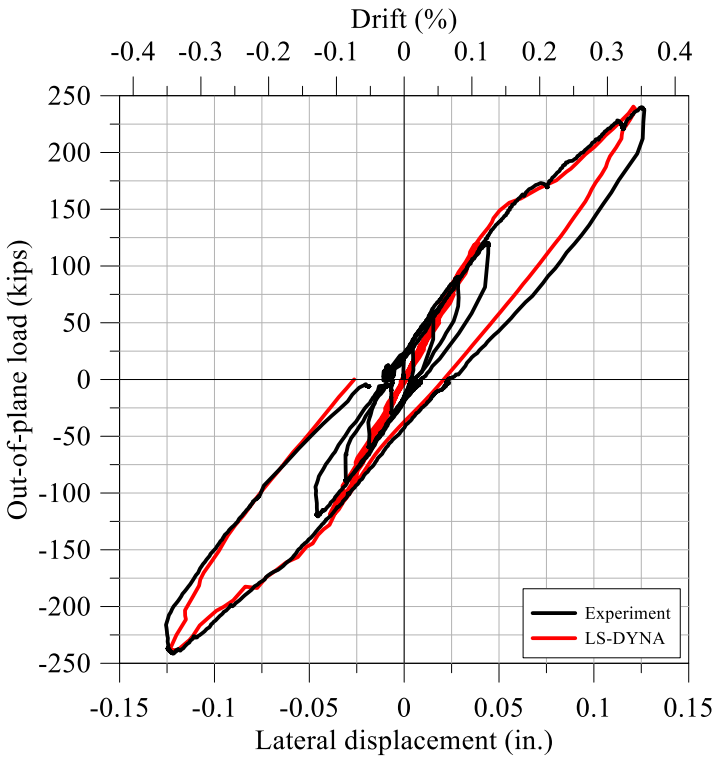

Figure 3-22: OOP force-displacement relationship, LS-DYNA and experiment, CNSC2

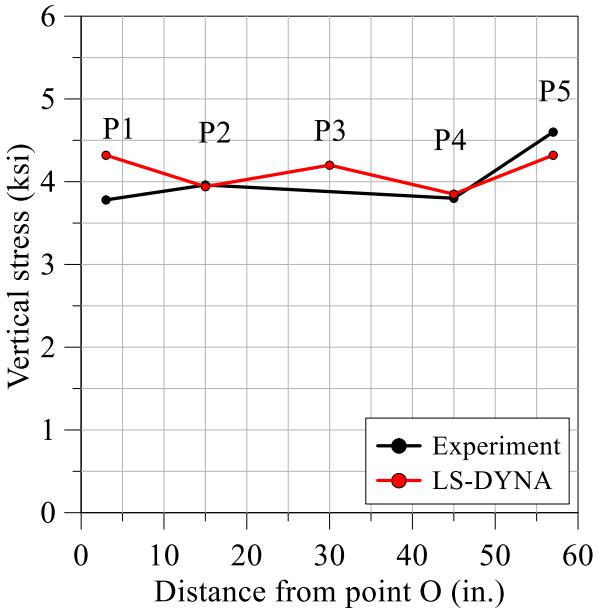

(a) OOP load = 60 kips

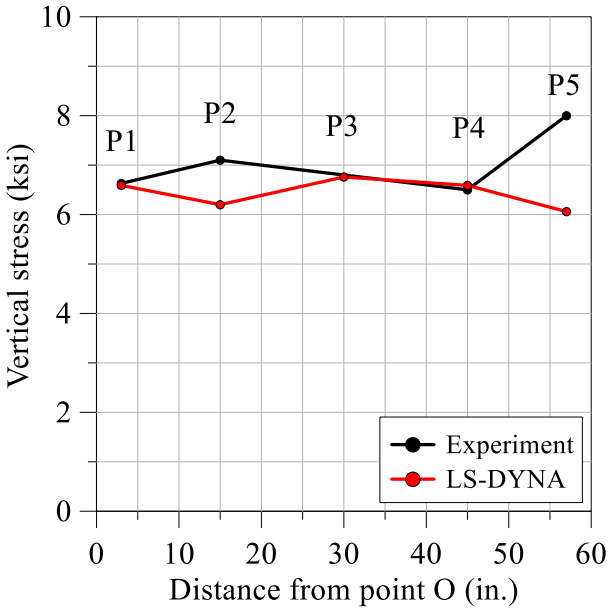

(b) OOP load = 90 kips

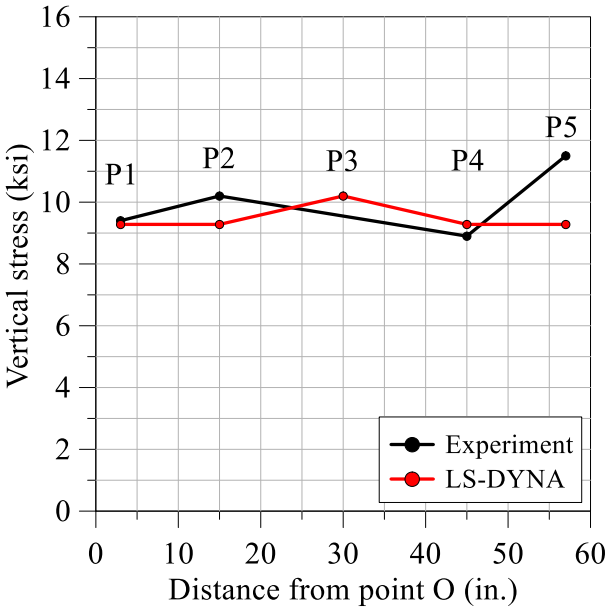

(c) OOP load = 120 kips

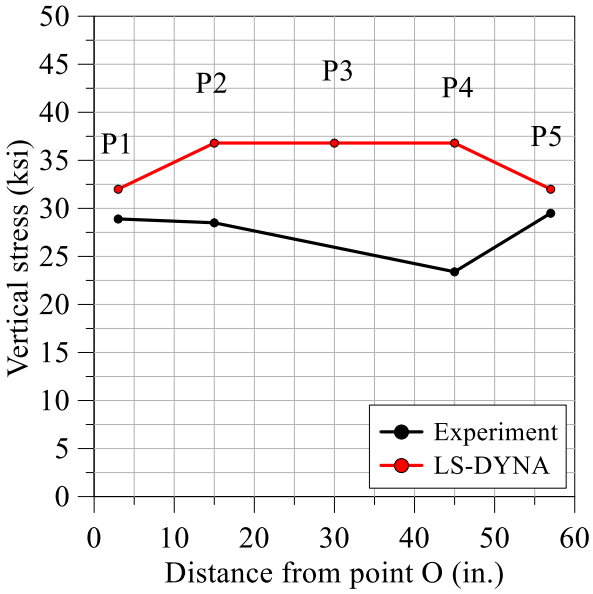

(d) OOP load = 240 kips

Figure 3-23: Distributions of vertical stress in the tension plate, CNSC2

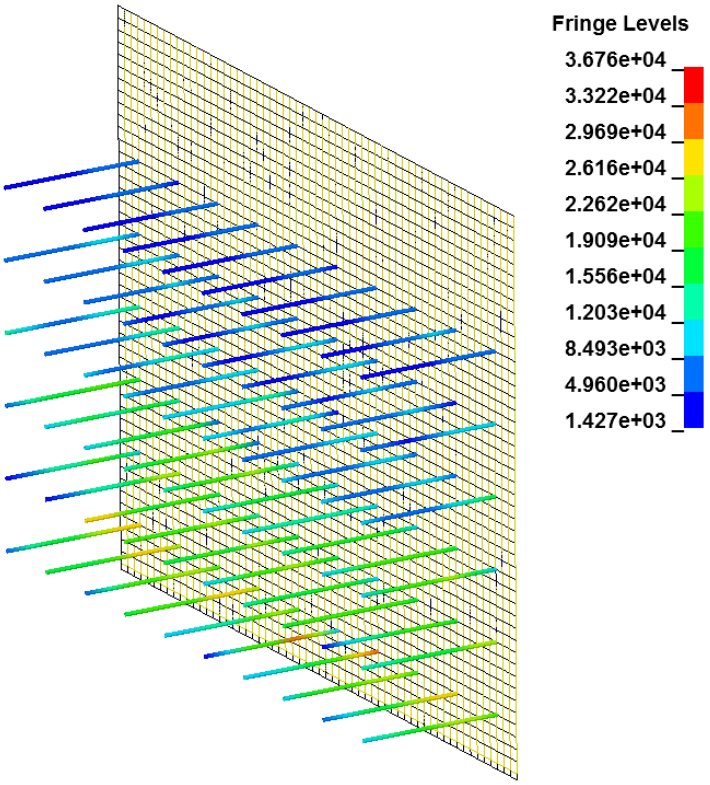

Figure 3-24: Distributions of axial stress in tie bars at instant before IP cyclic loading, CNSC2 (units of psi)

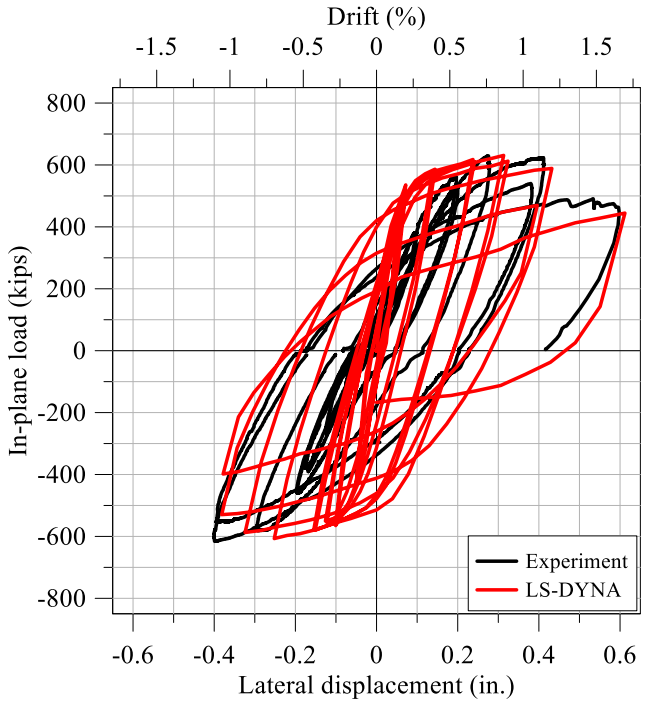

Figure 3-25: IP force-displacement relationship, LS-DYNA and experiment, CNSC2

The calculated equivalent viscous damping ratio, EVD, for the experiment and the numerical simulation are presented in Figure 3-26. The damping ratios predicted using the numerical model are significantly greater than those measured in the experiment. Figure 3-27a and Figure 3-27b present the IP force-displacement relationships for cycles 7 and 9, respectively; cycles 7 and 9 correspond to drift ratios of 0.55% and 0.79%, respectively. The numerical model overpredicts the peak force measured in the experiment in Cycle 7 but the values of the numerically predicted energy dissipation in these cycles are significantly greater than those calculated from the experiment, leading to greater values of EVD.

The measured and predicted damage to CNSC2 are shown in Figure 3-28. Local buckling of the steel faceplates and cracking of the concrete are seen in both the experiment and the simulation. Large concrete strains are predicted and crushing of concrete was observed at the toes of the wall.

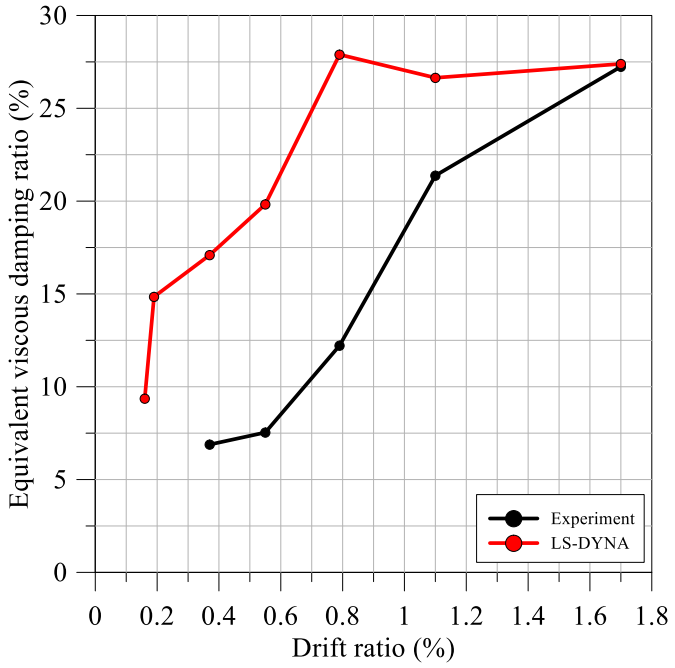

Figure 3-26: Equivalent viscous damping ratio, LS-DYNA and experiment, CNSC2

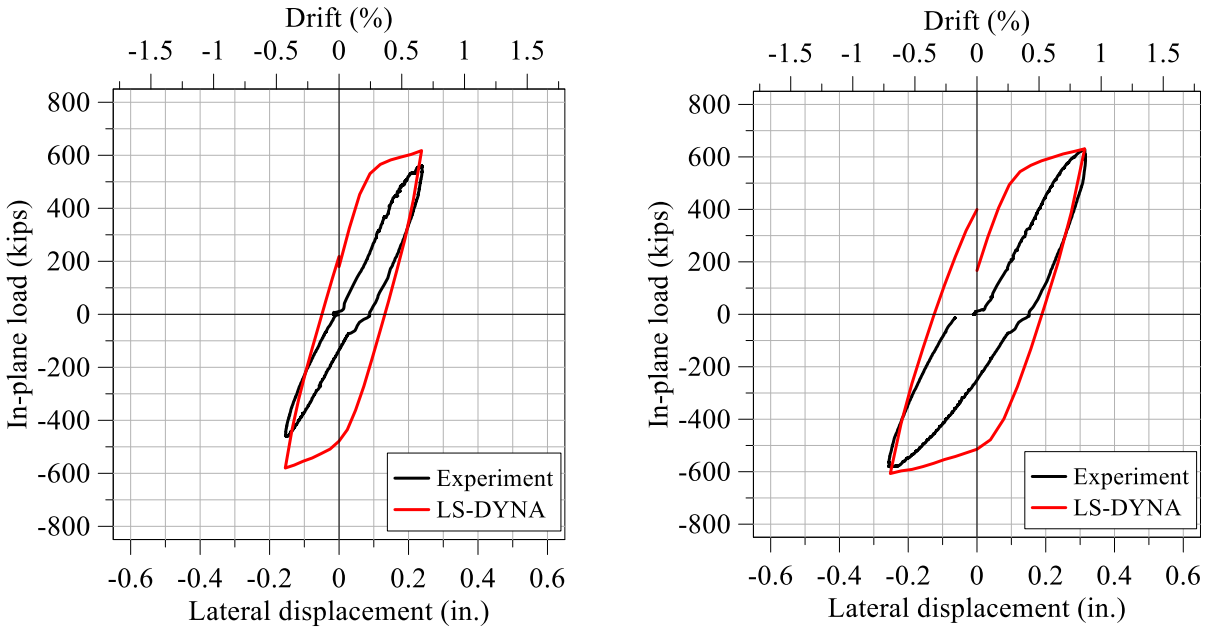

(a) Cycle 7, drift ratio = 0.55% (b) Cycle 9, drift ratio = 0.79%

Figure 3-27: Selected IP force-displacement relationships, LS-DYNA and experiment, CNSC2

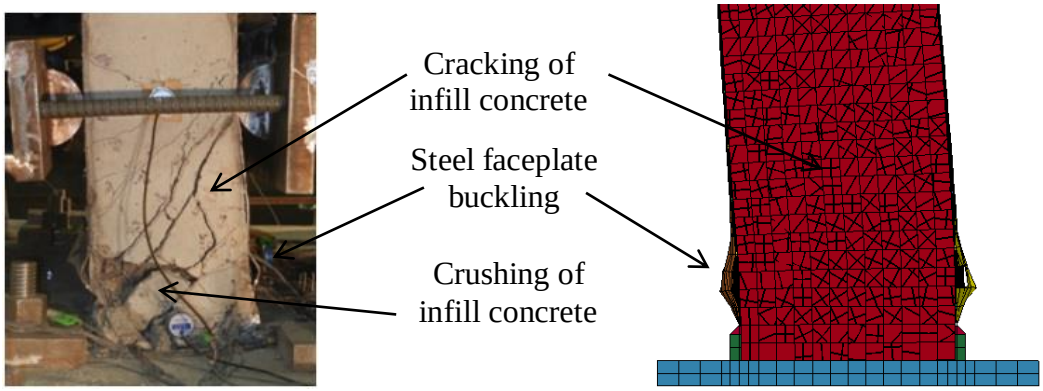

Figure 3-28: Observed and predicted damage to CNSC2

Figure 3-29a and Figure 3-29b show the LS-DYNA-predicted IP cyclic force-displacement relationships for the infill concrete and steel faceplates, respectively. The predicted IP force-displacement relationship of the pier is shown in grey to highlight the contribution of the infill concrete and steel faceplates to the total IP shear resistance. The steel faceplates dominate the behavior of the wall piers in the IP direction. The predicted hysteresis loops for the infill concrete and the steel faceplates are pinched, due to concrete cracking and faceplate buckling, respectively. The components of resistance in LS-DYNA-predicted OOP cyclic force history are presented in Figure 3-30; the total applied load is also displayed to highlight the contribution of each component to the OOP shear resistance. The infill concrete dominates the behavior in the

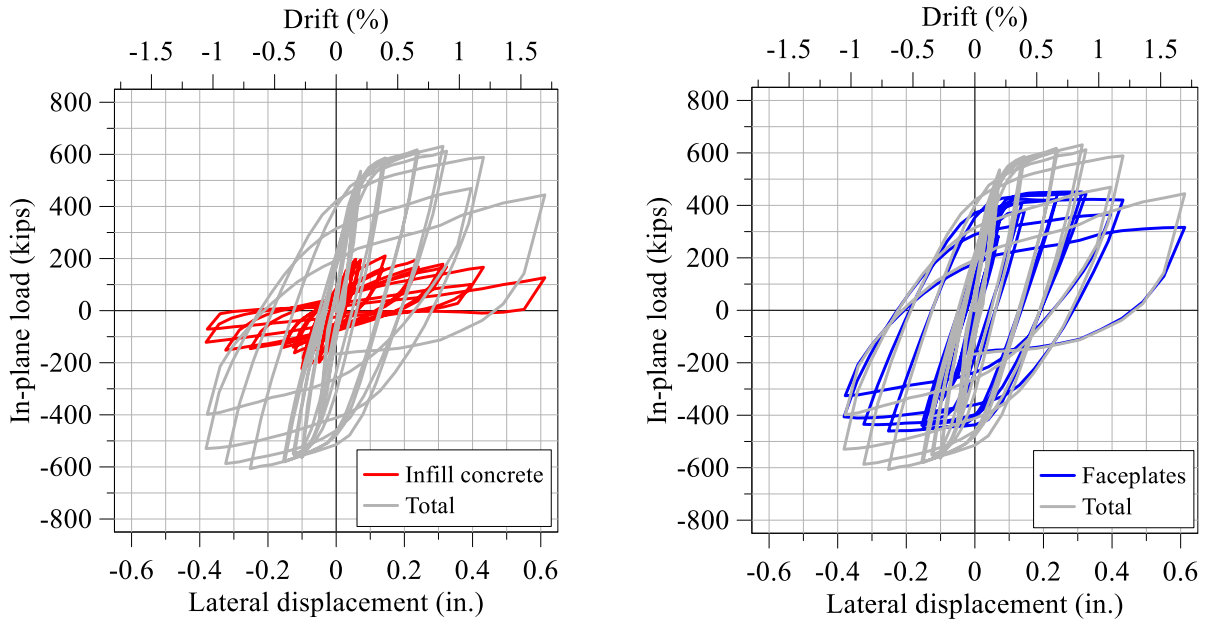

(a) Infill concrete (b) Steel faceplates

Figure 3-29: LS-DYNA-predicted IP cyclic force-displacement relationships, CNSC2

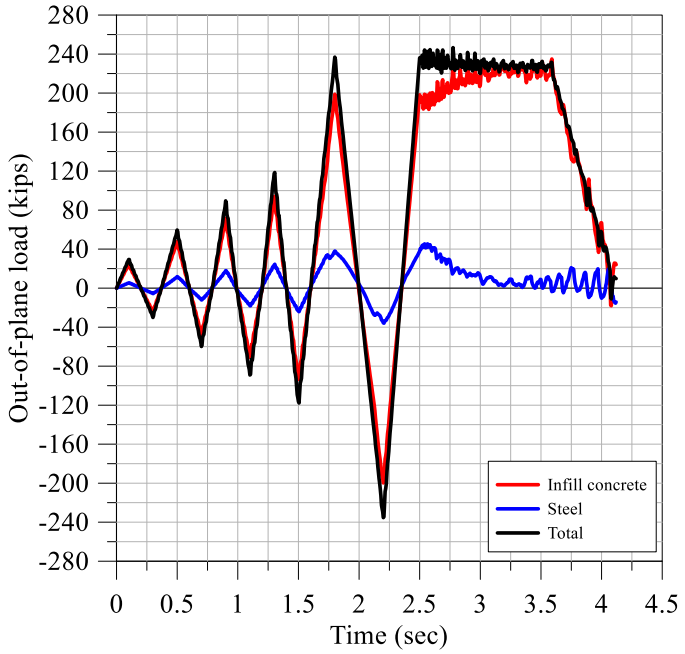

Figure 3-30: LS-DYNA-predicted components of the OOP cyclic force history, CNSC2

OOP direction: an expected result. The linear decay in the numerically applied OOP load in cycles 12 and 13, related to the relaxation of the OOP loading in the experiment, is shown in Figure 3-30.

The IP force-displacement relationship for the experiment and the LS-DYNA simulations with and without applied OOP load are presented in Figure 3-31. The application of the OOP load significantly reduces the IP capacity of the wall piers, although the initial stiffness and rates of reloading/unloading are not significantly affected. The backbone curves for the cyclic loadings of Figure 3-31 are shown in Figure 3-32. The application of the OOP load to the LS-DYNA model reduced the IP capacity by 22%.

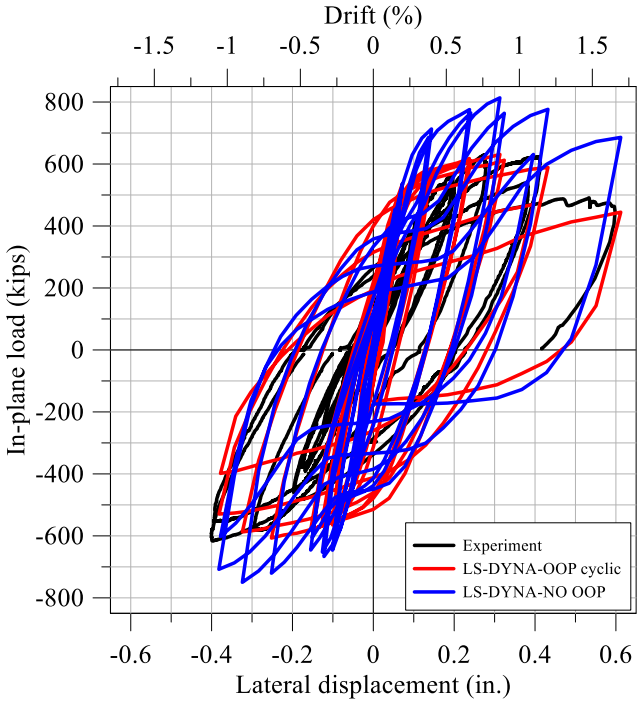

Figure 3-31: IP force-displacement relationships, CNSC2

3.3.3 CNSC3 Simulations

The uniaxial concrete compressive strength on the day of testing of CNSC3 was 5300 psi. The specimen was initially subjected to five cycles of OOP loading, at magnitudes of 50, 100, 150, 200, and 250 kips, respectively, before IP cyclic loading was imposed. The loading protocol used for the experiment and the simulation consisted of seven load steps with two fully reversed cycles per load step and a maximum drift of 0.56%: see Table 2-14.

The OOP force-displacement relationship for the experiment and numerical model are presented in Figure 3-33. Similar to the simulations of CNSC1 and CNSC2, the numerical model is slightly stiffer for OOP loading than that measured in the experiment. The distributions of

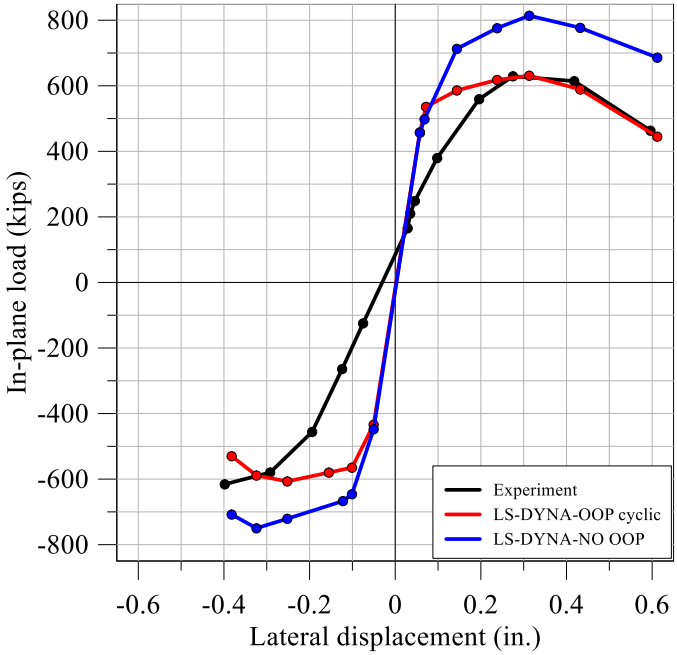

Figure 3-32: Backbone curves, CNSC2

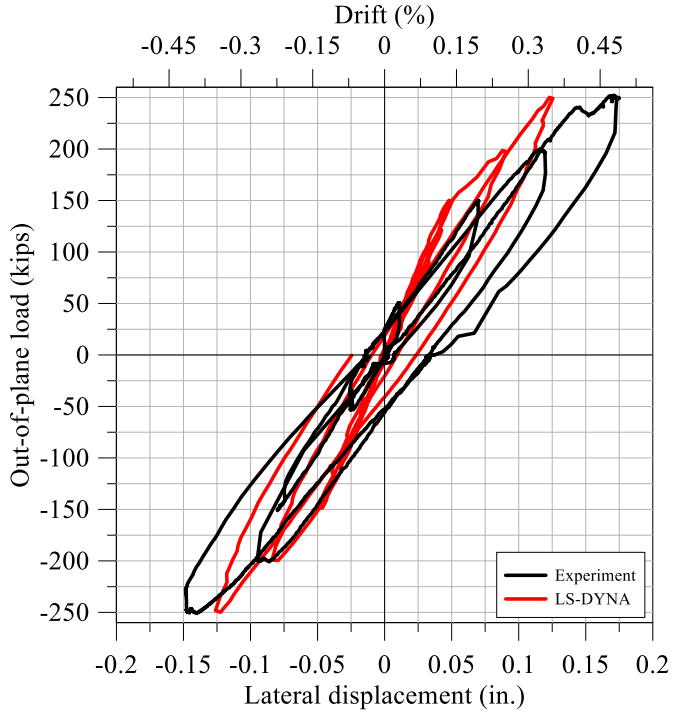

Figure 3-33: OOP force-displacement relationship, LS-DYNA and experiment, CNSC3

vertical stress on the West faceplate (see Figure 3-11) at OOP loads of 50, 150, 200, and 250 kips are presented in Figure 3-34a, Figure 3-34b, Figure 3-34c, and Figure 3-34d, respectively; the data from the cycle with an applied OOP load of 100 kips was lost. The location of points P1 through P5 on the tension faceplate are those described in Sections 1.1.1 and 3.3.2, for CNSC1 and CNSC2, respectively; the strain gage data at point P5 was not reliable and not plotted. The predicted and measured vertical stresses on the tension faceplate are in good agreement.

The distributions of axial stress in the tie bars at the instant before application of IP loading is shown in Figure 3-35; the stresses are shown in units of psi. The magnitude of applied load is 250 kips. The maximum axial stress is approximately 32 ksi, occurring in the bottom row of tie bars near the connection to the faceplate: smaller than the yield stress (=50 ksi).

The simulated and measured IP force-displacement relationships for CNSC3 are presented in Figure 3-36; the numerical model over predicted the peak IP capacity by 12% and did not predict the loss of IP capacity observed in the experiment. In the experiment, failure of CNSC3 was triggered by significant buckling of the steel faceplate at the Northeast corner of the wall and spalling of the infill concrete. The damage to the infill concrete was not predicted using the Winfrith concrete model, which assumes elastic-perfectly plastic behavior in compression. The numerical model predicted buckling of the East steel faceplate and concrete cracking on the North and South faces (seen in Figure 3-37). The Winfrith model enabled the development of large compressive strains in the infill concrete, but not damage in the form of spalling, for which erosion strains (a numerical workaround) would have to be specified. A new material model would be needed to capture this loss of strength at large compressive strains.

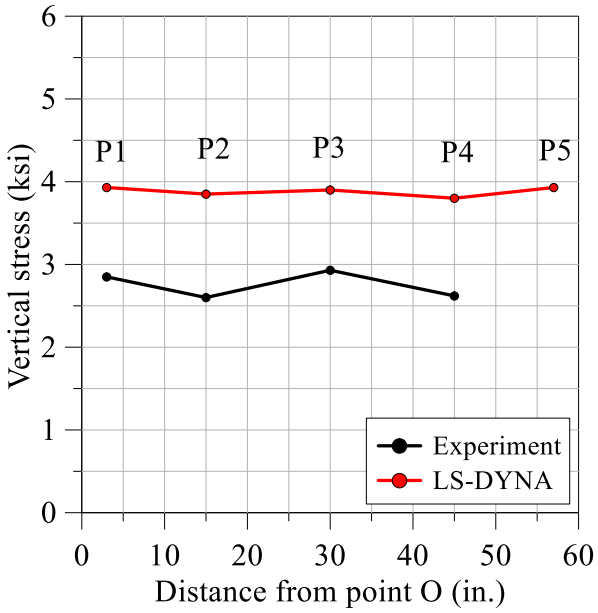

(a) OOP load = 50 kips

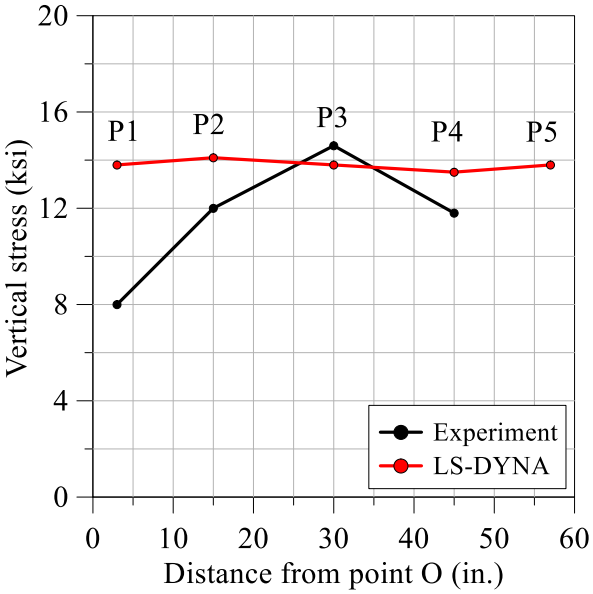

(b) OOP load = 150 kips

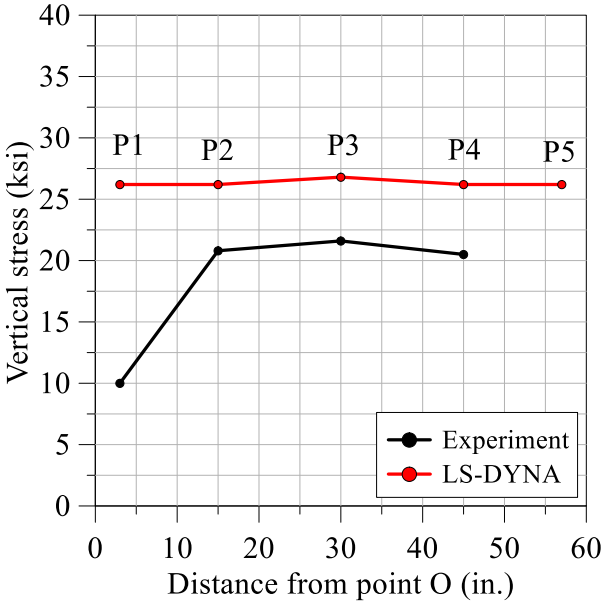

(c) OOP load = 200 kips

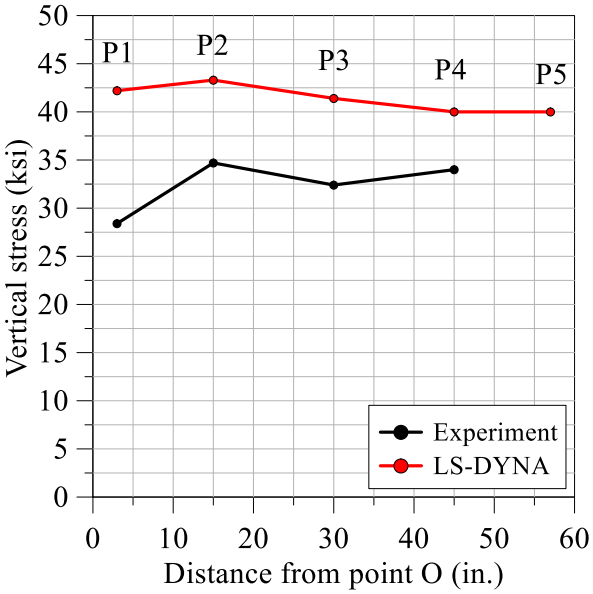

(d) OOP load = 250 kips

Figure 3-34: Distributions of vertical stress in the tension plate, CNSC3

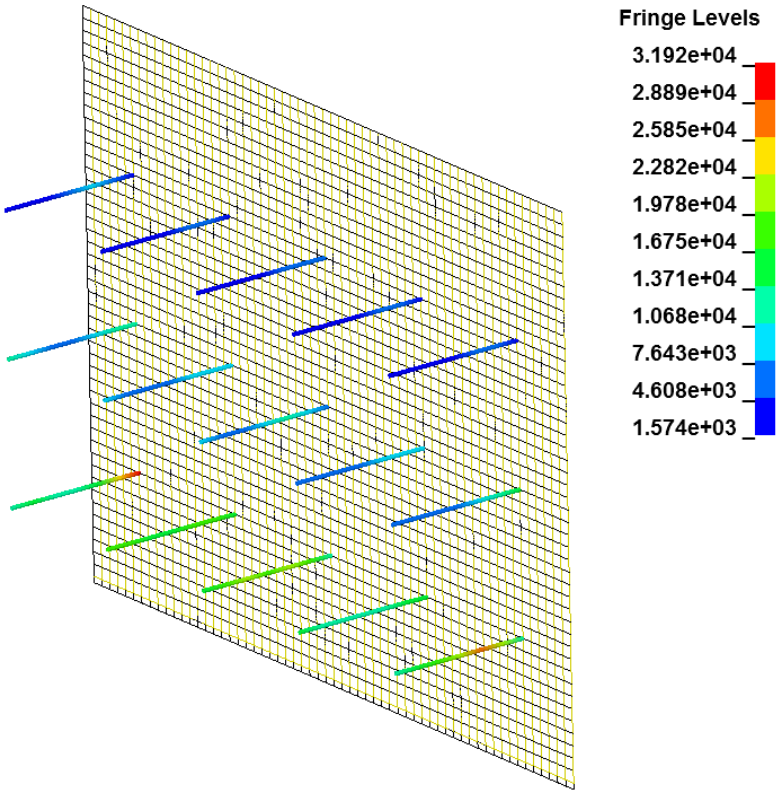

Figure 3-35: Distributions of axial stress in tie bars at instant before IP cyclic loading, CNSC3 (units of psi)

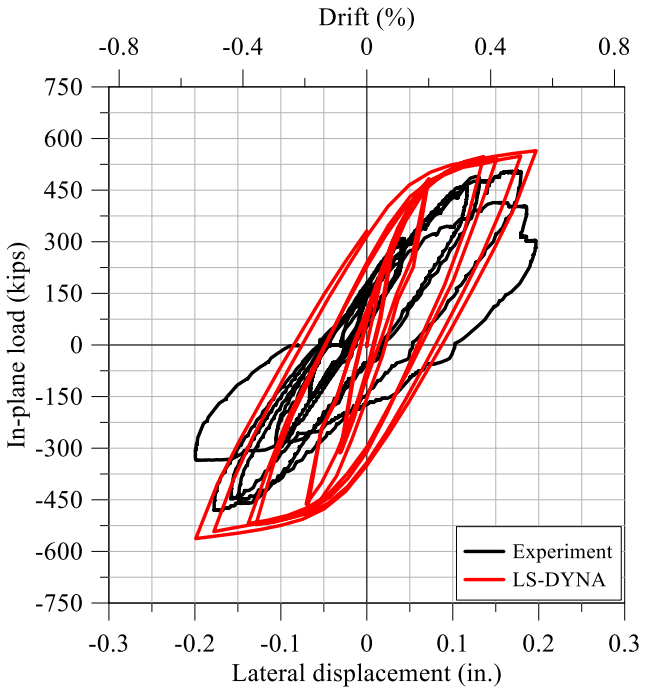

Figure 3-36: IP force-displacement relationship, LS-DYNA and experiment, CNSC3

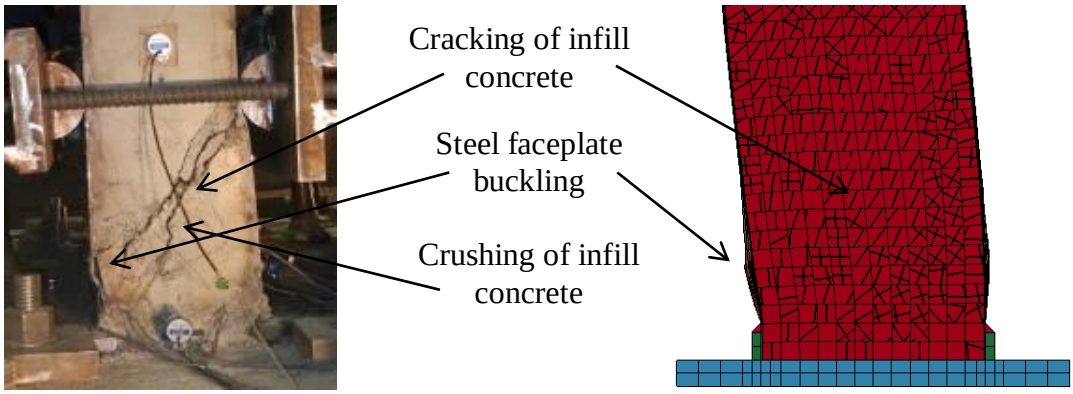

Figure 3-37: Observed and predicted damage to CNSC3

The equivalent viscous damping ratios, EVD, for the experiment and the numerical simulation are presented in Figure 3-38; the predicted values of damping are greater than those back-calculated from the experimental data because the energy dissipated per loop are greater. The IP force-displacement relationships for cycles 6 and 7, which correspond to drift ratios of 0.39% and 0.51%, are presented in Figure 3-39a and Figure 3-39b, respectively.

The predicted and measured equivalent viscous damping ratios are in relatively good agreement at a drift ratio of 0.56% (seen in Figure 3-38). The measured and predicted IP force-displacement relationships for cycle 8, corresponding to a drift ratio of 0.56%, are presented in Figure 3-40.

The damping ratios are similar because the energy dissipated per cycle and strain energy are both proportionally greater in the experiment.

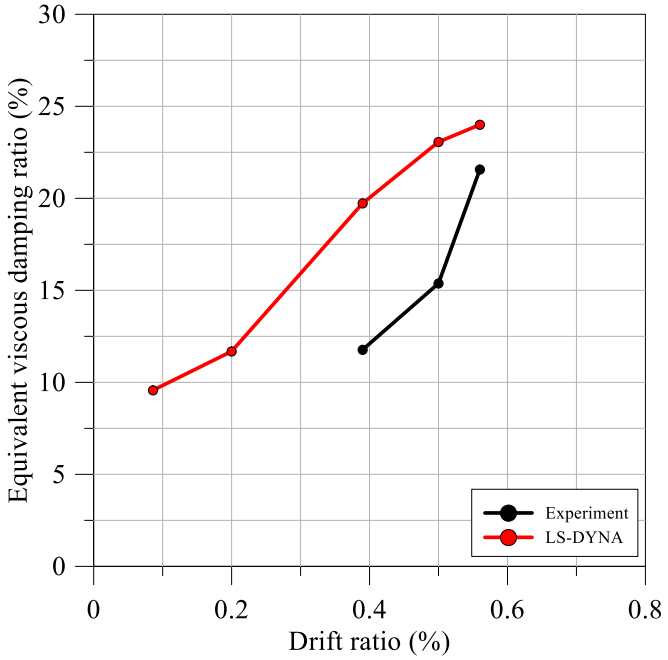

Figure 3-38: Equivalent viscous damping ratio, LS-DYNA and experiment, CNSC3

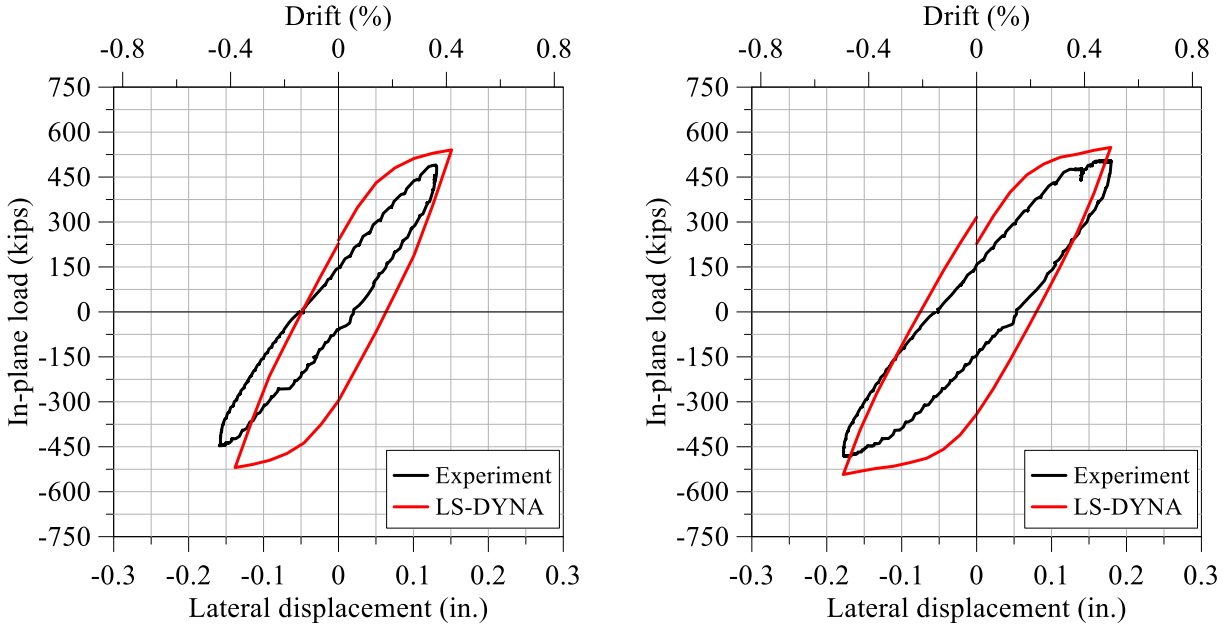

(a) Cycle 6, drift ratio = 0.39% (b) Cycle 7, drift ratio = 0.51%

Figure 3-39: Selected IP force-displacement relationships, LS-DYNA and experiment, CNSC3

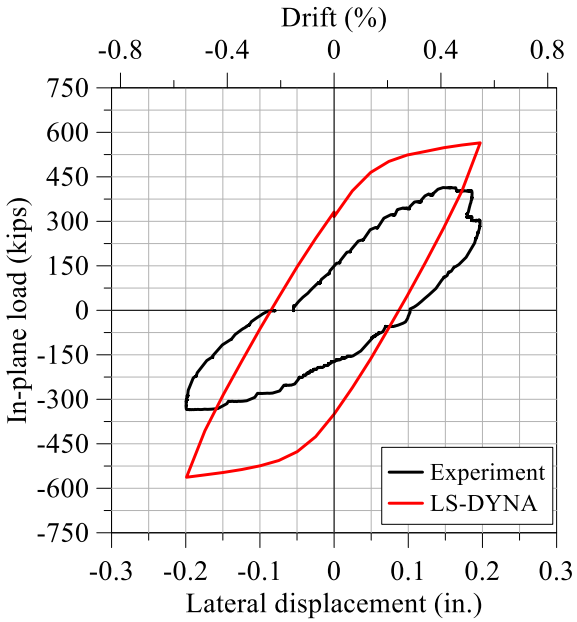

Figure 3-40: IP force-displacement relationship, cycle 8, drift ratio = 0.56%, LS-DYNA and experiment, CNSC3

Figure 3-41a and Figure 3-41b show the LS-DYNA-predicted IP cyclic force-displacement relationship of the infill concrete and steel faceplates, respectively. The predicted IP force-displacement relationship of the pier is shown in grey to highlight the contribution of the infill concrete and steel faceplates to the total IP shear resistance. Pinching of the hysteresis loops for the concrete and the steel faceplates in the simulations is minimal. The LS-DYNA-predicted OOP cyclic force history is presented in Figure 3-42; the infill concrete dominated the OOP behavior of the SC walls, as expected.

Figure 3-43 shows the IP force-displacement relationship for the experiment, and the LS-DYNA simulations with and without the applied OOP load. The corresponding backbone curves are presented in Figure 3-44. The application of OOP load reduces the IP capacity of the numerical model by 22%.

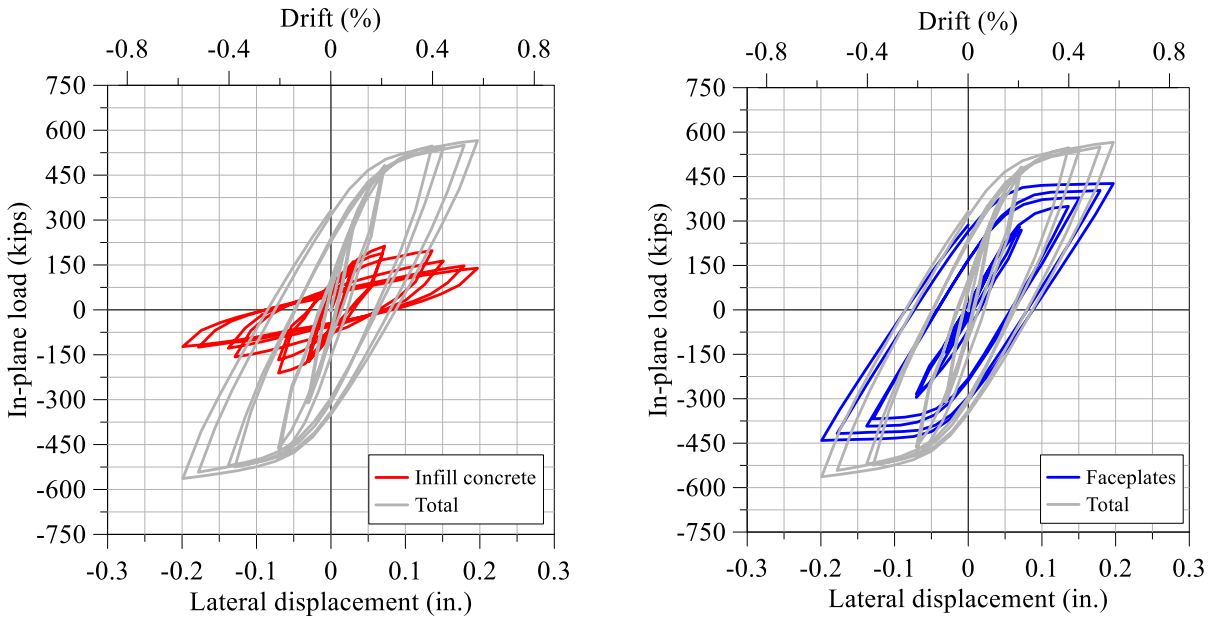

(a) Infill concrete (b) Steel faceplates

Figure 3-41: LS-DYNA-predicted IP cyclic force-displacement relationships, CNSC3

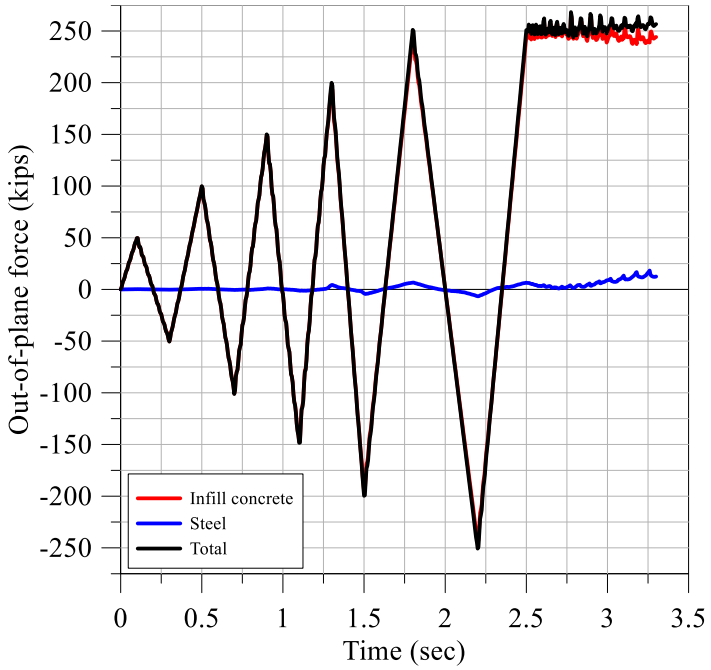

Figure 3-42: LS-DYNA-predicted components of the OOP cyclic force history, CNSC3

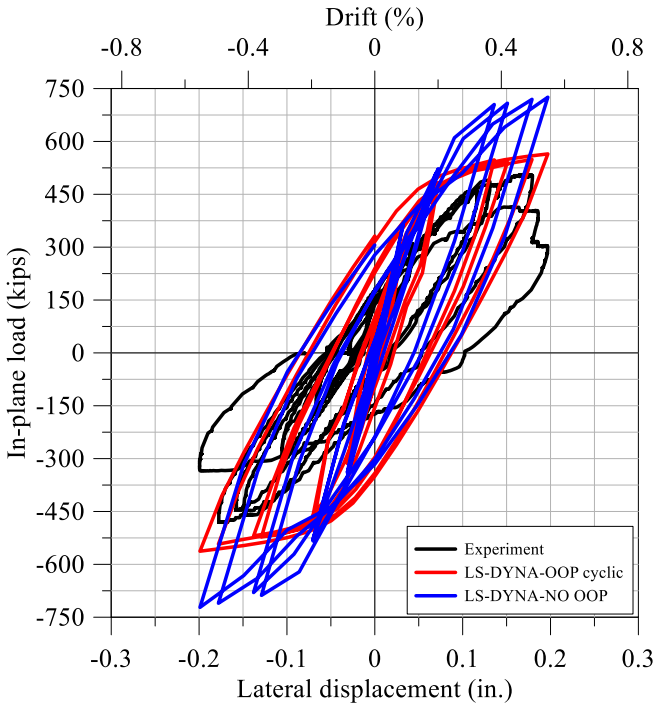

Figure 3-43: IP force displacement relationships, CNSC3

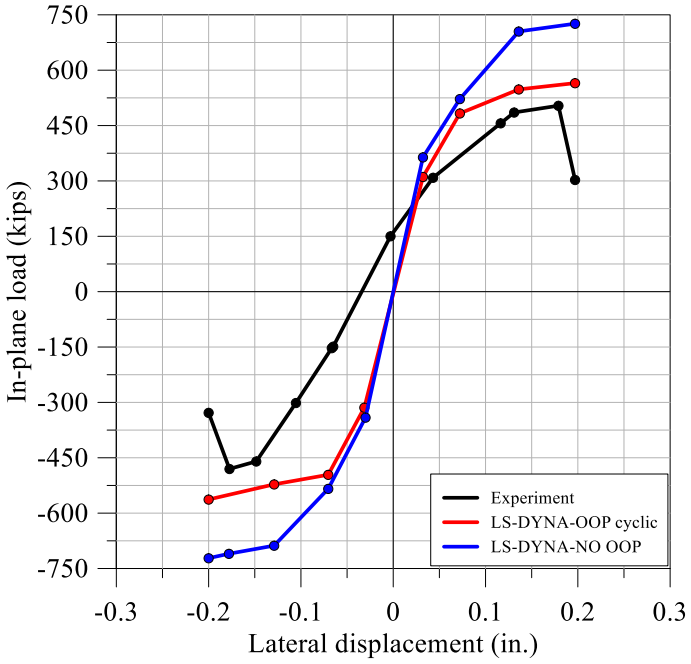

Figure 3-44: Backbone curves, CNSC3

3.3.4 Summary and Conclusions

The physical tests of CNSC1, CNSC2, and CNSC3, as described in Chapter 2, were simulated using the general-purpose finite element program LS-DYNA. Numerical models developed by Epackachi et al. (2014b; 2015) that were validated for the prediction of the IP response of SC wall piers were utilized as a starting point for this study. Predictions of the numerical models were compared with the measurements from experiments at both global and local levels, including cyclic force-displacement relationships (in-plane and out-of-plane), equivalent viscous damping ratios, vertical stresses in the steel faceplates induced by OOP load, and observed damage (e.g., cracking of the infill concrete and buckling of steel faceplates).

The numerical predictions for CNSC1 and CNSC2 agreed reasonably well with measurements from the experiments. The predicted IP stiffness of CNSC1 and CNSC2 were both significantly greater than those observed in the experiment because the foundation (and its flexibility) was not considered in the numerical models; the predicted values of OOP stiffness agreed reasonably well with those measured in the experiments. The predicted distributions of vertical stress on the tension faceplate (under OOP loading) at different levels of OOP load were similar to those measured in the experiments. The predictions of peak IP shear resistance, post-peak strength reduction, and rate of reloading/unloading stiffness for peak and post-peak IP strength cycles agreed reasonably well with the experimental results, with the best results for CNSC1, for which the OOP loading (and average shear stress) were the smallest of the three tests. The predicted values of EVD for IP response were greater than those calculated from the experimental data because the numerically predicted hysteresis loops were wider (more energy dissipated per cycle). The damage predicted using the numerical models (i.e., cracking of infill concrete and buckling of steel faceplates) was in good agreement with that observed in the experiments. Crushing and spalling of concrete, indicated by large compressive strains in the numerical models, could not be captured explicitly because the Winfrith model assumes elastic-perfectly-plastic behavior in compression. Erosion, as a numerical workaround was not implemented. Load distribution between the steel faceplates and the infill concrete in the IP and OOP directions was also investigated using the numerical model; the steel faceplates and the infill concrete dominate the behavior of the SC wall in the IP and OOP directions, respectively.

The predicted response of CNSC3 overestimated the measured peak strength by approximately 12%. The numerical model did not recover the loss of post-peak strength and stiffness calculated from the experimental data, which was likely due to the inability of the Winfrith model, in the absence of a calibrated erosion strain, to simulate loss of material. Under IP loading, the steel faceplates dictate seismic performance. Under OOP loading, the infill concrete dictates seismic response. Because the Winfrith model is unable to directly address loss of material, physical damage to the concrete under OOP loading (e.g., spalling), which should affect the IP behavior, including loss of strength and stiffness, cannot be captured directly.

This limitation of the numerical model will be accommodated in the parametric study presented in Chapter 4 by investigating the IP behavior of SC wall piers subjected to OOP shear stresses less than a threshold limit taken equal to the shear strength of concrete per ACI 318-14 (ACI, 2014). If the applied OOP shear stress exceeds the shear strength of the concrete and a sufficient number of tie bars are not available to mitigate crack growth, the IP response predicted using LS-DYNA will not be reliable. Concrete erosion could be used as a numerical workaround, but the chosen value of erosion strain requires calibration for which the authors have no data bar that for CNSC3. An updated numerical model may be able to address this issue but the development of such a model is far beyond the scope of this project.

The parametric study presented in Chapter 4 is used to develop a relationship between the level of applied OOP shear stress and the IP capacity of SC wall piers. The results of the parametric study, combined with the results of the CNSC experiments, are used to provide technical guidance on the analysis and design of SC wall piers subjected to combined IP and OOP loading.

SECTION 4
DEVELOPING DESIGN GUIDANCE FOR SC WALLS THROUGH PARAMETRIC STUDIES

4.1 Introduction

A parametric study was conducted using the numerical model of Chapter 3 to investigate the effect of OOP loading (magnitude and location) on the IP response of SC wall piers with different concrete compressive strength and tie bar spacing. Section 4.2 presents the parametric study and key results. Technical guidance for design of SC walls subjected to combined IP and OOP loading is presented in Section 4.3, and is based on the experiments of Chapter 2, the numerical simulations of Chapter 3, and the parametric study of Section 4.2.

4.2 Parametric Study

The simulations conducted in this parametric study are summarized in Table 4-1, where f_c' is the compressive strength, s is the tie bar spacing, d is the depth of the cross section (=12 inches), and a/d is the ratio of shear span to depth. Two values of compressive strength were considered in this study: 3500 and 5000 psi. Three values of a/d were considered for each value of compressive strength: 0.5, 1.5, and 3. The ratio a/d equal to 1.5 and 3 correspond to loading at the middle and top of the wall, respectively. For each value of a/d, three amplitudes of OOP shear stress were considered: $1\sqrt{f_c'}$, $2\sqrt{f_c'}$, and $3\sqrt{f_c'}$. All of these simulations were performed for two values of tie bar spacing: d and $d/2$.

Given the limitations of the Winfrith model described in Section 3.3.4, the SC wall piers in this parametric study were subjected to OOP shear stresses less than the expected shear strength of plain concrete, which is strongly dependent on the ratio of shear span-to-depth of the loaded member. Per Figure 6-13 in Wight (2015), the shear stress (strength) of concrete with a longitudinal reinforcement ratio of 1.5% (assuming one steel faceplate acts as longitudinal reinforcement when the wall is subjected to an OOP bending moment), in the absence of shear reinforcement, is between $2\sqrt{f_c'}$ and $3\sqrt{f_c'}$. (The data in this figure are from tests of shallow beams with a/d generally greater than or equal to 2.0. This range on maximum shear stress is for shallow (relatively thin) specimens, namely, 12 inches and smaller, and the design guidance presented later addresses the issue of wall thickness. Importantly, a/d for the specimens tested as part of this research project was 1.5, for which a greater shear stress at failure is expected.)

The lower end on this range of OOP shear stress, $2\sqrt{f_c'}$, is associated with good predictions of IP response using LS-DYNA: the CNSC1 simulations in Section 1.1.1 for which the maximum OOP shear stress was $1.96\sqrt{f_c'}$. For CNSC2 (CNSC3), inclined cracking was observed at an OOP load corresponding to a shear stress of $4.33\sqrt{f_c'}$ ($4.92\sqrt{f_c'}$). The predictions of the cyclic IP response of CNSC2 and CNSC3 using LS-DYNA were reasonable but much poorer than for CNSC1. Accordingly, on the basis of these observations, the maximum shear stress associated with OOP loading was limited to $3\sqrt{f_c'}$ for the parametric studies in order to have confidence in the numerical predictions.

Figure 4-1a, Figure 4-2a and Figure 4-3a present the cyclic IP force-displacement relationships of SC walls subjected to OOP loads associated with shear stresses of $1\sqrt{f_c'}$, $2\sqrt{f_c'}$, and $3\sqrt{f_c'}$ with a tie bar spacing of d, for a/d equal to 0.5, 1.5, and 3, respectively. The corresponding backbone curves for these simulations are presented in Figure 4-1b, Figure 4-2b and Figure 4-3b, respectively. The walls have a concrete compressive strength of 3500 psi and a tie bar spacing of 12 inches. The peak IP lateral loads of these nine SC walls are presented in Table 4-1: simulations 2 to 10. The peak lateral capacity of SC walls subjected to an OOP shear stress of $1\sqrt{f_c'}$, $2\sqrt{f_c'}$, and $3\sqrt{f_c'}$ for a/d equal to 0.5 (1.5) [3] reduced by 1 (2) [4]%, 5 (8) [16]%, and 11 (17) [29]%, respectively, from the IP strength with no applied OOP shear stress (=729 kips). The results of the simulations show that the magnitude and location of the OOP load have a significant effect on the IP capacity of the SC walls. The reductions in IP strength become more evident as the magnitude of the OOP load and the height of its application above the foundation are increased, which leads to larger bending moments and higher longitudinal stresses in the faceplates. Since the IP behavior of the SC walls is governed by the steel faceplates, additional stresses induced by the OOP load, of the amplitude considered here, reduce the IP capacity of the wall pier. The OOP load, of the amplitude considered here, does not have a significant effect on the initial stiffness, pinching, and rate of reloading/unloading of SC walls, as observed in Figure 4-1a, Figure 4-2a and Figure 4-3a.

Table 4-1: Summary of LS-DYNA simulations

Simulation	f_c' (psi)	Tie bar spacing, s (in.)	a / d	OOP Load	OOP load (kips)	IP capacity (kips)	% reduction in IP capacity
1	3500	d	-	0	-	729	-
2	3500	d	0.5	$1\sqrt{f_c'}$	43	720	1
3	3500	d	0.5	$2\sqrt{f_c'}$	85	690	5
4	3500	d	0.5	$3\sqrt{f_c'}$	128	651	11
5	3500	d	1.5	$1\sqrt{f_c'}$	43	712	2
6	3500	d	1.5	$2\sqrt{f_c'}$	85	671	8
7	3500	d	1.5	$3\sqrt{f_c'}$	128	607	17
8	3500	d	3	$1\sqrt{f_c'}$	43	698	4
9	3500	d	3	$2\sqrt{f_c'}$	85	613	16
10	3500	d	3	$3\sqrt{f_c'}$	128	520	29
11	3500	d / 2	-	0	-	759	-
12	3500	d / 2	0.5	$1\sqrt{f_c'}$	43	751	1
13	3500	d / 2	0.5	$2\sqrt{f_c'}$	85	741	3
14	3500	d / 2	0.5	$3\sqrt{f_c'}$	128	721	5
15	3500	d / 2	1.5	$1\sqrt{f_c'}$	43	745	2
16	3500	d / 2	1.5	$2\sqrt{f_c'}$	85	695	8
17	3500	d / 2	1.5	$3\sqrt{f_c'}$	128	645	15
18	3500	d / 2	3	$1\sqrt{f_c'}$	43	724	5
19	3500	d / 2	3	$2\sqrt{f_c'}$	85	646	15
20	3500	d / 2	3	$3\sqrt{f_c'}$	128	583	23
21	5000	d	-	0	-	765	-
22	5000	d	0.5	$1\sqrt{f_c'}$	51	753	2
23	5000	d	0.5	$2\sqrt{f_c'}$	102	723	6
24	5000	d	0.5	$3\sqrt{f_c'}$	153	709	7
25	5000	d	1.5	$1\sqrt{f_c'}$	51	742	3
26	5000	d	1.5	$2\sqrt{f_c'}$	102	704	8
27	5000	d	1.5	$3\sqrt{f_c'}$	153	637	17
28	5000	d	3	$1\sqrt{f_c'}$	51	729	5
29	5000	d	3	$2\sqrt{f_c'}$	102	649	15
30	5000	d	3	$3\sqrt{f_c'}$	153	577	25
31	5000	d / 2	-	0	-	793	-
32	5000	d / 2	0.5	$1\sqrt{f_c'}$	51	789	0.5

Table 4-1: Summary of LS-DYNA simulations (contd.)

33	5000	$d/2$	0.5	$2\sqrt{f_c'}$	102	770	3
34	5000	$d/2$	0.5	$3\sqrt{f_c'}$	153	763	4
35	5000	$d/2$	1.5	$1\sqrt{f_c'}$	51	785	1
36	5000	$d/2$	1.5	$2\sqrt{f_c'}$	102	744	6
37	5000	$d/2$	1.5	$3\sqrt{f_c'}$	153	697	12
38	5000	$d/2$	3	$1\sqrt{f_c'}$	51	763	4
39	5000	$d/2$	3	$2\sqrt{f_c'}$	102	700	12
40	5000	$d/2$	3	$3\sqrt{f_c'}$	153	637	20

To investigate the effect of OOP loading on the IP lateral capacity of SC walls with tie bar spacing smaller than d, the LS-DYNA models used in simulations 2 to 10 were revised with a tie bar spacing of $d/2$ (=6 inches). The IP force-displacement relationships for OOP shear stresses of $1\sqrt{f_c'}$, $2\sqrt{f_c'}$, and $3\sqrt{f_c'}$ for a/d equal to 0.5, 1.5, and 3 are presented in Figure 4-4a, Figure 4-5a, and Figure 4-6a, respectively: the peak IP strengths are presented in Table 4-1 through simulations 12 to 20. The corresponding backbone curves for these simulations are shown in Figure 4-4b, Figure 4-5b, and Figure 4-6b, respectively. The IP capacity is reduced by 23% for an OOP shear stress of $3\sqrt{f_c'}$ and a/d of 3 with respect to the IP strength with no OOP load (=759 kips); the reduction in IP capacity is slightly less than that observed for a tie bar spacing of d and an OOP shear stress of $3\sqrt{f_c'}$ and a/d of 3 (=29 %) (simulation 10).

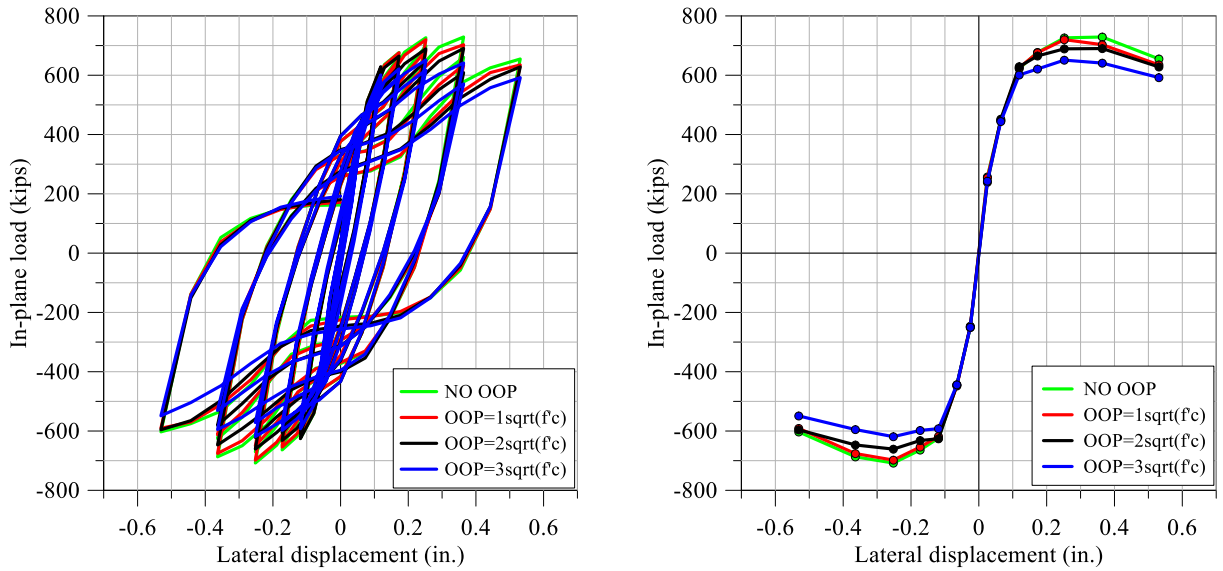

(a) IP force-displacement relationship (b) Backbone curves

Figure 4-1: IP behavior of SC walls, $a/d = 0.5$, $f_c' = 3500$ psi, $s = d$

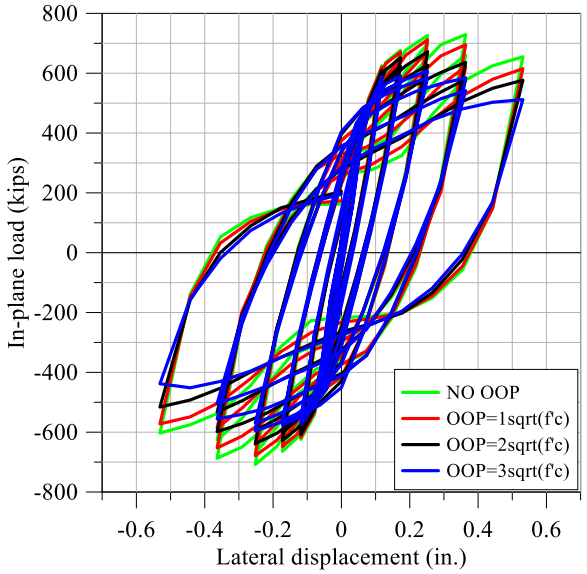

(a) IP force-displacement relationship

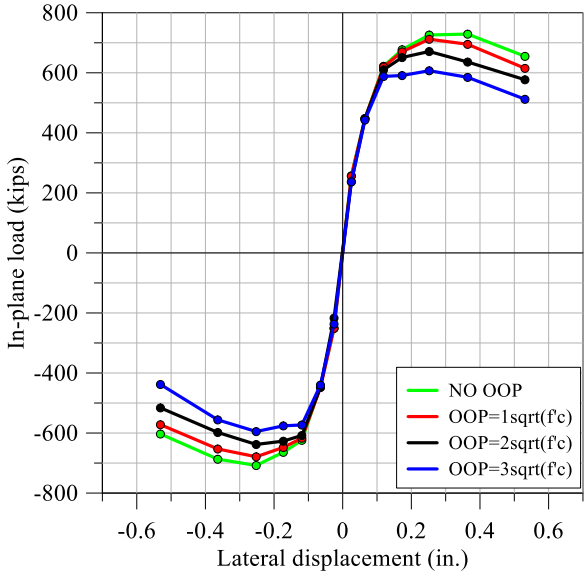

(b) Backbone curves

Figure 4-2: IP behavior of SC walls, $a/d = 1.5$, $f_c' = 3500$ psi, $s = d$

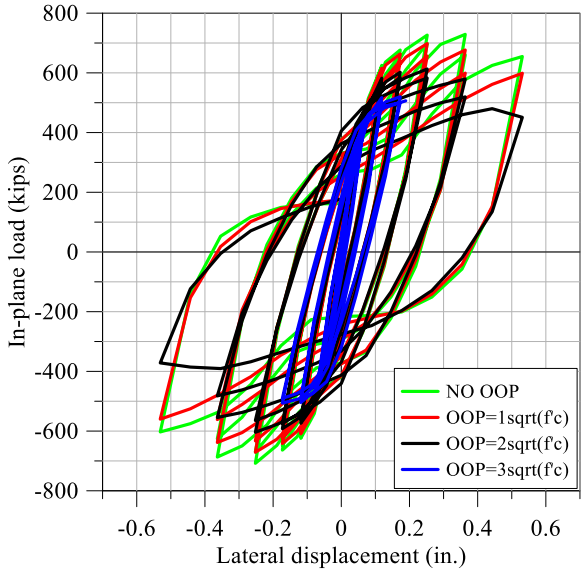

(a) IP force-displacement relationship

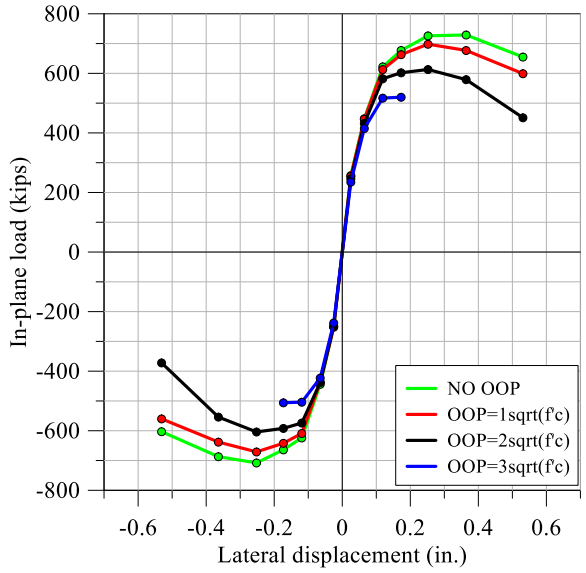

(b) Backbone curves

Figure 4-3: IP behavior of SC walls, $a/d = 3$, $f_c' = 3500$ psi, $s = d$

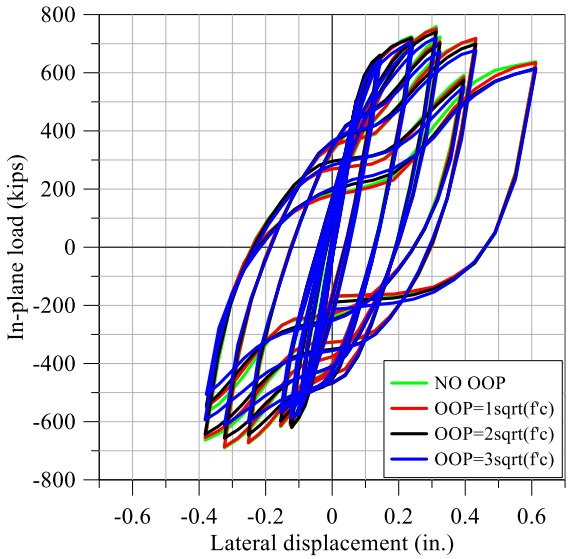

(a) IP force-displacement relationship

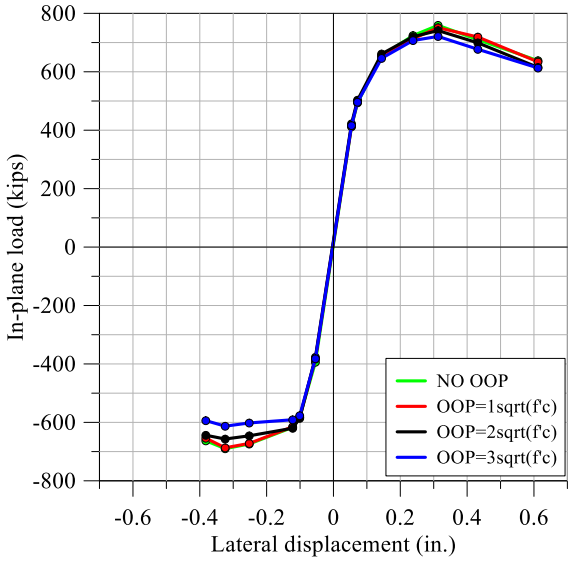

(b) Backbone curves

Figure 4-4: IP behavior of SC walls, $a/d = 0.5$, $f_c' = 3500$ psi, $s = d/2$

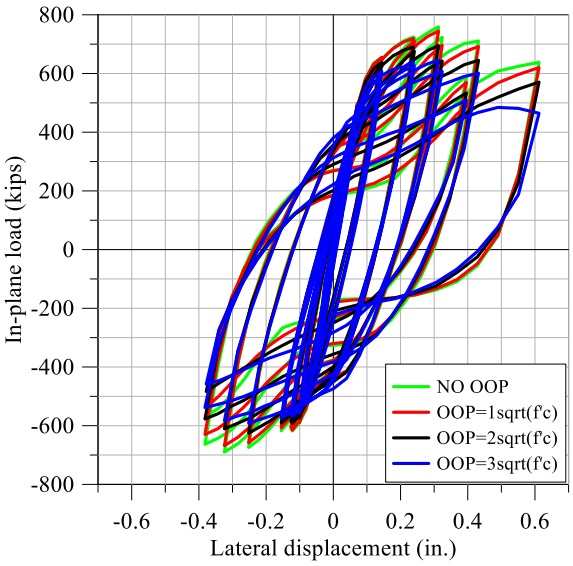

(a) IP force-displacement relationship

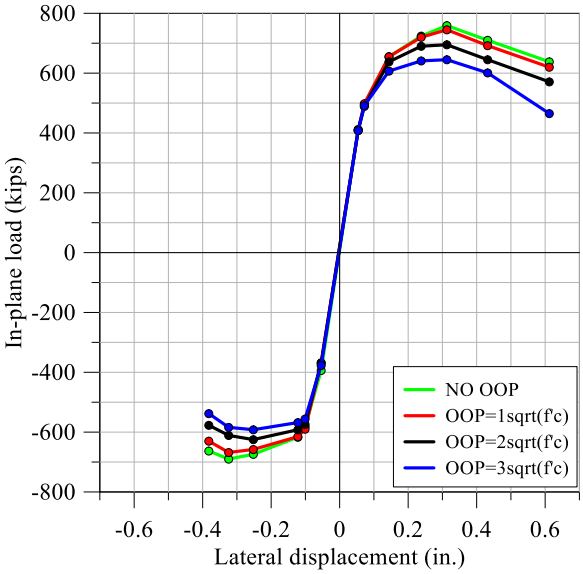

(b) Backbone curves

Figure 4-5: IP behavior of SC walls, $a/d = 1.5$, $f_c' = 3500$ psi, $s = d/2$

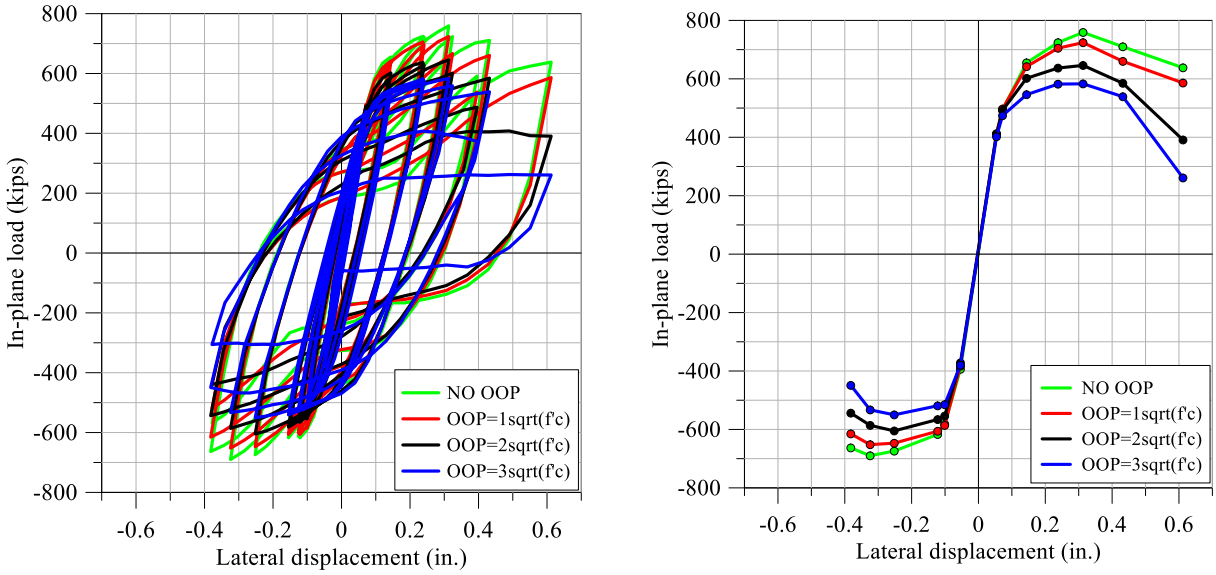

(a) IP force-displacement relationship (b) Backbone curves

Figure 4-6: IP behavior of SC walls, $a/d = 3$, $f_c' = 3500$ psi, $s = d/2$

The LS-DYNA models used in simulations 2 to 10 were repeated with a higher concrete uniaxial compressive strength: 5000 psi. The increase from 3500 psi to 5000 psi increased the IP capacity, in the absence of OOP load, by 5%. The percentage increase in IP strength was expected to be small because the IP behavior is dominated by the steel faceplates.

Figure 4-7a, Figure 4-8a, and Figure 4-9a present the cyclic IP force-displacement relationships of SC walls subjected to OOP shear stresses of $1\sqrt{f_c'}$, $2\sqrt{f_c'}$, and $3\sqrt{f_c'}$ for a/d equal to 0.5, 1.5, and 3, respectively. Figure 4-7b, Figure 4-8b, and Figure 4-9b present the corresponding backbone curves for these simulations, respectively, for a/d of 0.5, 1.5, and 3. The peak IP lateral loads of these nine SC walls are presented in Table 4-1 through simulations 22 to 30. The peak lateral capacity of SC walls subjected to an OOP shear stress of $1\sqrt{f_c'}$, $2\sqrt{f_c'}$, and $3\sqrt{f_c'}$ for a/d equal to 0.5 (1.5) [3] reduced by 2 (3) [5]%, 6 (8) [15]%, and 7 (17) [25]%, respectively, from the IP strength with no OOP load (=765 kips). The percentage reductions in IP capacity are similar to those obtained for 3500 psi concrete (simulations 2 to 10).

Simulations 22 to 30 were repeated with a tie bar spacing of $d/2$. The IP force-displacement relationships for OOP shear stresses of $1\sqrt{f_c'}$, $2\sqrt{f_c'}$, and $3\sqrt{f_c'}$ for a/d equal to 0.5, 1.5, and 3 are presented in Figure 4-10a, Figure 4-11a, Figure 4-12a, respectively. Results are summarized in Table 4-1: simulations 31 to 40. The corresponding backbone curves for a/d values of 0.5, 1.5, and 3 are presented in Figure 4-10b, Figure 4-11b, Figure 4-12b, respectively. The IP

capacity was reduced by 20% for an OOP shear stress of $3\sqrt{f_c'}$ and a/d of 3 (simulation 40) with respect to the IP strength with no OOP load (=793 kips); the reduction in IP capacity is slightly less than that observed for a tie bar spacing of d and an OOP load of $3\sqrt{f_c'}$ and a/d of 3 (simulation 30). As the magnitude and height of application of the OOP load are increased, the reductions in IP capacity are slightly less for a tie bar spacing of $d/2$ compared to that of a tie bar spacing of d; the same trends are observed for concrete compressive strengths of 3500 and 5000 psi.

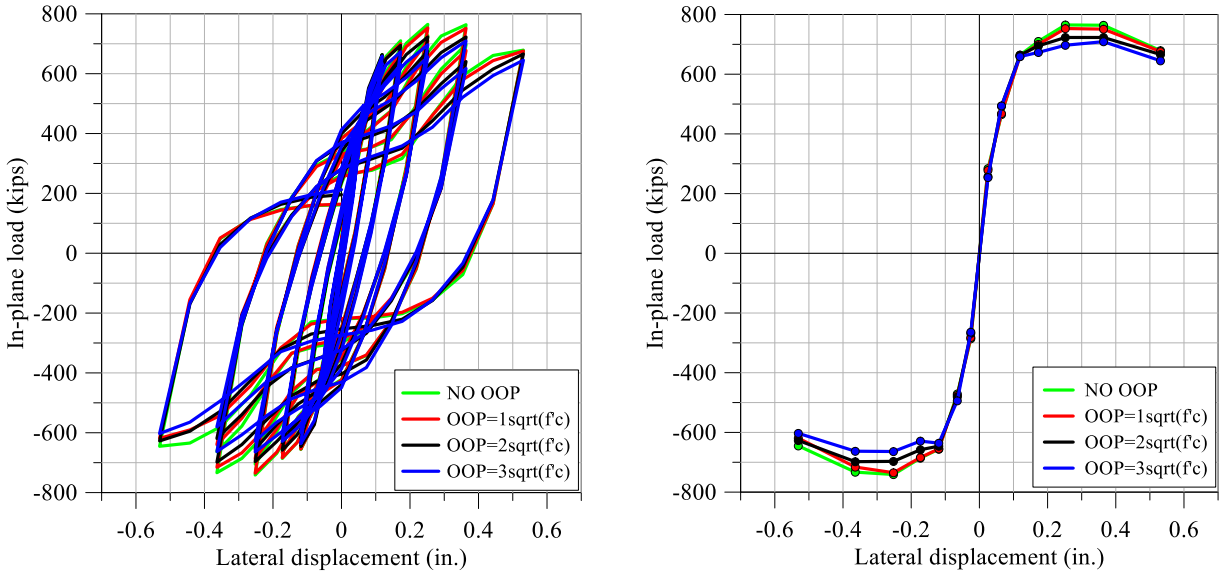

(a) IP force-displacement relationship (b) Backbone curves

Figure 4-7: IP behavior of SC walls, $a/d = 0.5$, $f_c' = 5000$ psi, $s = d$

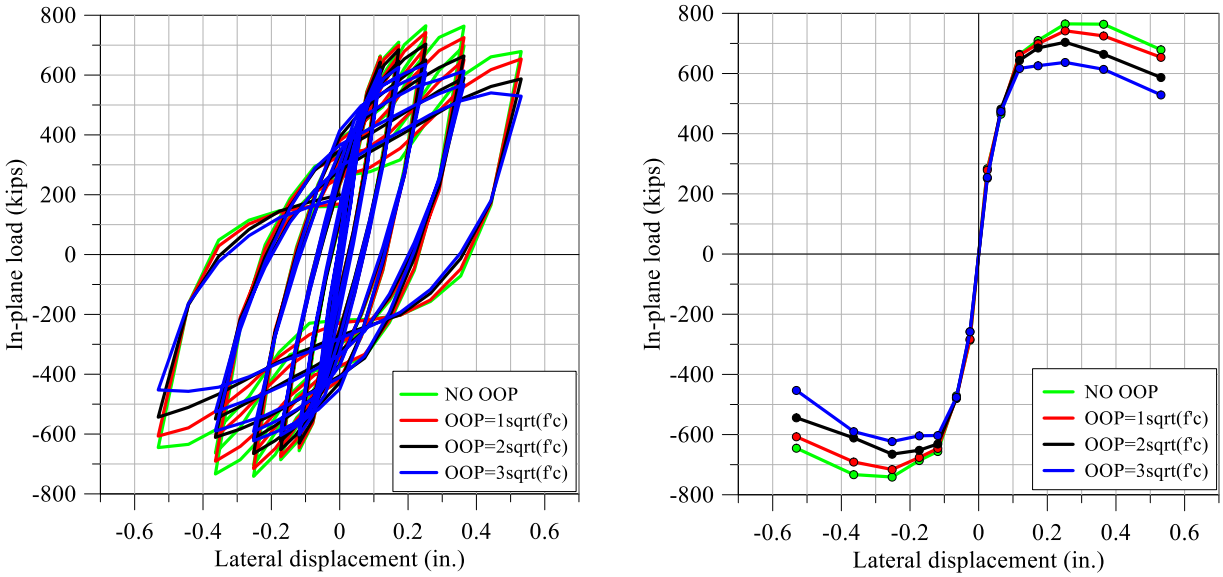

(a) IP force-displacement relationship (b) Backbone curves

Figure 4-8: IP behavior of SC walls, $a/d = 1.5$, $f_c' = 5000$ psi, $s = d$

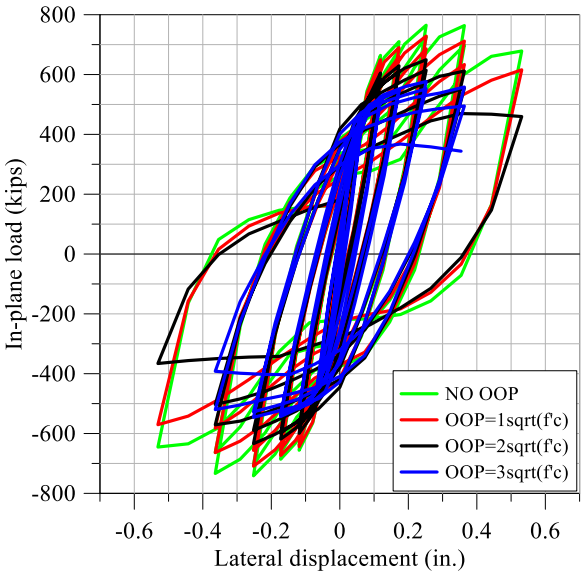

(a) IP force-displacement relationship

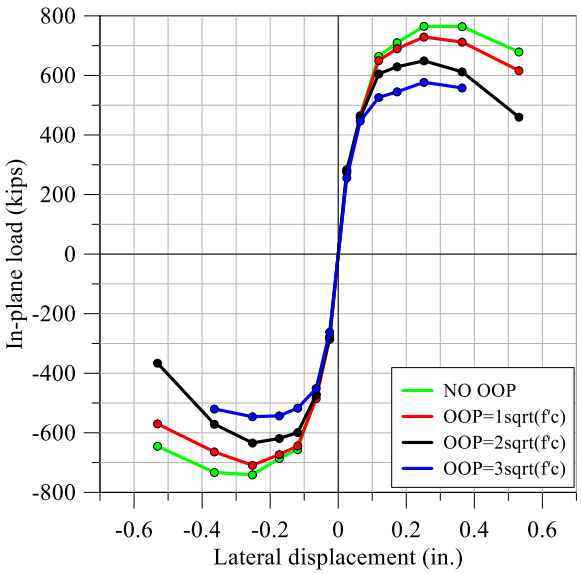

(b) Backbone curves

Figure 4-9: IP behavior of SC walls, $a/d = 3$, $f_c' = 5000$ psi, $s = d$

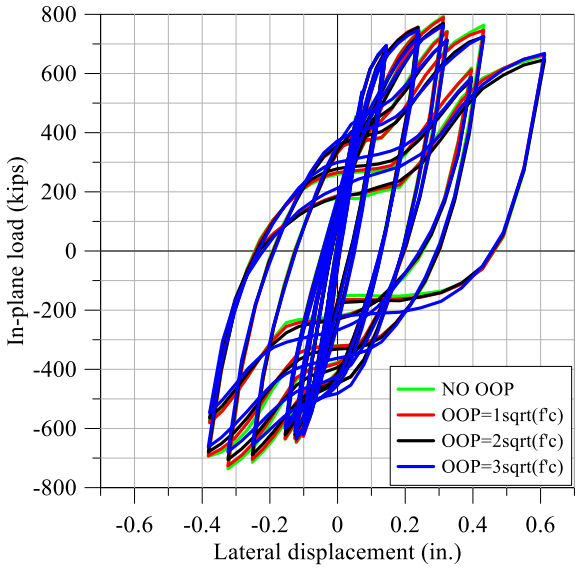

(a) IP force-displacement relationship

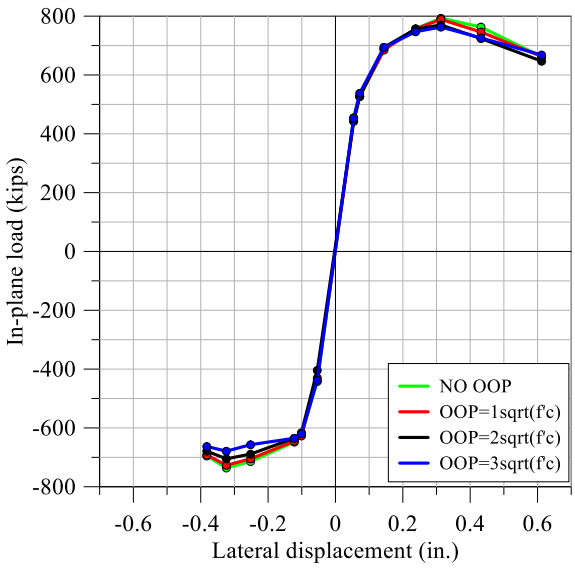

(b) Backbone curves

Figure 4-10: IP behavior of SC walls, $a/d = 0.5$, $f_c' = 5000$ psi, $s = d/2$

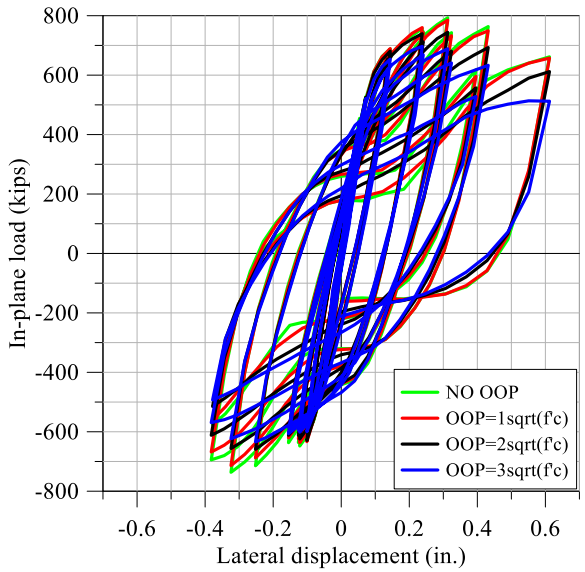

(a) IP force-displacement relationship

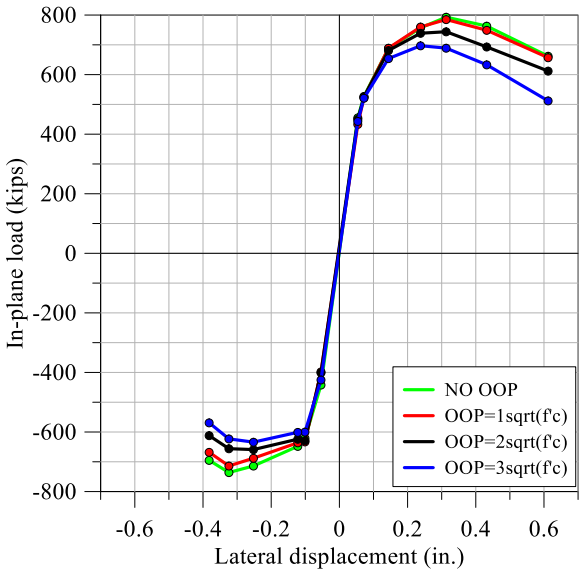

(b) Backbone curves

Figure 4-11: IP behavior of SC walls, $a/d=1.5$, $f_c'=5000$ psi, $s=d/2$

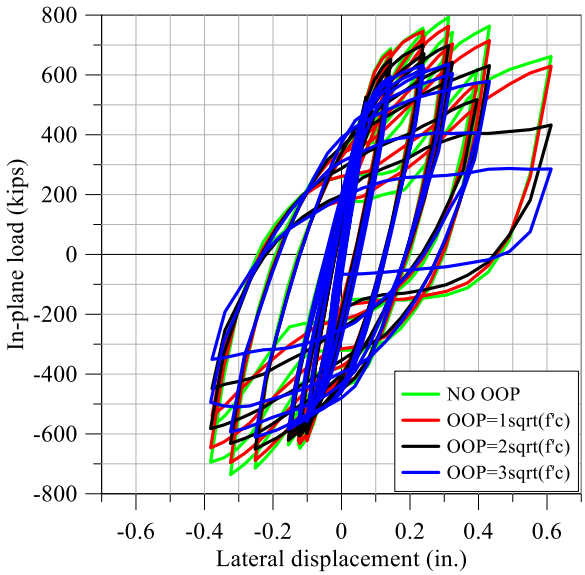

(a) IP force-displacement relationship

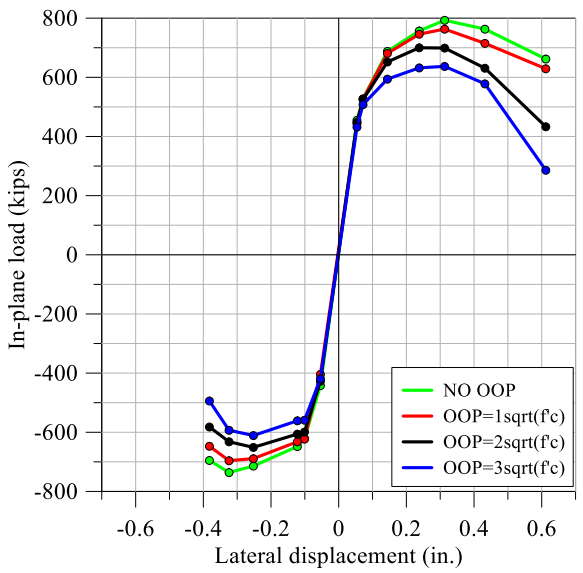

(b) Backbone curves

Figure 4-12: IP behavior of SC walls, $a/d=3$, $f_c'=5000$ psi, $s=d/2$

4.3 Technical Guidance

Technical guidance for design of SC walls subjected to combined IP and OOP loading is provided in this section, and is based on the experiments of Chapter 2, the numerical simulations of Chapter 3, and the parametric study of Section 4.2. The results of the experiments were used to validate the numerical models and provide technical guidance on the displacement ductility capacity of SC wall piers. The parametric studies were used to provide technical guidance on the effects of OOP loading (height and location) on IP capacity.

Figure 4-13 presents the IP force-displacement backbone curves for experiments CNSC1, CNSC2, and CNSC3, normalized by their respective IP capacities, IP_c. The backbone curves for CNSC2 and CNSC3 were shifted to the origin to allow for a direct comparison of their IP performance with that of CNSC1.

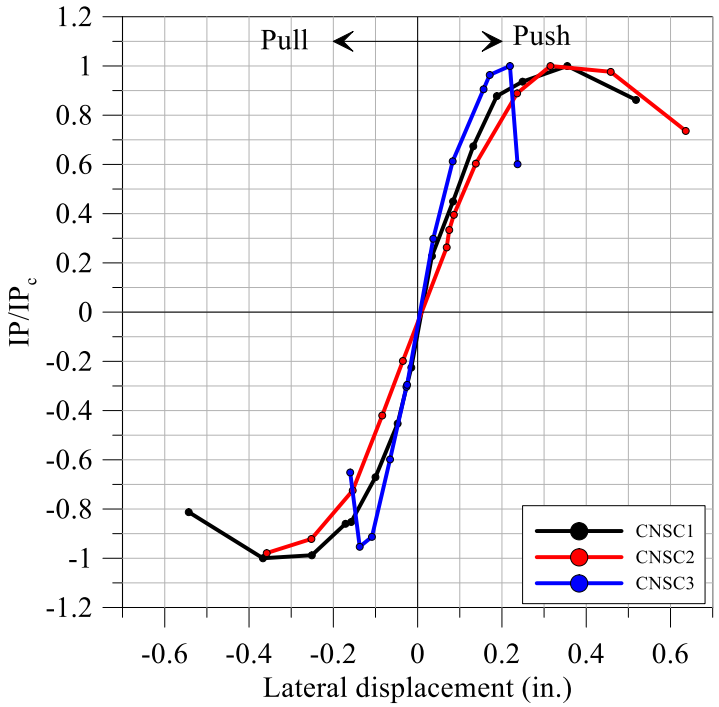

Figure 4-13: Normalized backbone curves, CNSC experiments

With the exception of tie bar spacing and concrete uniaxial compressive strength, the construction of the CNSC specimens was identical. Epackachi et al. (2014a) showed that connector (studs and tie rods) spacing had little effect on IP stiffness at levels of lateral load smaller than the peak value. The uniaxial compressive strengths of the concrete in CNSC1,

CNSC2 and CNSC3, on the first day of testing, were 7700 psi, 5300 psi, and 5300 psi, respectively. Based on these concrete strengths, the initial stiffness of CNSC1 should have been greater than that of both CNSC2 and CNSC3. Per Figure 4-13, the initial stiffness of CNSC1 is greater than that of CNSC2 in both the first and third quadrants: the expected result; but not greater than that of CNSC3: an unexpected result, especially given that CNSC3 was damaged under OOP loading prior to IP loading and CNSC1 was not.

On the basis of the normalized backbone curves of Figure 4-13, it is evident that a) identical wall piers with low OOP shear stress (e.g., CNSC1) are more deformable (ductile) than those with high OOP shear stress (CNSC3), b) the installation of cross ties at spacing $d/2$, where d is the thickness of the wall, results in a more deformable (ductile) SC wall than if the ties are spaced at distance d, and c) high OOP shear stress (and coexisting moment) in an SC wall pier may lead to non-ductile response IP, namely, no IP deformation capacity beyond the displacement associated with peak strength.

Displacement ductility has been a traditional seismic measure of component and system performance. For the three walls tested as part of this project, and assuming a maximum displacement equal to the displacement at which the resistance drops below 80% of the peak value, the maximum ductility of CNSC1 (CNSC2) [CNSC3] is approximately 3 (2) [1].

The peak resistances of CNSC1, CNSC2 and CNSC3 were 735 kips, 629 kips, and 504 kips, respectively. The greater strength of CNSC1 can be attributed in part to a) higher compressive strength (7700 psi versus 5300 psi) for the infill concrete, and b) a relatively low OOP shear stress. A comparison of the peak resistance of CNSC2 and CNSC3 makes clear the importance to IP strength of limiting damage due to OOP shear forces, which can be accomplished in part by the provision of closely spaced cross ties. The only meaningful difference between CNSC2 and CNSC3 was tie bar spacing because the compressive strength of the infill concrete was the same in both specimens and the maximum OOP shear stress was very similar: $4.73\sqrt{f_c'}$ for CNSC2 and $4.92\sqrt{f_c'}$ for CNSC3. In this instance, the provision of closely spaced tie bars (at $d/2$) enabled a much greater peak IP resistance (629 versus 504 kips).

Results from the parametric studies were mined to develop draft guidance for when to consider co-existing OOP shearing forces for IP design of SC wall piers. The relationships between applied OOP shear stress (normalized by $\sqrt{f_c'}$) and the peak IP capacity, IP_{OOP} (normalized by

the IP capacity with no applied OOP load, $IP_{NO\ OOP}$) for a uniaxial concrete compressive strength of 3500 psi and a tie bar spacing of 12 inches are presented in Figure 4-14. The curves are shown for a/d equal to 0.5, 1.5, and 3. A similar plot is shown in Figure 4-15 for a tie bar spacing of 6 inches. As the magnitude of OOP shear stress and the ratio of shear span-to-depth increase, larger longitudinal stresses develop in the steel faceplates, reducing IP capacity. The reduction in tie bar spacing from d to $d/2$, slightly improved the IP capacity performance of the SC walls for the larger magnitudes of OOP shear stress and ratios of shear span-to-depth considered in this parametric study; the benefits of reduced tie bar spacing are expected to increase as the magnitude of the OOP shear stress exceeds the inclined cracking load of the concrete.

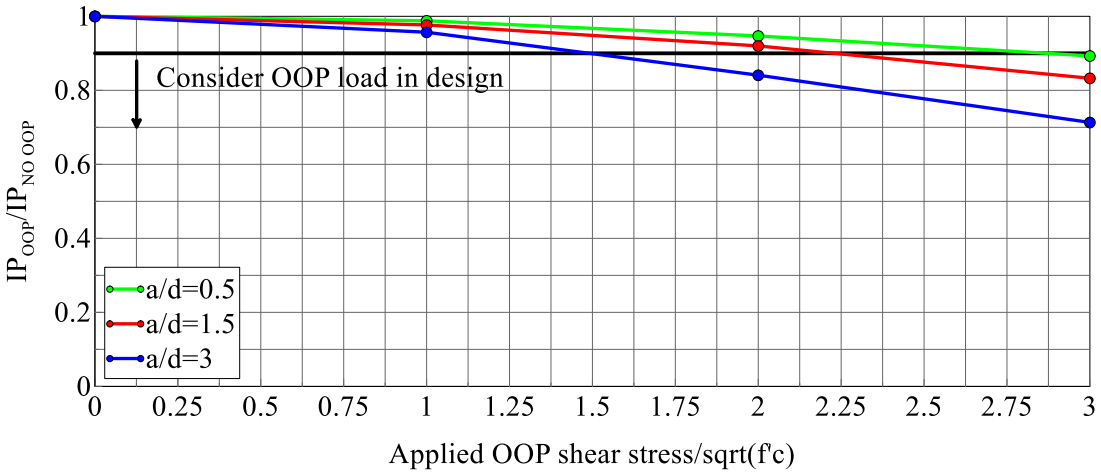

Figure 4-14: IP capacity vs. applied OOP shear stress, $f_c' = 3500$ psi, $s = d$

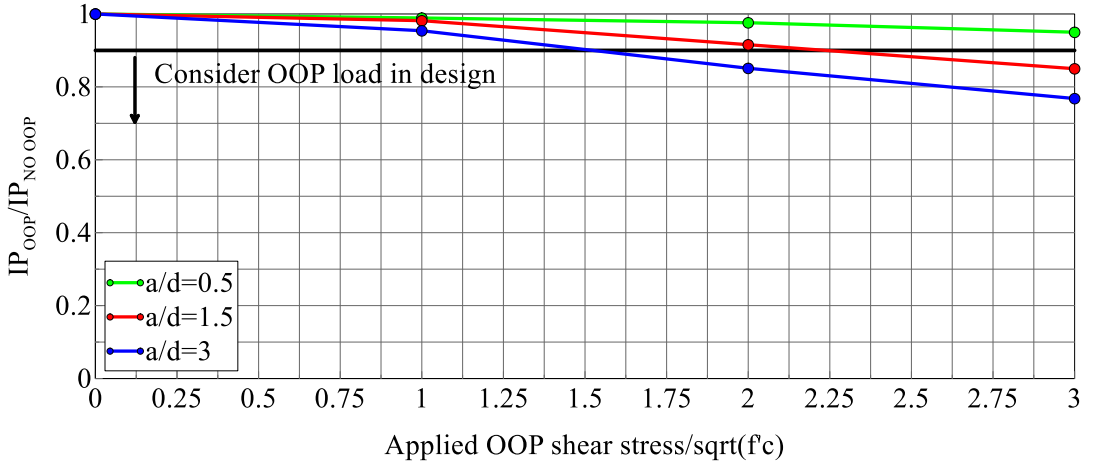

Figure 4-15: IP capacity vs. applied OOP shear stress, $f_c' = 3500$ psi, $s = d/2$

Figure 4-16 and Figure 4-17 present the information of Figure 4-14 and Figure 4-15, but for a uniaxial concrete compressive strength of 5000 psi. The trends are identical to those described in the previous paragraph.

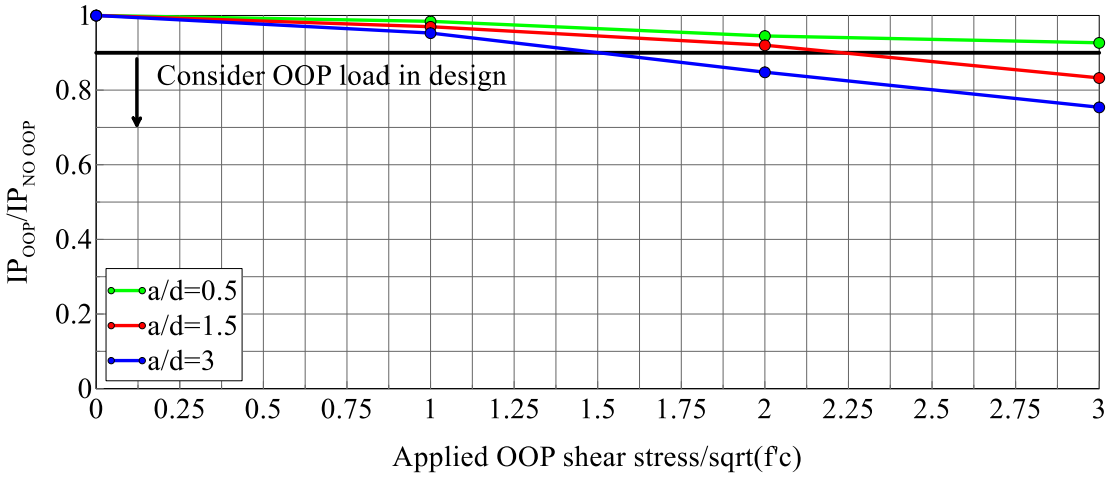

Figure 4-16: IP capacity vs. applied OOP shear stress, $f_c' = 5000$ psi , $s = d$

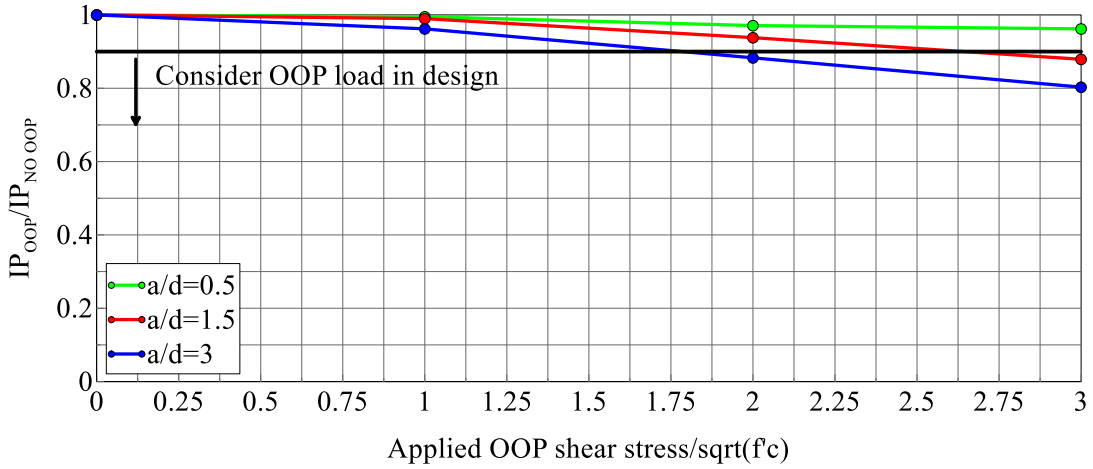

Figure 4-17: IP capacity vs. applied OOP shear stress, $f_c' = 5000$ psi , $s = d / 2$

The discussions above address the effect of OOP loading on IP capacity. Two issues that ought to be addressed in a future study, which will likely be specific to Canadian nuclear practice, are a) the strength reduction factors to be used for IP shear capacity calculations, b) strength reduction factors for OOP shear capacity calculations, c) strength reduction factors for combined IP and OOP loading. ASCE 43-05 (ASCE, 2005) provides guidance on how these factors should be calculated, which depend on whether the actions are ductile or non-ductile. A goal with predictive equations for design strength (strength reduction factor multiplied by a nominal

strength) is to achieve an exceedance probability of 98%.

The walls tested as part of this project had a thickness of 12 inches. It is well established that the shear strength of plain reinforced concrete elements is negatively affected by section depth, namely, an increase in depth (thickness for walls) will lead to a decrease in the average shear stress at failure. A ballot measure to address this issue has passed review by the ASCE Dynamic Analysis of Nuclear Structures Committee, which reduces nominal shear stress with depth, to a minimum value of approximately $1\sqrt{f_c'}$ to achieve the component-level target probability goals of ASCE 43.

Based on the physical testing of SC wall piers CNSC1, CNSC2, and CNSC3 and the observed trends in the parametric studies, the following design guidance is proposed for the construction of SC wall piers subjected to combined IP and OOP loadings

- OOP shear forces and bending moments can damage both infill concrete (shear force) and the steel faceplates (bending moment). Damage to the infill concrete will depend on a) the ratio of shear span to wall thickness, and b) the amplitude of the OOP loading. Damage to the steel faceplates will also depend on these two parameters.
- The effects of OOP loading should be addressed explicitly for design basis calculations. Damage to the infill concrete under IP loading will degrade OOP shear capacity, which is essentially a function of the capacity of the infill concrete only. The steel faceplates should not yield significantly (sufficient to buckle inelastically) under combined IP and OOP design basis loadings, with an appropriate margin (through a strength reduction factor) to achieve a 98% exceedance probability.
- The OOP shear strength of the infill concrete should address the effect of wall thickness on maximum average shear stress.
- A tie bar spacing of no greater than $d/2$ is recommended for SC wall piers subjected to OOP loads that exceed the design shear strength of plain concrete, accounting for depth effects, and calculated using a strength reduction factor suitable to achieve an exceedance probability of 98% per ASCE 43 (see above).
- Tie bars should be used instead of shear studs near the base of an SC wall in zones where concrete crushing and spalling is possible, to preserve the integrity of the cross section and provide point restraint to the faceplates to delay their inelastic buckling.

- Figure 4-14, Figure 4-15, Figure 4-16, and Figure 4-17 could be used to help identify magnitudes of OOP shear stress and ratios of shear span-to-depth (wall thickness) beyond which OOP loadings ought be considered for design basis calculations of IP strength. The threshold shown in the figures is a 10% reduction in peak strength. Importantly, the negative impact of significant member thickness (as described above) is not addressed here.

Although not part of the scope of this project, it is important to consider the effects of beyond design basis loadings on the seismic performance of SC walls and wall piers. In the United States, one path to demonstrating adequate performance in shaking more intense than design basis is to ensure that the resulting design will perform its intended function with 95% confidence of a probability of failure of 5% or less for shaking equal to 167% design basis. For many components this requires the risk analyst to utilize deformation capacity beyond yield (or ductility) to justify adequate performance. On the basis of the tests of CNSC3 (and to a lesser degree CNSC2), this risk-oriented performance target may require that design basis strength of SC walls under OOP loading be limited to shear stress of less than $1\sqrt{f_c'}$, or even less if the wall has a thickness greater than 12 inches.

SECTION 5
SUMMARY AND GUIDANCE FOR SEISMIC DESIGN OF SC WALL PIERS

5.1 Summary

A study was undertaken to investigate the effects of OOP loading on the IP behavior of SC composite wall piers, with a focus on the magnitude of the OOP load and the effect of tie bar spacing. Numerical simulations and physical testing were performed to develop draft guidance for consideration by CNSC.

Three medium-scale rectangular SC wall specimens were built and tested under force-controlled monotonic OOP loading and displacement-control cyclic IP loading at the Bowen Laboratory at Purdue University. The results of the experiments indicate that the OOP load has a significant effect on the IP behavior of SC composite shear walls, in particular, the deformation capacity and peak resistance; the effects become very significant as the applied OOP load develops an average shear stress that is greater than the inclined cracking load of the concrete.

The three experiments were simulated using the general-purpose finite element program LS-DYNA. The numerical model was based on a validated model for IP loading that was developed by Epackachi et al. (2014a, 2015) for a prior project. The model was evaluated for OOP loading using data from tests of plain reinforced concrete beams (i.e., no shear reinforcement) and reasonable comparisons were obtained. The predictions of the numerical models of the tested wall piers were compared with global and local measurements made in the experiments, including cyclic force-displacement relationships (IP and OOP), equivalent viscous damping ratios, vertical stresses in the steel faceplates induced by OOP loading, and observed damage (i.e., cracking of the infill concrete and buckling of the steel faceplates). The predictions of response for CNSC1 (low OOP shear stress) were very good, reasonable for CNSC2 (high OOP shear stress but tie bars at spacing $d/2$) and somewhat poor for CNSC3 (high OOP shear stress and tie bars at spacing d). One reason for the poorer predictions for CNSC2 and CNSC3 can be traced to the use of the Winfrith model, which assumes elastic perfectly plastic behavior in compression.

A parametric study was conducted using the numerical model described above to investigate the

effect of OOP loading (magnitude and location) on the IP response of SC wall piers. Different concrete compressive strengths and tie bar spacing were considered. Results of the parametric studies showed that OOP load (or shear stress) has a significant effect on the IP capacity of SC wall piers, and that the effects become very significant as the ratio of shear span-to-depth and the magnitude of the OOP load are increased.

5.2 Guidance for the Analysis and Design of SC Walls

An important objective of this project was to formulate design guidance for SC walls subjected to combined IP and OOP loading. The following guidance is offered for consideration of CNSC:

1. The effects of OOP loading should be addressed explicitly for design basis calculations. The steel faceplates should not yield significantly (sufficient to buckle inelastically) under combined IP and OOP design basis loadings, with an appropriate margin (through a strength reduction factor) to achieve a 98% exceedance probability per ASCE 43-05.

2. The OOP shear strength of the infill concrete should address the effect of wall thickness on maximum average shear stress. The balloted code change provision in ASCE 43-** could be used for this purpose.

3. A maximum tie bar spacing of $d/2$ is recommended for SC walls subjected to OOP loads that exceed the nominal design strength of plain concrete, reduced as appropriate for wall thickness, and calculated using a strength reduction factor suitable to achieve a 98% exceedance probability per ASCE 43-05.

4. Tie bars should be used instead of shear studs near the base of an SC wall in zones where concrete crushing and spalling is possible, to preserve the integrity of the cross section and provide point restraint to the faceplates to delay their inelastic buckling.

5. Limits on IP and OOP design basis strength of SC walls should recognize the need for capacity in the event of beyond design basis shaking.

A numerical model has been developed in LS-DYNA, which is capable of predicting the IP cyclic response of SC wall piers, and the combined IP and OOP cyclic response of SC walls provided the OOP shear stresses are relatively low, of the order of $2\sqrt{f_c'}$ for shallow (relatively

thin) walls. The model is described in detail in Chapters 3 and 4 of this report.

Charts have been developed, and presented in Chapter 4, to identify what combinations of OOP shear stress and ratios of shear span to depth (wall thickness) may result in significant reductions in IP shear capacity. These charts could be used for preliminary design of SC wall piers.

SECTION 6
REFERENCES

American Concrete Institute (ACI). (2006). "Code requirements for nuclear safety-related concrete structures and commentary," *ACI 349-06*, Farmington Hills, MI.

American Concrete Institute (ACI). (2014). "Building code requirements for structural concrete and commentary," *ACI 318-14*, Farmington Hills, MI.

American Institute of Steel Construction (AISC). (2015). "Specification for safety-related steel structures for nuclear facilities including supplement no. 1," *ANSI/AISC N690s1-15*, Chicago, IL.

American Society of Civil Engineers (ASCE). (2005). "Seismic design criteria for structures, systems and components in nuclear facilities," *ASCE/SEI Standard 43-05*, Reston, VA.

Bhardwaj, S. R., Kurt, E. G., Terranova, B., Varma, A. H., Whittaker, A. S., and Orbovic, N. (2015). "Preliminary investigation of the effects of out-of-plane loading on the in-plane behavior of SC walls," *Transactions, 23rd International Conference on Structural Mechanics in Reactor Technology (SMiRT)*, Manchester, United Kingdom, August.

Bresler, B., and Scordelis, A. C. (1963). "Shear strength of reinforced concrete beams," ACI Journal Proceedings, 60 (1): 51-74.

Chopra, A. (2011). *Dynamics of Structures*, Fourth Edition, Prentice-Hall.

Comite Euro-international du Beton (CEB). (1993). "CEB-FIP model code 1990," Thomas Telford, London, England.

Epackachi, S., Nguyen, N., Kurt, E., Whittaker, A. and Varma, A. H. (2014a). "In-plane behavior of rectangular steel-plate composite shear walls," *Journal of Structural Engineering*, 141 (7), 04014176.

Epackachi, S., Nguyen, N., Kurt, E., Whittaker, A., and Varma, A. H. (2014b) "Numerical and experimental investigation of the in-plane behavior of rectangular steel-plate composite walls," *Proceedings, ASCE Structures Congress*, Portland, OR, April.

Epackachi, S., Whittaker, A., Varma, A. H., and Kurt, E. (2015). "Finite element modeling of steel-plate concrete composite wall piers," *Engineering Structures*, 100: 369-384.

Kurt, E. G., Varma, A. H., Booth, P., and Whittaker, A. S. (2013). "SC wall piers and basemat connections: numerical investigation of behavior and design," *Transactions, 22nd International Conference on Structural Mechanics in Reactor Technology (SMiRT)*, San Francisco, USA, August.

Kurt, E., Varma, A. H., Epackachi, S., and Whittaker, A. (2015) "Rectangular SC wall piers: summary of seismic behavior and design," *Proceedings, ASCE Structures Congress*, Portland, OR, April.

Livermore Software Technology Corporation (LSTC). (2012). *LS-DYNA keyword user's manual V971*, Livermore, CA.

Mphonde, A. G., and Frantz, G. C. (1984). "Shear tests of high- and low-strength concrete beams without stirrups," ACI Journal Proceedings, 81 (4): 350-357.

Sener, K. C., and Varma, A. H. (2014). "Steel-plate composite walls: experimental database and design for out-of-plane shear," *Journal of Constructional Steel Research*, 100: 197-210.

Sener, K. C., Varma, A. H., and Ayhan, D. (2015). "Steel-plate composite (SC) walls: out-of-plane flexural behavior, database, and design," *Journal of Constructional Steel Research*, 108: 46-59.

Seo, J., Varma, A. H., Sener, K. C., and Ayhan, D. (2016). "Steel-plate composite (SC) walls: in-plane shear behavior, database, and design," *Journal of Constructional Steel Research*, 119: 202-215.

Varma, A. H., Zhang, K., Chi, H., Booth, P. N., and Baker, T. (2011). "In-plane shear behavior of SC composite walls: theory vs. experiment," *Transactions, 21st International Conference on Structural Mechanics in Reactor Technology (SMiRT)*, New Delhi, India, November.

Wight, J. (2015). *Reinforced Concrete, Mechanics and Design*, Seventh Edition, Pearson.

Wittmann, F. H., Rokugo, K., Bruehwiler, E., Mihashi, H., and Simonin, P. (1988). "Fracture energy and strain softening of concrete as determined by means of compact tension specimens," *Materials and Structures*, 21: 21-32.

Yang, Y., Jingbo, L., Nie, X., and Fan, J. (2016). "Experimental research on out-of-plane cyclic behavior of steel-plate composite walls," *Journal of Earthquake and Tsunami*, 10: 1-16.

MCEER Technical Reports

MCEER publishes technical reports on a variety of subjects written by authors funded through MCEER. These reports can be downloaded from the MCEER website at http://www.buffalo.edu/mceer. They can also be requested through NTIS, P.O. Box 1425, Springfield, Virginia 22151. NTIS accession numbers are shown in parenthesis, if available.

NCEER-87-0001 "First-Year Program in Research, Education and Technology Transfer," 3/5/87, (PB88-134275, A04, MF-A01).

NCEER-87-0002 "Experimental Evaluation of Instantaneous Optimal Algorithms for Structural Control," by R.C. Lin, T.T. Soong and A.M. Reinhorn, 4/20/87, (PB88-134341, A04, MF-A01).

NCEER-87-0003 "Experimentation Using the Earthquake Simulation Facilities at University at Buffalo," by A.M. Reinhorn and R.L. Ketter, not available.

NCEER-87-0004 "The System Characteristics and Performance of a Shaking Table," by J.S. Hwang, K.C. Chang and G.C. Lee, 6/1/87, (PB88-134259, A03, MF-A01). This report is available only through NTIS (see address given above).

NCEER-87-0005 "A Finite Element Formulation for Nonlinear Viscoplastic Material Using a Q Model," by O. Gyebi and G. Dasgupta, 11/2/87, (PB88-213764, A08, MF-A01).

NCEER-87-0006 "Symbolic Manipulation Program (SMP) - Algebraic Codes for Two and Three Dimensional Finite Element Formulations," by X. Lee and G. Dasgupta, 11/9/87, (PB88-218522, A05, MF-A01).

NCEER-87-0007 "Instantaneous Optimal Control Laws for Tall Buildings Under Seismic Excitations," by J.N. Yang, A. Akbarpour and P. Ghaemmaghami, 6/10/87, (PB88-134333, A06, MF-A01). This report is only available through NTIS (see address given above).

NCEER-87-0008 "IDARC: Inelastic Damage Analysis of Reinforced Concrete Frame - Shear-Wall Structures," by Y.J. Park, A.M. Reinhorn and S.K. Kunnath, 7/20/87, (PB88-134325, A09, MF-A01). This report is only available through NTIS (see address given above).

NCEER-87-0009 "Liquefaction Potential for New York State: A Preliminary Report on Sites in Manhattan and Buffalo," by M. Budhu, V. Vijayakumar, R.F. Giese and L. Baumgras, 8/31/87, (PB88-163704, A03, MF-A01). This report is available only through NTIS (see address given above).

NCEER-87-0010 "Vertical and Torsional Vibration of Foundations in Inhomogeneous Media," by A.S. Veletsos and K.W. Dotson, 6/1/87, (PB88-134291, A03, MF-A01). This report is only available through NTIS (see address given above).

NCEER-87-0011 "Seismic Probabilistic Risk Assessment and Seismic Margins Studies for Nuclear Power Plants," by Howard H.M. Hwang, 6/15/87, (PB88-134267, A03, MF-A01). This report is only available through NTIS (see address given above).

NCEER-87-0012 "Parametric Studies of Frequency Response of Secondary Systems Under Ground-Acceleration Excitations," by Y. Yong and Y.K. Lin, 6/10/87, (PB88-134309, A03, MF-A01). This report is only available through NTIS (see address given above).

NCEER-87-0013 "Frequency Response of Secondary Systems Under Seismic Excitation," by J.A. HoLung, J. Cai and Y.K. Lin, 7/31/87, (PB88-134317, A05, MF-A01). This report is only available through NTIS (see address given above).

NCEER-87-0014 "Modelling Earthquake Ground Motions in Seismically Active Regions Using Parametric Time Series Methods," by G.W. Ellis and A.S. Cakmak, 8/25/87, (PB88-134283, A08, MF-A01). This report is only available through NTIS (see address given above).

NCEER-87-0015 "Detection and Assessment of Seismic Structural Damage," by E. DiPasquale and A.S. Cakmak, 8/25/87, (PB88-163712, A05, MF-A01). This report is only available through NTIS (see address given above).

NCEER-87-0016 "Pipeline Experiment at Parkfield, California," by J. Isenberg and E. Richardson, 9/15/87, (PB88-163720, A03, MF-A01). This report is available only through NTIS (see address given above).

NCEER-87-0017 "Digital Simulation of Seismic Ground Motion," by M. Shinozuka, G. Deodatis and T. Harada, 8/31/87, (PB88-155197, A04, MF-A01). This report is available only through NTIS (see address given above).

NCEER-87-0018 "Practical Considerations for Structural Control: System Uncertainty, System Time Delay and Truncation of Small Control Forces," J.N. Yang and A. Akbarpour, 8/10/87, (PB88-163738, A08, MF-A01). This report is only available through NTIS (see address given above).

NCEER-87-0019 "Modal Analysis of Nonclassically Damped Structural Systems Using Canonical Transformation," by J.N. Yang, S. Sarkani and F.X. Long, 9/27/87, (PB88-187851, A04, MF-A01).

NCEER-87-0020 "A Nonstationary Solution in Random Vibration Theory," by J.R. Red-Horse and P.D. Spanos, 11/3/87, (PB88-163746, A03, MF-A01).

NCEER-87-0021 "Horizontal Impedances for Radially Inhomogeneous Viscoelastic Soil Layers," by A.S. Veletsos and K.W. Dotson, 10/15/87, (PB88-150859, A04, MF-A01).

NCEER-87-0022 "Seismic Damage Assessment of Reinforced Concrete Members," by Y.S. Chung, C. Meyer and M. Shinozuka, 10/9/87, (PB88-150867, A05, MF-A01). This report is available only through NTIS (see address given above).

NCEER-87-0023 "Active Structural Control in Civil Engineering," by T.T. Soong, 11/11/87, (PB88-187778, A03, MF-A01).

NCEER-87-0024 "Vertical and Torsional Impedances for Radially Inhomogeneous Viscoelastic Soil Layers," by K.W. Dotson and A.S. Veletsos, 12/87, (PB88-187786, A03, MF-A01).

NCEER-87-0025 "Proceedings from the Symposium on Seismic Hazards, Ground Motions, Soil-Liquefaction and Engineering Practice in Eastern North America," October 20-22, 1987, edited by K.H. Jacob, 12/87, (PB88-188115, A23, MF-A01). This report is available only through NTIS (see address given above).

NCEER-87-0026 "Report on the Whittier-Narrows, California, Earthquake of October 1, 1987," by J. Pantelic and A. Reinhorn, 11/87, (PB88-187752, A03, MF-A01). This report is available only through NTIS (see address given above).

NCEER-87-0027 "Design of a Modular Program for Transient Nonlinear Analysis of Large 3-D Building Structures," by S. Srivastav and J.F. Abel, 12/30/87, (PB88-187950, A05, MF-A01). This report is only available through NTIS (see address given above).

NCEER-87-0028 "Second-Year Program in Research, Education and Technology Transfer," 3/8/88, (PB88-219480, A04, MF-A01).

NCEER-88-0001 "Workshop on Seismic Computer Analysis and Design of Buildings With Interactive Graphics," by W. McGuire, J.F. Abel and C.H. Conley, 1/18/88, (PB88-187760, A03, MF-A01). This report is only available through NTIS (see address given above).

NCEER-88-0002 "Optimal Control of Nonlinear Flexible Structures," by J.N. Yang, F.X. Long and D. Wong, 1/22/88, (PB88-213772, A06, MF-A01).

NCEER-88-0003 "Substructuring Techniques in the Time Domain for Primary-Secondary Structural Systems," by G.D. Manolis and G. Juhn, 2/10/88, (PB88-213780, A04, MF-A01).

NCEER-88-0004 "Iterative Seismic Analysis of Primary-Secondary Systems," by A. Singhal, L.D. Lutes and P.D. Spanos, 2/23/88, (PB88-213798, A04, MF-A01).

NCEER-88-0005 "Stochastic Finite Element Expansion for Random Media," by P.D. Spanos and R. Ghanem, 3/14/88, (PB88-213806, A03, MF-A01).

NCEER-88-0006 "Combining Structural Optimization and Structural Control," by F.Y. Cheng and C.P. Pantelides, 1/10/88, (PB88-213814, A05, MF-A01).

NCEER-88-0007 "Seismic Performance Assessment of Code-Designed Structures," by H.H-M. Hwang, J-W. Jaw and H-J. Shau, 3/20/88, (PB88-219423, A04, MF-A01). This report is only available through NTIS (see address given above).

NCEER-88-0008 "Reliability Analysis of Code-Designed Structures Under Natural Hazards," by H.H-M. Hwang, H. Ushiba and M. Shinozuka, 2/29/88, (PB88-229471, A07, MF-A01). This report is only available through NTIS (see address given above).

NCEER-88-0009 "Seismic Fragility Analysis of Shear Wall Structures," by J-W Jaw and H.H-M. Hwang, 4/30/88, (PB89-102867, A04, MF-A01).

NCEER-88-0010 "Base Isolation of a Multi-Story Building Under a Harmonic Ground Motion - A Comparison of Performances of Various Systems," by F-G Fan, G. Ahmadi and I.G. Tadjbakhsh, 5/18/88, (PB89-122238, A06, MF-A01). This report is only available through NTIS (see address given above).

NCEER-88-0011 "Seismic Floor Response Spectra for a Combined System by Green's Functions," by F.M. Lavelle, L.A. Bergman and P.D. Spanos, 5/1/88, (PB89-102875, A03, MF-A01).

NCEER-88-0012 "A New Solution Technique for Randomly Excited Hysteretic Structures," by G.Q. Cai and Y.K. Lin, 5/16/88, (PB89-102883, A03, MF-A01).

NCEER-88-0013 "A Study of Radiation Damping and Soil-Structure Interaction Effects in the Centrifuge," by K. Weissman, supervised by J.H. Prevost, 5/24/88, (PB89-144703, A06, MF-A01).

NCEER-88-0014 "Parameter Identification and Implementation of a Kinematic Plasticity Model for Frictional Soils," by J.H. Prevost and D.V. Griffiths, not available.

NCEER-88-0015 "Two- and Three- Dimensional Dynamic Finite Element Analyses of the Long Valley Dam," by D.V. Griffiths and J.H. Prevost, 6/17/88, (PB89-144711, A04, MF-A01).

NCEER-88-0016 "Damage Assessment of Reinforced Concrete Structures in Eastern United States," by A.M. Reinhorn, M.J. Seidel, S.K. Kunnath and Y.J. Park, 6/15/88, (PB89-122220, A04, MF-A01). This report is only available through NTIS (see address given above).

NCEER-88-0017 "Dynamic Compliance of Vertically Loaded Strip Foundations in Multilayered Viscoelastic Soils," by S. Ahmad and A.S.M. Israil, 6/17/88, (PB89-102891, A04, MF-A01).

NCEER-88-0018 "An Experimental Study of Seismic Structural Response With Added Viscoelastic Dampers," by R.C. Lin, Z. Liang, T.T. Soong and R.H. Zhang, 6/30/88, (PB89-122212, A05, MF-A01). This report is available only through NTIS (see address given above).

NCEER-88-0019 "Experimental Investigation of Primary - Secondary System Interaction," by G.D. Manolis, G. Juhn and A.M. Reinhorn, 5/27/88, (PB89-122204, A04, MF-A01).

NCEER-88-0020 "A Response Spectrum Approach For Analysis of Nonclassically Damped Structures," by J.N. Yang, S. Sarkani and F.X. Long, 4/22/88, (PB89-102909, A04, MF-A01).

NCEER-88-0021 "Seismic Interaction of Structures and Soils: Stochastic Approach," by A.S. Veletsos and A.M. Prasad, 7/21/88, (PB89-122196, A04, MF-A01). This report is only available through NTIS (see address given above).

NCEER-88-0022 "Identification of the Serviceability Limit State and Detection of Seismic Structural Damage," by E. DiPasquale and A.S. Cakmak, 6/15/88, (PB89-122188, A05, MF-A01). This report is available only through NTIS (see address given above).

NCEER-88-0023 "Multi-Hazard Risk Analysis: Case of a Simple Offshore Structure," by B.K. Bhartia and E.H. Vanmarcke, 7/21/88, (PB89-145213, A05, MF-A01).

NCEER-88-0024 "Automated Seismic Design of Reinforced Concrete Buildings," by Y.S. Chung, C. Meyer and M. Shinozuka, 7/5/88, (PB89-122170, A06, MF-A01). This report is available only through NTIS (see address given above).

NCEER-88-0025 "Experimental Study of Active Control of MDOF Structures Under Seismic Excitations," by L.L. Chung, R.C. Lin, T.T. Soong and A.M. Reinhorn, 7/10/88, (PB89-122600, A04, MF-A01).

NCEER-88-0026 "Earthquake Simulation Tests of a Low-Rise Metal Structure," by J.S. Hwang, K.C. Chang, G.C. Lee and R.L. Ketter, 8/1/88, (PB89-102917, A04, MF-A01).

NCEER-88-0027 "Systems Study of Urban Response and Reconstruction Due to Catastrophic Earthquakes," by F. Kozin and H.K. Zhou, 9/22/88, (PB90-162348, A04, MF-A01).

NCEER-88-0028 "Seismic Fragility Analysis of Plane Frame Structures," by H.H-M. Hwang and Y.K. Low, 7/31/88, (PB89-131445, A06, MF-A01).

NCEER-88-0029 "Response Analysis of Stochastic Structures," by A. Kardara, C. Bucher and M. Shinozuka, 9/22/88, (PB89-174429, A04, MF-A01).

NCEER-88-0030 "Nonnormal Accelerations Due to Yielding in a Primary Structure," by D.C.K. Chen and L.D. Lutes, 9/19/88, (PB89-131437, A04, MF-A01).

NCEER-88-0031 "Design Approaches for Soil-Structure Interaction," by A.S. Veletsos, A.M. Prasad and Y. Tang, 12/30/88, (PB89-174437, A03, MF-A01). This report is available only through NTIS (see address given above).

NCEER-88-0032 "A Re-evaluation of Design Spectra for Seismic Damage Control," by C.J. Turkstra and A.G. Tallin, 11/7/88, (PB89-145221, A05, MF-A01).

NCEER-88-0033 "The Behavior and Design of Noncontact Lap Splices Subjected to Repeated Inelastic Tensile Loading," by V.E. Sagan, P. Gergely and R.N. White, 12/8/88, (PB89-163737, A08, MF-A01).

NCEER-88-0034 "Seismic Response of Pile Foundations," by S.M. Mamoon, P.K. Banerjee and S. Ahmad, 11/1/88, (PB89-145239, A04, MF-A01).

NCEER-88-0035 "Modeling of R/C Building Structures With Flexible Floor Diaphragms (IDARC2)," by A.M. Reinhorn, S.K. Kunnath and N. Panahshahi, 9/7/88, (PB89-207153, A07, MF-A01).

NCEER-88-0036 "Solution of the Dam-Reservoir Interaction Problem Using a Combination of FEM, BEM with Particular Integrals, Modal Analysis, and Substructuring," by C-S. Tsai, G.C. Lee and R.L. Ketter, 12/31/88, (PB89-207146, A04, MF-A01).

NCEER-88-0037 "Optimal Placement of Actuators for Structural Control," by F.Y. Cheng and C.P. Pantelides, 8/15/88, (PB89-162846, A05, MF-A01).

NCEER-88-0038 "Teflon Bearings in Aseismic Base Isolation: Experimental Studies and Mathematical Modeling," by A. Mokha, M.C. Constantinou and A.M. Reinhorn, 12/5/88, (PB89-218457, A10, MF-A01). This report is available only through NTIS (see address given above).

NCEER-88-0039 "Seismic Behavior of Flat Slab High-Rise Buildings in the New York City Area," by P. Weidlinger and M. Ettouney, 10/15/88, (PB90-145681, A04, MF-A01).

NCEER-88-0040 "Evaluation of the Earthquake Resistance of Existing Buildings in New York City," by P. Weidlinger and M. Ettouney, 10/15/88, not available.

NCEER-88-0041 "Small-Scale Modeling Techniques for Reinforced Concrete Structures Subjected to Seismic Loads," by W. Kim, A. El-Attar and R.N. White, 11/22/88, (PB89-189625, A05, MF-A01).

NCEER-88-0042 "Modeling Strong Ground Motion from Multiple Event Earthquakes," by G.W. Ellis and A.S. Cakmak, 10/15/88, (PB89-174445, A03, MF-A01).

NCEER-88-0043 "Nonstationary Models of Seismic Ground Acceleration," by M. Grigoriu, S.E. Ruiz and E. Rosenblueth, 7/15/88, (PB89-189617, A04, MF-A01).

NCEER-88-0044 "SARCF User's Guide: Seismic Analysis of Reinforced Concrete Frames," by Y.S. Chung, C. Meyer and M. Shinozuka, 11/9/88, (PB89-174452, A08, MF-A01).

NCEER-88-0045 "First Expert Panel Meeting on Disaster Research and Planning," edited by J. Pantelic and J. Stoyle, 9/15/88, (PB89-174460, A05, MF-A01).

NCEER-88-0046 "Preliminary Studies of the Effect of Degrading Infill Walls on the Nonlinear Seismic Response of Steel Frames," by C.Z. Chrysostomou, P. Gergely and J.F. Abel, 12/19/88, (PB89-208383, A05, MF-A01).

NCEER-88-0047 "Reinforced Concrete Frame Component Testing Facility - Design, Construction, Instrumentation and Operation," by S.P. Pessiki, C. Conley, T. Bond, P. Gergely and R.N. White, 12/16/88, (PB89-174478, A04, MF-A01).

NCEER-89-0001 "Effects of Protective Cushion and Soil Compliancy on the Response of Equipment Within a Seismically Excited Building," by J.A. HoLung, 2/16/89, (PB89-207179, A04, MF-A01).

NCEER-89-0002 "Statistical Evaluation of Response Modification Factors for Reinforced Concrete Structures," by H.H-M. Hwang and J-W. Jaw, 2/17/89, (PB89-207187, A05, MF-A01).

NCEER-89-0003 "Hysteretic Columns Under Random Excitation," by G-Q. Cai and Y.K. Lin, 1/9/89, (PB89-196513, A03, MF-A01).

NCEER-89-0004 "Experimental Study of `Elephant Foot Bulge' Instability of Thin-Walled Metal Tanks," by Z-H. Jia and R.L. Ketter, 2/22/89, (PB89-207195, A03, MF-A01).

NCEER-89-0005 "Experiment on Performance of Buried Pipelines Across San Andreas Fault," by J. Isenberg, E. Richardson and T.D. O'Rourke, 3/10/89, (PB89-218440, A04, MF-A01). This report is available only through NTIS (see address given above).

NCEER-89-0006 "A Knowledge-Based Approach to Structural Design of Earthquake-Resistant Buildings," by M. Subramani, P. Gergely, C.H. Conley, J.F. Abel and A.H. Zaghw, 1/15/89, (PB89-218465, A06, MF-A01).

NCEER-89-0007 "Liquefaction Hazards and Their Effects on Buried Pipelines," by T.D. O'Rourke and P.A. Lane, 2/1/89, (PB89-218481, A09, MF-A01).

NCEER-89-0008 "Fundamentals of System Identification in Structural Dynamics," by H. Imai, C-B. Yun, O. Maruyama and M. Shinozuka, 1/26/89, (PB89-207211, A04, MF-A01).

NCEER-89-0009 "Effects of the 1985 Michoacan Earthquake on Water Systems and Other Buried Lifelines in Mexico," by A.G. Ayala and M.J. O'Rourke, 3/8/89, (PB89-207229, A06, MF-A01).

NCEER-89-R010 "NCEER Bibliography of Earthquake Education Materials," by K.E.K. Ross, Second Revision, 9/1/89, (PB90-125352, A05, MF-A01). This report is replaced by NCEER-92-0018.

NCEER-89-0011 "Inelastic Three-Dimensional Response Analysis of Reinforced Concrete Building Structures (IDARC-3D), Part I - Modeling," by S.K. Kunnath and A.M. Reinhorn, 4/17/89, (PB90-114612, A07, MF-A01). This report is available only through NTIS (see address given above).

NCEER-89-0012 "Recommended Modifications to ATC-14," by C.D. Poland and J.O. Malley, 4/12/89, (PB90-108648, A15, MF-A01).

NCEER-89-0013 "Repair and Strengthening of Beam-to-Column Connections Subjected to Earthquake Loading," by M. Corazao and A.J. Durrani, 2/28/89, (PB90-109885, A06, MF-A01).

NCEER-89-0014 "Program EXKAL2 for Identification of Structural Dynamic Systems," by O. Maruyama, C-B. Yun, M. Hoshiya and M. Shinozuka, 5/19/89, (PB90-109877, A09, MF-A01).

NCEER-89-0015 "Response of Frames With Bolted Semi-Rigid Connections, Part I - Experimental Study and Analytical Predictions," by P.J. DiCorso, A.M. Reinhorn, J.R. Dickerson, J.B. Radziminski and W.L. Harper, 6/1/89, not available.

NCEER-89-0016 "ARMA Monte Carlo Simulation in Probabilistic Structural Analysis," by P.D. Spanos and M.P. Mignolet, 7/10/89, (PB90-109893, A03, MF-A01).

NCEER-89-P017 "Preliminary Proceedings from the Conference on Disaster Preparedness - The Place of Earthquake Education in Our Schools," Edited by K.E.K. Ross, 6/23/89, (PB90-108606, A03, MF-A01).

NCEER-89-0017 "Proceedings from the Conference on Disaster Preparedness - The Place of Earthquake Education in Our Schools," Edited by K.E.K. Ross, 12/31/89, (PB90-207895, A012, MF-A02). This report is available only through NTIS (see address given above).

NCEER-89-0018 "Multidimensional Models of Hysteretic Material Behavior for Vibration Analysis of Shape Memory Energy Absorbing Devices, by E.J. Graesser and F.A. Cozzarelli, 6/7/89, (PB90-164146, A04, MF-A01).

NCEER-89-0019 "Nonlinear Dynamic Analysis of Three-Dimensional Base Isolated Structures (3D-BASIS)," by S. Nagarajaiah, A.M. Reinhorn and M.C. Constantinou, 8/3/89, (PB90-161936, A06, MF-A01). This report has been replaced by NCEER-93-0011.

NCEER-89-0020 "Structural Control Considering Time-Rate of Control Forces and Control Rate Constraints," by F.Y. Cheng and C.P. Pantelides, 8/3/89, (PB90-120445, A04, MF-A01).

NCEER-89-0021 "Subsurface Conditions of Memphis and Shelby County," by K.W. Ng, T-S. Chang and H-H.M. Hwang, 7/26/89, (PB90-120437, A03, MF-A01).

NCEER-89-0022 "Seismic Wave Propagation Effects on Straight Jointed Buried Pipelines," by K. Elhmadi and M.J. O'Rourke, 8/24/89, (PB90-162322, A10, MF-A02).

NCEER-89-0023 "Workshop on Serviceability Analysis of Water Delivery Systems," edited by M. Grigoriu, 3/6/89, (PB90-127424, A03, MF-A01).

NCEER-89-0024 "Shaking Table Study of a 1/5 Scale Steel Frame Composed of Tapered Members," by K.C. Chang, J.S. Hwang and G.C. Lee, 9/18/89, (PB90-160169, A04, MF-A01).

NCEER-89-0025 "DYNA1D: A Computer Program for Nonlinear Seismic Site Response Analysis - Technical Documentation," by Jean H. Prevost, 9/14/89, (PB90-161944, A07, MF-A01). This report is available only through NTIS (see address given above).

NCEER-89-0026 "1:4 Scale Model Studies of Active Tendon Systems and Active Mass Dampers for Aseismic Protection," by A.M. Reinhorn, T.T. Soong, R.C. Lin, Y.P. Yang, Y. Fukao, H. Abe and M. Nakai, 9/15/89, (PB90-173246, A10, MF-A02). This report is available only through NTIS (see address given above).

NCEER-89-0027 "Scattering of Waves by Inclusions in a Nonhomogeneous Elastic Half Space Solved by Boundary Element Methods," by P.K. Hadley, A. Askar and A.S. Cakmak, 6/15/89, (PB90-145699, A07, MF-A01).

NCEER-89-0028 "Statistical Evaluation of Deflection Amplification Factors for Reinforced Concrete Structures," by H.H.M. Hwang, J-W. Jaw and A.L. Ch'ng, 8/31/89, (PB90-164633, A05, MF-A01).

NCEER-89-0029 "Bedrock Accelerations in Memphis Area Due to Large New Madrid Earthquakes," by H.H.M. Hwang, C.H.S. Chen and G. Yu, 11/7/89, (PB90-162330, A04, MF-A01).

NCEER-89-0030 "Seismic Behavior and Response Sensitivity of Secondary Structural Systems," by Y.Q. Chen and T.T. Soong, 10/23/89, (PB90-164658, A08, MF-A01).

NCEER-89-0031 "Random Vibration and Reliability Analysis of Primary-Secondary Structural Systems," by Y. Ibrahim, M. Grigoriu and T.T. Soong, 11/10/89, (PB90-161951, A04, MF-A01).

NCEER-89-0032 "Proceedings from the Second U.S. - Japan Workshop on Liquefaction, Large Ground Deformation and Their Effects on Lifelines, September 26-29, 1989," Edited by T.D. O'Rourke and M. Hamada, 12/1/89, (PB90-209388, A22, MF-A03).

NCEER-89-0033 "Deterministic Model for Seismic Damage Evaluation of Reinforced Concrete Structures," by J.M. Bracci, A.M. Reinhorn, J.B. Mander and S.K. Kunnath, 9/27/89, (PB91-108803, A06, MF-A01).

NCEER-89-0034 "On the Relation Between Local and Global Damage Indices," by E. DiPasquale and A.S. Cakmak, 8/15/89, (PB90-173865, A05, MF-A01).

NCEER-89-0035 "Cyclic Undrained Behavior of Nonplastic and Low Plasticity Silts," by A.J. Walker and H.E. Stewart, 7/26/89, (PB90-183518, A10, MF-A01).

NCEER-89-0036 "Liquefaction Potential of Surficial Deposits in the City of Buffalo, New York," by M. Budhu, R. Giese and L. Baumgrass, 1/17/89, (PB90-208455, A04, MF-A01).

NCEER-89-0037 "A Deterministic Assessment of Effects of Ground Motion Incoherence," by A.S. Veletsos and Y. Tang, 7/15/89, (PB90-164294, A03, MF-A01).

NCEER-89-0038 "Workshop on Ground Motion Parameters for Seismic Hazard Mapping," July 17-18, 1989, edited by R.V. Whitman, 12/1/89, (PB90-173923, A04, MF-A01).

NCEER-89-0039 "Seismic Effects on Elevated Transit Lines of the New York City Transit Authority," by C.J. Costantino, C.A. Miller and E. Heymsfield, 12/26/89, (PB90-207887, A06, MF-A01).

NCEER-89-0040 "Centrifugal Modeling of Dynamic Soil-Structure Interaction," by K. Weissman, Supervised by J.H. Prevost, 5/10/89, (PB90-207879, A07, MF-A01).

NCEER-89-0041 "Linearized Identification of Buildings With Cores for Seismic Vulnerability Assessment," by I-K. Ho and A.E. Aktan, 11/1/89, (PB90-251943, A07, MF-A01).

NCEER-90-0001 "Geotechnical and Lifeline Aspects of the October 17, 1989 Loma Prieta Earthquake in San Francisco," by T.D. O'Rourke, H.E. Stewart, F.T. Blackburn and T.S. Dickerman, 1/90, (PB90-208596, A05, MF-A01).

NCEER-90-0002 "Nonnormal Secondary Response Due to Yielding in a Primary Structure," by D.C.K. Chen and L.D. Lutes, 2/28/90, (PB90-251976, A07, MF-A01).

NCEER-90-0003 "Earthquake Education Materials for Grades K-12," by K.E.K. Ross, 4/16/90, (PB91-251984, A05, MF-A05). This report has been replaced by NCEER-92-0018.

NCEER-90-0004 "Catalog of Strong Motion Stations in Eastern North America," by R.W. Busby, 4/3/90, (PB90-251984, A05, MF-A01).

NCEER-90-0005 "NCEER Strong-Motion Data Base: A User Manual for the GeoBase Release (Version 1.0 for the Sun3)," by P. Friberg and K. Jacob, 3/31/90 (PB90-258062, A04, MF-A01).

NCEER-90-0006 "Seismic Hazard Along a Crude Oil Pipeline in the Event of an 1811-1812 Type New Madrid Earthquake," by H.H.M. Hwang and C-H.S. Chen, 4/16/90, (PB90-258054, A04, MF-A01).

NCEER-90-0007 "Site-Specific Response Spectra for Memphis Sheahan Pumping Station," by H.H.M. Hwang and C.S. Lee, 5/15/90, (PB91-108811, A05, MF-A01).

NCEER-90-0008 "Pilot Study on Seismic Vulnerability of Crude Oil Transmission Systems," by T. Ariman, R. Dobry, M. Grigoriu, F. Kozin, M. O'Rourke, T. O'Rourke and M. Shinozuka, 5/25/90, (PB91-108837, A06, MF-A01).

NCEER-90-0009 "A Program to Generate Site Dependent Time Histories: EQGEN," by G.W. Ellis, M. Srinivasan and A.S. Cakmak, 1/30/90, (PB91-108829, A04, MF-A01).

NCEER-90-0010 "Active Isolation for Seismic Protection of Operating Rooms," by M.E. Talbott, Supervised by M. Shinozuka, 6/8/9, (PB91-110205, A05, MF-A01).

NCEER-90-0011 "Program LINEARID for Identification of Linear Structural Dynamic Systems," by C-B. Yun and M. Shinozuka, 6/25/90, (PB91-110312, A08, MF-A01).

NCEER-90-0012 "Two-Dimensional Two-Phase Elasto-Plastic Seismic Response of Earth Dams," by A.N. Yiagos, Supervised by J.H. Prevost, 6/20/90, (PB91-110197, A13, MF-A02).

NCEER-90-0013 "Secondary Systems in Base-Isolated Structures: Experimental Investigation, Stochastic Response and Stochastic Sensitivity," by G.D. Manolis, G. Juhn, M.C. Constantinou and A.M. Reinhorn, 7/1/90, (PB91-110320, A08, MF-A01).

NCEER-90-0014 "Seismic Behavior of Lightly-Reinforced Concrete Column and Beam-Column Joint Details," by S.P. Pessiki, C.H. Conley, P. Gergely and R.N. White, 8/22/90, (PB91-108795, A11, MF-A02).

NCEER-90-0015 "Two Hybrid Control Systems for Building Structures Under Strong Earthquakes," by J.N. Yang and A. Danielians, 6/29/90, (PB91-125393, A04, MF-A01).

NCEER-90-0016 "Instantaneous Optimal Control with Acceleration and Velocity Feedback," by J.N. Yang and Z. Li, 6/29/90, (PB91-125401, A03, MF-A01).

NCEER-90-0017 "Reconnaissance Report on the Northern Iran Earthquake of June 21, 1990," by M. Mehrain, 10/4/90, (PB91-125377, A03, MF-A01).

NCEER-90-0018 "Evaluation of Liquefaction Potential in Memphis and Shelby County," by T.S. Chang, P.S. Tang, C.S. Lee and H. Hwang, 8/10/90, (PB91-125427, A09, MF-A01).

NCEER-90-0019 "Experimental and Analytical Study of a Combined Sliding Disc Bearing and Helical Steel Spring Isolation System," by M.C. Constantinou, A.S. Mokha and A.M. Reinhorn, 10/4/90, (PB91-125385, A06, MF-A01). This report is available only through NTIS (see address given above).

NCEER-90-0020 "Experimental Study and Analytical Prediction of Earthquake Response of a Sliding Isolation System with a Spherical Surface," by A.S. Mokha, M.C. Constantinou and A.M. Reinhorn, 10/11/90, (PB91-125419, A05, MF-A01).

NCEER-90-0021 "Dynamic Interaction Factors for Floating Pile Groups," by G. Gazetas, K. Fan, A. Kaynia and E. Kausel, 9/10/90, (PB91-170381, A05, MF-A01).

NCEER-90-0022 "Evaluation of Seismic Damage Indices for Reinforced Concrete Structures," by S. Rodriguez-Gomez and A.S. Cakmak, 9/30/90, PB91-171322, A06, MF-A01).

NCEER-90-0023 "Study of Site Response at a Selected Memphis Site," by H. Desai, S. Ahmad, E.S. Gazetas and M.R. Oh, 10/11/90, (PB91-196857, A03, MF-A01).

NCEER-90-0024 "A User's Guide to Strongmo: Version 1.0 of NCEER's Strong-Motion Data Access Tool for PCs and Terminals," by P.A. Friberg and C.A.T. Susch, 11/15/90, (PB91-171272, A03, MF-A01).

NCEER-90-0025 "A Three-Dimensional Analytical Study of Spatial Variability of Seismic Ground Motions," by L-L. Hong and A.H.-S. Ang, 10/30/90, (PB91-170399, A09, MF-A01).

NCEER-90-0026 "MUMOID User's Guide - A Program for the Identification of Modal Parameters," by S. Rodriguez-Gomez and E. DiPasquale, 9/30/90, (PB91-171298, A04, MF-A01).

NCEER-90-0027 "SARCF-II User's Guide - Seismic Analysis of Reinforced Concrete Frames," by S. Rodriguez-Gomez, Y.S. Chung and C. Meyer, 9/30/90, (PB91-171280, A05, MF-A01).

NCEER-90-0028 "Viscous Dampers: Testing, Modeling and Application in Vibration and Seismic Isolation," by N. Makris and M.C. Constantinou, 12/20/90 (PB91-190561, A06, MF-A01).

NCEER-90-0029 "Soil Effects on Earthquake Ground Motions in the Memphis Area," by H. Hwang, C.S. Lee, K.W. Ng and T.S. Chang, 8/2/90, (PB91-190751, A05, MF-A01).

NCEER-91-0001 "Proceedings from the Third Japan-U.S. Workshop on Earthquake Resistant Design of Lifeline Facilities and Countermeasures for Soil Liquefaction, December 17-19, 1990," edited by T.D. O'Rourke and M. Hamada, 2/1/91, (PB91-179259, A99, MF-A04).

NCEER-91-0002 "Physical Space Solutions of Non-Proportionally Damped Systems," by M. Tong, Z. Liang and G.C. Lee, 1/15/91, (PB91-179242, A04, MF-A01).

NCEER-91-0003 "Seismic Response of Single Piles and Pile Groups," by K. Fan and G. Gazetas, 1/10/91, (PB92-174994, A04, MF-A01).

NCEER-91-0004 "Damping of Structures: Part 1 - Theory of Complex Damping," by Z. Liang and G. Lee, 10/10/91, (PB92-197235, A12, MF-A03).

NCEER-91-0005 "3D-BASIS - Nonlinear Dynamic Analysis of Three Dimensional Base Isolated Structures: Part II," by S. Nagarajaiah, A.M. Reinhorn and M.C. Constantinou, 2/28/91, (PB91-190553, A07, MF-A01). This report has been replaced by NCEER-93-0011.

NCEER-91-0006 "A Multidimensional Hysteretic Model for Plasticity Deforming Metals in Energy Absorbing Devices," by E.J. Graesser and F.A. Cozzarelli, 4/9/91, (PB92-108364, A04, MF-A01).

NCEER-91-0007 "A Framework for Customizable Knowledge-Based Expert Systems with an Application to a KBES for Evaluating the Seismic Resistance of Existing Buildings," by E.G. Ibarra-Anaya and S.J. Fenves, 4/9/91, (PB91-210930, A08, MF-A01).

NCEER-91-0008 "Nonlinear Analysis of Steel Frames with Semi-Rigid Connections Using the Capacity Spectrum Method," by G.G. Deierlein, S-H. Hsieh, Y-J. Shen and J.F. Abel, 7/2/91, (PB92-113828, A05, MF-A01).

NCEER-91-0009 "Earthquake Education Materials for Grades K-12," by K.E.K. Ross, 4/30/91, (PB91-212142, A06, MF-A01). This report has been replaced by NCEER-92-0018.

NCEER-91-0010 "Phase Wave Velocities and Displacement Phase Differences in a Harmonically Oscillating Pile," by N. Makris and G. Gazetas, 7/8/91, (PB92-108356, A04, MF-A01).

NCEER-91-0011 "Dynamic Characteristics of a Full-Size Five-Story Steel Structure and a 2/5 Scale Model," by K.C. Chang, G.C. Yao, G.C. Lee, D.S. Hao and Y.C. Yeh," 7/2/91, (PB93-116648, A06, MF-A02).

NCEER-91-0012 "Seismic Response of a 2/5 Scale Steel Structure with Added Viscoelastic Dampers," by K.C. Chang, T.T. Soong, S-T. Oh and M.L. Lai, 5/17/91, (PB92-110816, A05, MF-A01).

NCEER-91-0013 "Earthquake Response of Retaining Walls; Full-Scale Testing and Computational Modeling," by S. Alampalli and A-W.M. Elgamal, 6/20/91, not available.

NCEER-91-0014 "3D-BASIS-M: Nonlinear Dynamic Analysis of Multiple Building Base Isolated Structures," by P.C. Tsopelas, S. Nagarajaiah, M.C. Constantinou and A.M. Reinhorn, 5/28/91, (PB92-113885, A09, MF-A02).

NCEER-91-0015 "Evaluation of SEAOC Design Requirements for Sliding Isolated Structures," by D. Theodossiou and M.C. Constantinou, 6/10/91, (PB92-114602, A11, MF-A03).

NCEER-91-0016 "Closed-Loop Modal Testing of a 27-Story Reinforced Concrete Flat Plate-Core Building," by H.R. Somaprasad, T. Toksoy, H. Yoshiyuki and A.E. Aktan, 7/15/91, (PB92-129980, A07, MF-A02).

NCEER-91-0017 "Shake Table Test of a 1/6 Scale Two-Story Lightly Reinforced Concrete Building," by A.G. El-Attar, R.N. White and P. Gergely, 2/28/91, (PB92-222447, A06, MF-A02).

NCEER-91-0018 "Shake Table Test of a 1/8 Scale Three-Story Lightly Reinforced Concrete Building," by A.G. El-Attar, R.N. White and P. Gergely, 2/28/91, (PB93-116630, A08, MF-A02).

NCEER-91-0019 "Transfer Functions for Rigid Rectangular Foundations," by A.S. Veletsos, A.M. Prasad and W.H. Wu, 7/31/91, not available.

NCEER-91-0020 "Hybrid Control of Seismic-Excited Nonlinear and Inelastic Structural Systems," by J.N. Yang, Z. Li and A. Danielians, 8/1/91, (PB92-143171, A06, MF-A02).

NCEER-91-0021 "The NCEER-91 Earthquake Catalog: Improved Intensity-Based Magnitudes and Recurrence Relations for U.S. Earthquakes East of New Madrid," by L. Seeber and J.G. Armbruster, 8/28/91, (PB92-176742, A06, MF-A02).

NCEER-91-0022 "Proceedings from the Implementation of Earthquake Planning and Education in Schools: The Need for Change - The Roles of the Changemakers," by K.E.K. Ross and F. Winslow, 7/23/91, (PB92-129998, A12, MF-A03).

NCEER-91-0023 "A Study of Reliability-Based Criteria for Seismic Design of Reinforced Concrete Frame Buildings," by H.H.M. Hwang and H-M. Hsu, 8/10/91, (PB92-140235, A09, MF-A02).

NCEER-91-0024 "Experimental Verification of a Number of Structural System Identification Algorithms," by R.G. Ghanem, H. Gavin and M. Shinozuka, 9/18/91, (PB92-176577, A18, MF-A04).

NCEER-91-0025 "Probabilistic Evaluation of Liquefaction Potential," by H.H.M. Hwang and C.S. Lee," 11/25/91, (PB92-143429, A05, MF-A01).

NCEER-91-0026 "Instantaneous Optimal Control for Linear, Nonlinear and Hysteretic Structures - Stable Controllers," by J.N. Yang and Z. Li, 11/15/91, (PB92-163807, A04, MF-A01).

NCEER-91-0027 "Experimental and Theoretical Study of a Sliding Isolation System for Bridges," by M.C. Constantinou, A. Kartoum, A.M. Reinhorn and P. Bradford, 11/15/91, (PB92-176973, A10, MF-A03).

NCEER-92-0001 "Case Studies of Liquefaction and Lifeline Performance During Past Earthquakes, Volume 1: Japanese Case Studies," Edited by M. Hamada and T. O'Rourke, 2/17/92, (PB92-197243, A18, MF-A04).

NCEER-92-0002 "Case Studies of Liquefaction and Lifeline Performance During Past Earthquakes, Volume 2: United States Case Studies," Edited by T. O'Rourke and M. Hamada, 2/17/92, (PB92-197250, A20, MF-A04).

NCEER-92-0003 "Issues in Earthquake Education," Edited by K. Ross, 2/3/92, (PB92-222389, A07, MF-A02).

NCEER-92-0004 "Proceedings from the First U.S. - Japan Workshop on Earthquake Protective Systems for Bridges," Edited by I.G. Buckle, 2/4/92, (PB94-142239, A99, MF-A06).

NCEER-92-0005 "Seismic Ground Motion from a Haskell-Type Source in a Multiple-Layered Half-Space," A.P. Theoharis, G. Deodatis and M. Shinozuka, 1/2/92, not available.

NCEER-92-0006 "Proceedings from the Site Effects Workshop," Edited by R. Whitman, 2/29/92, (PB92-197201, A04, MF-A01).

NCEER-92-0007 "Engineering Evaluation of Permanent Ground Deformations Due to Seismically-Induced Liquefaction," by M.H. Baziar, R. Dobry and A-W.M. Elgamal, 3/24/92, (PB92-222421, A13, MF-A03).

NCEER-92-0008 "A Procedure for the Seismic Evaluation of Buildings in the Central and Eastern United States," by C.D. Poland and J.O. Malley, 4/2/92, (PB92-222439, A20, MF-A04).

NCEER-92-0009 "Experimental and Analytical Study of a Hybrid Isolation System Using Friction Controllable Sliding Bearings," by M.Q. Feng, S. Fujii and M. Shinozuka, 5/15/92, (PB93-150282, A06, MF-A02).

NCEER-92-0010 "Seismic Resistance of Slab-Column Connections in Existing Non-Ductile Flat-Plate Buildings," by A.J. Durrani and Y. Du, 5/18/92, (PB93-116812, A06, MF-A02).

NCEER-92-0011 "The Hysteretic and Dynamic Behavior of Brick Masonry Walls Upgraded by Ferrocement Coatings Under Cyclic Loading and Strong Simulated Ground Motion," by H. Lee and S.P. Prawel, 5/11/92, not available.

NCEER-92-0012 "Study of Wire Rope Systems for Seismic Protection of Equipment in Buildings," by G.F. Demetriades, M.C. Constantinou and A.M. Reinhorn, 5/20/92, (PB93-116655, A08, MF-A02).

NCEER-92-0013 "Shape Memory Structural Dampers: Material Properties, Design and Seismic Testing," by P.R. Witting and F.A. Cozzarelli, 5/26/92, (PB93-116663, A05, MF-A01).

NCEER-92-0014 "Longitudinal Permanent Ground Deformation Effects on Buried Continuous Pipelines," by M.J. O'Rourke, and C. Nordberg, 6/15/92, (PB93-116671, A08, MF-A02).

NCEER-92-0015 "A Simulation Method for Stationary Gaussian Random Functions Based on the Sampling Theorem," by M. Grigoriu and S. Balopoulou, 6/11/92, (PB93-127496, A05, MF-A01).

NCEER-92-0016 "Gravity-Load-Designed Reinforced Concrete Buildings: Seismic Evaluation of Existing Construction and Detailing Strategies for Improved Seismic Resistance," by G.W. Hoffmann, S.K. Kunnath, A.M. Reinhorn and J.B. Mander, 7/15/92, (PB94-142007, A08, MF-A02).

NCEER-92-0017 "Observations on Water System and Pipeline Performance in the Limón Area of Costa Rica Due to the April 22, 1991 Earthquake," by M. O'Rourke and D. Ballantyne, 6/30/92, (PB93-126811, A06, MF-A02).

NCEER-92-0018 "Fourth Edition of Earthquake Education Materials for Grades K-12," Edited by K.E.K. Ross, 8/10/92, (PB93-114023, A07, MF-A02).

NCEER-92-0019 "Proceedings from the Fourth Japan-U.S. Workshop on Earthquake Resistant Design of Lifeline Facilities and Countermeasures for Soil Liquefaction," Edited by M. Hamada and T.D. O'Rourke, 8/12/92, (PB93-163939, A99, MF-E11).

NCEER-92-0020 "Active Bracing System: A Full Scale Implementation of Active Control," by A.M. Reinhorn, T.T. Soong, R.C. Lin, M.A. Riley, Y.P. Wang, S. Aizawa and M. Higashino, 8/14/92, (PB93-127512, A06, MF-A02).

NCEER-92-0021 "Empirical Analysis of Horizontal Ground Displacement Generated by Liquefaction-Induced Lateral Spreads," by S.F. Bartlett and T.L. Youd, 8/17/92, (PB93-188241, A06, MF-A02).

NCEER-92-0022 "IDARC Version 3.0: Inelastic Damage Analysis of Reinforced Concrete Structures," by S.K. Kunnath, A.M. Reinhorn and R.F. Lobo, 8/31/92, (PB93-227502, A07, MF-A02).

NCEER-92-0023 "A Semi-Empirical Analysis of Strong-Motion Peaks in Terms of Seismic Source, Propagation Path and Local Site Conditions, by M. Kamiyama, M.J. O'Rourke and R. Flores-Berrones, 9/9/92, (PB93-150266, A08, MF-A02).

NCEER-92-0024 "Seismic Behavior of Reinforced Concrete Frame Structures with Nonductile Details, Part I: Summary of Experimental Findings of Full Scale Beam-Column Joint Tests," by A. Beres, R.N. White and P. Gergely, 9/30/92, (PB93-227783, A05, MF-A01).

NCEER-92-0025 "Experimental Results of Repaired and Retrofitted Beam-Column Joint Tests in Lightly Reinforced Concrete Frame Buildings," by A. Beres, S. El-Borgi, R.N. White and P. Gergely, 10/29/92, (PB93-227791, A05, MF-A01).

NCEER-92-0026 "A Generalization of Optimal Control Theory: Linear and Nonlinear Structures," by J.N. Yang, Z. Li and S. Vongchavalitkul, 11/2/92, (PB93-188621, A05, MF-A01).

NCEER-92-0027 "Seismic Resistance of Reinforced Concrete Frame Structures Designed Only for Gravity Loads: Part I - Design and Properties of a One-Third Scale Model Structure," by J.M. Bracci, A.M. Reinhorn and J.B. Mander, 12/1/92, (PB94-104502, A08, MF-A02).

NCEER-92-0028 "Seismic Resistance of Reinforced Concrete Frame Structures Designed Only for Gravity Loads: Part II - Experimental Performance of Subassemblages," by L.E. Aycardi, J.B. Mander and A.M. Reinhorn, 12/1/92, (PB94-104510, A08, MF-A02).

NCEER-92-0029 "Seismic Resistance of Reinforced Concrete Frame Structures Designed Only for Gravity Loads: Part III - Experimental Performance and Analytical Study of a Structural Model," by J.M. Bracci, A.M. Reinhorn and J.B. Mander, 12/1/92, (PB93-227528, A09, MF-A01).

NCEER-92-0030 "Evaluation of Seismic Retrofit of Reinforced Concrete Frame Structures: Part I - Experimental Performance of Retrofitted Subassemblages," by D. Choudhuri, J.B. Mander and A.M. Reinhorn, 12/8/92, (PB93-198307, A07, MF-A02).

NCEER-92-0031 "Evaluation of Seismic Retrofit of Reinforced Concrete Frame Structures: Part II - Experimental Performance and Analytical Study of a Retrofitted Structural Model," by J.M. Bracci, A.M. Reinhorn and J.B. Mander, 12/8/92, (PB93-198315, A09, MF-A03).

NCEER-92-0032 "Experimental and Analytical Investigation of Seismic Response of Structures with Supplemental Fluid Viscous Dampers," by M.C. Constantinou and M.D. Symans, 12/21/92, (PB93-191435, A10, MF-A03). This report is available only through NTIS (see address given above).

NCEER-92-0033 "Reconnaissance Report on the Cairo, Egypt Earthquake of October 12, 1992," by M. Khater, 12/23/92, (PB93-188621, A03, MF-A01).

NCEER-92-0034 "Low-Level Dynamic Characteristics of Four Tall Flat-Plate Buildings in New York City," by H. Gavin, S. Yuan, J. Grossman, E. Pekelis and K. Jacob, 12/28/92, (PB93-188217, A07, MF-A02).

NCEER-93-0001 "An Experimental Study on the Seismic Performance of Brick-Infilled Steel Frames With and Without Retrofit," by J.B. Mander, B. Nair, K. Wojtkowski and J. Ma, 1/29/93, (PB93-227510, A07, MF-A02).

NCEER-93-0002 "Social Accounting for Disaster Preparedness and Recovery Planning," by S. Cole, E. Pantoja and V. Razak, 2/22/93, (PB94-142114, A12, MF-A03).

NCEER-93-0003 "Assessment of 1991 NEHRP Provisions for Nonstructural Components and Recommended Revisions," by T.T. Soong, G. Chen, Z. Wu, R-H. Zhang and M. Grigoriu, 3/1/93, (PB93-188639, A06, MF-A02).

NCEER-93-0004 "Evaluation of Static and Response Spectrum Analysis Procedures of SEAOC/UBC for Seismic Isolated Structures," by C.W. Winters and M.C. Constantinou, 3/23/93, (PB93-198299, A10, MF-A03).

NCEER-93-0005 "Earthquakes in the Northeast - Are We Ignoring the Hazard? A Workshop on Earthquake Science and Safety for Educators," edited by K.E.K. Ross, 4/2/93, (PB94-103066, A09, MF-A02).

NCEER-93-0006 "Inelastic Response of Reinforced Concrete Structures with Viscoelastic Braces," by R.F. Lobo, J.M. Bracci, K.L. Shen, A.M. Reinhorn and T.T. Soong, 4/5/93, (PB93-227486, A05, MF-A02).

NCEER-93-0007 "Seismic Testing of Installation Methods for Computers and Data Processing Equipment," by K. Kosar, T.T. Soong, K.L. Shen, J.A. HoLung and Y.K. Lin, 4/12/93, (PB93-198299, A07, MF-A02).

NCEER-93-0008 "Retrofit of Reinforced Concrete Frames Using Added Dampers," by A. Reinhorn, M. Constantinou and C. Li, not available.

NCEER-93-0009 "Seismic Behavior and Design Guidelines for Steel Frame Structures with Added Viscoelastic Dampers," by K.C. Chang, M.L. Lai, T.T. Soong, D.S. Hao and Y.C. Yeh, 5/1/93, (PB94-141959, A07, MF-A02).

NCEER-93-0010 "Seismic Performance of Shear-Critical Reinforced Concrete Bridge Piers," by J.B. Mander, S.M. Waheed, M.T.A. Chaudhary and S.S. Chen, 5/12/93, (PB93-227494, A08, MF-A02).

NCEER-93-0011 "3D-BASIS-TABS: Computer Program for Nonlinear Dynamic Analysis of Three Dimensional Base Isolated Structures," by S. Nagarajaiah, C. Li, A.M. Reinhorn and M.C. Constantinou, 8/2/93, (PB94-141819, A09, MF-A02).

NCEER-93-0012 "Effects of Hydrocarbon Spills from an Oil Pipeline Break on Ground Water," by O.J. Helweg and H.H.M. Hwang, 8/3/93, (PB94-141942, A06, MF-A02).

NCEER-93-0013 "Simplified Procedures for Seismic Design of Nonstructural Components and Assessment of Current Code Provisions," by M.P. Singh, L.E. Suarez, E.E. Matheu and G.O. Maldonado, 8/4/93, (PB94-141827, A09, MF-A02).

NCEER-93-0014 "An Energy Approach to Seismic Analysis and Design of Secondary Systems," by G. Chen and T.T. Soong, 8/6/93, (PB94-142767, A11, MF-A03).

NCEER-93-0015 "Proceedings from School Sites: Becoming Prepared for Earthquakes - Commemorating the Third Anniversary of the Loma Prieta Earthquake," Edited by F.E. Winslow and K.E.K. Ross, 8/16/93, (PB94-154275, A16, MF-A02).

NCEER-93-0016 "Reconnaissance Report of Damage to Historic Monuments in Cairo, Egypt Following the October 12, 1992 Dahshur Earthquake," by D. Sykora, D. Look, G. Croci, E. Karaesmen and E. Karaesmen, 8/19/93, (PB94-142221, A08, MF-A02).

NCEER-93-0017 "The Island of Guam Earthquake of August 8, 1993," by S.W. Swan and S.K. Harris, 9/30/93, (PB94-141843, A04, MF-A01).

NCEER-93-0018 "Engineering Aspects of the October 12, 1992 Egyptian Earthquake," by A.W. Elgamal, M. Amer, K. Adalier and A. Abul-Fadl, 10/7/93, (PB94-141983, A05, MF-A01).

NCEER-93-0019 "Development of an Earthquake Motion Simulator and its Application in Dynamic Centrifuge Testing," by I. Krstelj, Supervised by J.H. Prevost, 10/23/93, (PB94-181773, A-10, MF-A03).

NCEER-93-0020 "NCEER-Taisei Corporation Research Program on Sliding Seismic Isolation Systems for Bridges: Experimental and Analytical Study of a Friction Pendulum System (FPS)," by M.C. Constantinou, P. Tsopelas, Y-S. Kim and S. Okamoto, 11/1/93, (PB94-142775, A08, MF-A02).

NCEER-93-0021 "Finite Element Modeling of Elastomeric Seismic Isolation Bearings," by L.J. Billings, Supervised by R. Shepherd, 11/8/93, not available.

NCEER-93-0022 "Seismic Vulnerability of Equipment in Critical Facilities: Life-Safety and Operational Consequences," by K. Porter, G.S. Johnson, M.M. Zadeh, C. Scawthorn and S. Eder, 11/24/93, (PB94-181765, A16, MF-A03).

NCEER-93-0023 "Hokkaido Nansei-oki, Japan Earthquake of July 12, 1993, by P.I. Yanev and C.R. Scawthorn, 12/23/93, (PB94-181500, A07, MF-A01).

NCEER-94-0001 "An Evaluation of Seismic Serviceability of Water Supply Networks with Application to the San Francisco Auxiliary Water Supply System," by I. Markov, Supervised by M. Grigoriu and T. O'Rourke, 1/21/94, (PB94-204013, A07, MF-A02).

NCEER-94-0002 "NCEER-Taisei Corporation Research Program on Sliding Seismic Isolation Systems for Bridges: Experimental and Analytical Study of Systems Consisting of Sliding Bearings, Rubber Restoring Force Devices and Fluid Dampers," Volumes I and II, by P. Tsopelas, S. Okamoto, M.C. Constantinou, D. Ozaki and S. Fujii, 2/4/94, (PB94-181740, A09, MF-A02 and PB94-181757, A12, MF-A03).

NCEER-94-0003 "A Markov Model for Local and Global Damage Indices in Seismic Analysis," by S. Rahman and M. Grigoriu, 2/18/94, (PB94-206000, A12, MF-A03).

NCEER-94-0004 "Proceedings from the NCEER Workshop on Seismic Response of Masonry Infills," edited by D.P. Abrams, 3/1/94, (PB94-180783, A07, MF-A02).

NCEER-94-0005 "The Northridge, California Earthquake of January 17, 1994: General Reconnaissance Report," edited by J.D. Goltz, 3/11/94, (PB94-193943, A10, MF-A03).

NCEER-94-0006 "Seismic Energy Based Fatigue Damage Analysis of Bridge Columns: Part I - Evaluation of Seismic Capacity," by G.A. Chang and J.B. Mander, 3/14/94, (PB94-219185, A11, MF-A03).

NCEER-94-0007 "Seismic Isolation of Multi-Story Frame Structures Using Spherical Sliding Isolation Systems," by T.M. Al-Hussaini, V.A. Zayas and M.C. Constantinou, 3/17/94, (PB94-193745, A09, MF-A02).

NCEER-94-0008 "The Northridge, California Earthquake of January 17, 1994: Performance of Highway Bridges," edited by I.G. Buckle, 3/24/94, (PB94-193851, A06, MF-A02).

NCEER-94-0009 "Proceedings of the Third U.S.-Japan Workshop on Earthquake Protective Systems for Bridges," edited by I.G. Buckle and I. Friedland, 3/31/94, (PB94-195815, A99, MF-A06).

NCEER-94-0010 "3D-BASIS-ME: Computer Program for Nonlinear Dynamic Analysis of Seismically Isolated Single and Multiple Structures and Liquid Storage Tanks," by P.C. Tsopelas, M.C. Constantinou and A.M. Reinhorn, 4/12/94, (PB94-204922, A09, MF-A02).

NCEER-94-0011 "The Northridge, California Earthquake of January 17, 1994: Performance of Gas Transmission Pipelines," by T.D. O'Rourke and M.C. Palmer, 5/16/94, (PB94-204989, A05, MF-A01).

NCEER-94-0012 "Feasibility Study of Replacement Procedures and Earthquake Performance Related to Gas Transmission Pipelines," by T.D. O'Rourke and M.C. Palmer, 5/25/94, (PB94-206638, A09, MF-A02).

NCEER-94-0013 "Seismic Energy Based Fatigue Damage Analysis of Bridge Columns: Part II - Evaluation of Seismic Demand," by G.A. Chang and J.B. Mander, 6/1/94, (PB95-18106, A08, MF-A02).

NCEER-94-0014 "NCEER-Taisei Corporation Research Program on Sliding Seismic Isolation Systems for Bridges: Experimental and Analytical Study of a System Consisting of Sliding Bearings and Fluid Restoring Force/Damping Devices," by P. Tsopelas and M.C. Constantinou, 6/13/94, (PB94-219144, A10, MF-A03).

NCEER-94-0015 "Generation of Hazard-Consistent Fragility Curves for Seismic Loss Estimation Studies," by H. Hwang and J-R. Huo, 6/14/94, (PB95-181996, A09, MF-A02).

NCEER-94-0016 "Seismic Study of Building Frames with Added Energy-Absorbing Devices," by W.S. Pong, C.S. Tsai and G.C. Lee, 6/20/94, (PB94-219136, A10, A03).

NCEER-94-0017 "Sliding Mode Control for Seismic-Excited Linear and Nonlinear Civil Engineering Structures," by J. Yang, J. Wu, A. Agrawal and Z. Li, 6/21/94, (PB95-138483, A06, MF-A02).

NCEER-94-0018 "3D-BASIS-TABS Version 2.0: Computer Program for Nonlinear Dynamic Analysis of Three Dimensional Base Isolated Structures," by A.M. Reinhorn, S. Nagarajaiah, M.C. Constantinou, P. Tsopelas and R. Li, 6/22/94, (PB95-182176, A08, MF-A02).

NCEER-94-0019 "Proceedings of the International Workshop on Civil Infrastructure Systems: Application of Intelligent Systems and Advanced Materials on Bridge Systems," Edited by G.C. Lee and K.C. Chang, 7/18/94, (PB95-252474, A20, MF-A04).

NCEER-94-0020 "Study of Seismic Isolation Systems for Computer Floors," by V. Lambrou and M.C. Constantinou, 7/19/94, (PB95-138533, A10, MF-A03).

NCEER-94-0021 "Proceedings of the U.S.-Italian Workshop on Guidelines for Seismic Evaluation and Rehabilitation of Unreinforced Masonry Buildings," Edited by D.P. Abrams and G.M. Calvi, 7/20/94, (PB95-138749, A13, MF-A03).

NCEER-94-0022 "NCEER-Taisei Corporation Research Program on Sliding Seismic Isolation Systems for Bridges: Experimental and Analytical Study of a System Consisting of Lubricated PTFE Sliding Bearings and Mild Steel Dampers," by P. Tsopelas and M.C. Constantinou, 7/22/94, (PB95-182184, A08, MF-A02).

NCEER-94-0023 “Development of Reliability-Based Design Criteria for Buildings Under Seismic Load,” by Y.K. Wen, H. Hwang and M. Shinozuka, 8/1/94, (PB95-211934, A08, MF-A02).

NCEER-94-0024 “Experimental Verification of Acceleration Feedback Control Strategies for an Active Tendon System,” by S.J. Dyke, B.F. Spencer, Jr., P. Quast, M.K. Sain, D.C. Kaspari, Jr. and T.T. Soong, 8/29/94, (PB95-212320, A05, MF-A01).

NCEER-94-0025 “Seismic Retrofitting Manual for Highway Bridges,” Edited by I.G. Buckle and I.F. Friedland, published by the Federal Highway Administration (PB95-212676, A15, MF-A03).

NCEER-94-0026 “Proceedings from the Fifth U.S.-Japan Workshop on Earthquake Resistant Design of Lifeline Facilities and Countermeasures Against Soil Liquefaction,” Edited by T.D. O’Rourke and M. Hamada, 11/7/94, (PB95-220802, A99, MF-E08).

NCEER-95-0001 "Experimental and Analytical Investigation of Seismic Retrofit of Structures with Supplemental Damping: Part 1 - Fluid Viscous Damping Devices," by A.M. Reinhorn, C. Li and M.C. Constantinou, 1/3/95, (PB95-266599, A09, MF-A02).

NCEER-95-0002 "Experimental and Analytical Study of Low-Cycle Fatigue Behavior of Semi-Rigid Top-And-Seat Angle Connections," by G. Pekcan, J.B. Mander and S.S. Chen, 1/5/95, (PB95-220042, A07, MF-A02).

NCEER-95-0003 "NCEER-ATC Joint Study on Fragility of Buildings," by T. Anagnos, C. Rojahn and A.S. Kiremidjian, 1/20/95, (PB95-220026, A06, MF-A02).

NCEER-95-0004 "Nonlinear Control Algorithms for Peak Response Reduction," by Z. Wu, T.T. Soong, V. Gattulli and R.C. Lin, 2/16/95, (PB95-220349, A05, MF-A01).

NCEER-95-0005 "Pipeline Replacement Feasibility Study: A Methodology for Minimizing Seismic and Corrosion Risks to Underground Natural Gas Pipelines," by R.T. Eguchi, H.A. Seligson and D.G. Honegger, 3/2/95, (PB95-252326, A06, MF-A02).

NCEER-95-0006 "Evaluation of Seismic Performance of an 11-Story Frame Building During the 1994 Northridge Earthquake," by F. Naeim, R. DiSulio, K. Benuska, A. Reinhorn and C. Li, not available.

NCEER-95-0007 "Prioritization of Bridges for Seismic Retrofitting," by N. Basöz and A.S. Kiremidjian, 4/24/95, (PB95-252300, A08, MF-A02).

NCEER-95-0008 "Method for Developing Motion Damage Relationships for Reinforced Concrete Frames," by A. Singhal and A.S. Kiremidjian, 5/11/95, (PB95-266607, A06, MF-A02).

NCEER-95-0009 "Experimental and Analytical Investigation of Seismic Retrofit of Structures with Supplemental Damping: Part II - Friction Devices," by C. Li and A.M. Reinhorn, 7/6/95, (PB96-128087, A11, MF-A03).

NCEER-95-0010 "Experimental Performance and Analytical Study of a Non-Ductile Reinforced Concrete Frame Structure Retrofitted with Elastomeric Spring Dampers," by G. Pekcan, J.B. Mander and S.S. Chen, 7/14/95, (PB96-137161, A08, MF-A02).

NCEER-95-0011 "Development and Experimental Study of Semi-Active Fluid Damping Devices for Seismic Protection of Structures," by M.D. Symans and M.C. Constantinou, 8/3/95, (PB96-136940, A23, MF-A04).

NCEER-95-0012 "Real-Time Structural Parameter Modification (RSPM): Development of Innervated Structures," by Z. Liang, M. Tong and G.C. Lee, 4/11/95, (PB96-137153, A06, MF-A01).

NCEER-95-0013 "Experimental and Analytical Investigation of Seismic Retrofit of Structures with Supplemental Damping: Part III - Viscous Damping Walls," by A.M. Reinhorn and C. Li, 10/1/95, (PB96-176409, A11, MF-A03).

NCEER-95-0014 "Seismic Fragility Analysis of Equipment and Structures in a Memphis Electric Substation," by J-R. Huo and H.H.M. Hwang, 8/10/95, (PB96-128087, A09, MF-A02).

NCEER-95-0015 "The Hanshin-Awaji Earthquake of January 17, 1995: Performance of Lifelines," Edited by M. Shinozuka, 11/3/95, (PB96-176383, A15, MF-A03).

NCEER-95-0016 "Highway Culvert Performance During Earthquakes," by T.L. Youd and C.J. Beckman, available as NCEER-96-0015.

NCEER-95-0017 "The Hanshin-Awaji Earthquake of January 17, 1995: Performance of Highway Bridges," Edited by I.G. Buckle, 12/1/95, not available.

NCEER-95-0018 "Modeling of Masonry Infill Panels for Structural Analysis," by A.M. Reinhorn, A. Madan, R.E. Valles, Y. Reichmann and J.B. Mander, 12/8/95, (PB97-110886, MF-A01, A06).

NCEER-95-0019 "Optimal Polynomial Control for Linear and Nonlinear Structures," by A.K. Agrawal and J.N. Yang, 12/11/95, (PB96-168737, A07, MF-A02).

NCEER-95-0020 "Retrofit of Non-Ductile Reinforced Concrete Frames Using Friction Dampers," by R.S. Rao, P. Gergely and R.N. White, 12/22/95, (PB97-133508, A10, MF-A02).

NCEER-95-0021 "Parametric Results for Seismic Response of Pile-Supported Bridge Bents," by G. Mylonakis, A. Nikolaou and G. Gazetas, 12/22/95, (PB97-100242, A12, MF-A03).

NCEER-95-0022 "Kinematic Bending Moments in Seismically Stressed Piles," by A. Nikolaou, G. Mylonakis and G. Gazetas, 12/23/95, (PB97-113914, MF-A03, A13).

NCEER-96-0001 "Dynamic Response of Unreinforced Masonry Buildings with Flexible Diaphragms," by A.C. Costley and D.P. Abrams," 10/10/96, (PB97-133573, MF-A03, A15).

NCEER-96-0002 "State of the Art Review: Foundations and Retaining Structures," by I. Po Lam, not available.

NCEER-96-0003 "Ductility of Rectangular Reinforced Concrete Bridge Columns with Moderate Confinement," by N. Wehbe, M. Saiidi, D. Sanders and B. Douglas, 11/7/96, (PB97-133557, A06, MF-A02).

NCEER-96-0004 "Proceedings of the Long-Span Bridge Seismic Research Workshop," edited by I.G. Buckle and I.M. Friedland, not available.

NCEER-96-0005 "Establish Representative Pier Types for Comprehensive Study: Eastern United States," by J. Kulicki and Z. Prucz, 5/28/96, (PB98-119217, A07, MF-A02).

NCEER-96-0006 "Establish Representative Pier Types for Comprehensive Study: Western United States," by R. Imbsen, R.A. Schamber and T.A. Osterkamp, 5/28/96, (PB98-118607, A07, MF-A02).

NCEER-96-0007 "Nonlinear Control Techniques for Dynamical Systems with Uncertain Parameters," by R.G. Ghanem and M.I. Bujakov, 5/27/96, (PB97-100259, A17, MF-A03).

NCEER-96-0008 "Seismic Evaluation of a 30-Year Old Non-Ductile Highway Bridge Pier and Its Retrofit," by J.B. Mander, B. Mahmoodzadegan, S. Bhadra and S.S. Chen, 5/31/96, (PB97-110902, MF-A03, A10).

NCEER-96-0009 "Seismic Performance of a Model Reinforced Concrete Bridge Pier Before and After Retrofit," by J.B. Mander, J.H. Kim and C.A. Ligozio, 5/31/96, (PB97-110910, MF-A02, A10).

NCEER-96-0010 "IDARC2D Version 4.0: A Computer Program for the Inelastic Damage Analysis of Buildings," by R.E. Valles, A.M. Reinhorn, S.K. Kunnath, C. Li and A. Madan, 6/3/96, (PB97-100234, A17, MF-A03).

NCEER-96-0011 "Estimation of the Economic Impact of Multiple Lifeline Disruption: Memphis Light, Gas and Water Division Case Study," by S.E. Chang, H.A. Seligson and R.T. Eguchi, 8/16/96, (PB97-133490, A11, MF-A03).

NCEER-96-0012 "Proceedings from the Sixth Japan-U.S. Workshop on Earthquake Resistant Design of Lifeline Facilities and Countermeasures Against Soil Liquefaction, Edited by M. Hamada and T. O'Rourke, 9/11/96, (PB97-133581, A99, MF-A06).

NCEER-96-0013 "Chemical Hazards, Mitigation and Preparedness in Areas of High Seismic Risk: A Methodology for Estimating the Risk of Post-Earthquake Hazardous Materials Release," by H.A. Seligson, R.T. Eguchi, K.J. Tierney and K. Richmond, 11/7/96, (PB97-133565, MF-A02, A08).

NCEER-96-0014 "Response of Steel Bridge Bearings to Reversed Cyclic Loading," by J.B. Mander, D-K. Kim, S.S. Chen and G.J. Premus, 11/13/96, (PB97-140735, A12, MF-A03).

NCEER-96-0015 "Highway Culvert Performance During Past Earthquakes," by T.L. Youd and C.J. Beckman, 11/25/96, (PB97-133532, A06, MF-A01).

NCEER-97-0001 "Evaluation, Prevention and Mitigation of Pounding Effects in Building Structures," by R.E. Valles and A.M. Reinhorn, 2/20/97, (PB97-159552, A14, MF-A03).

NCEER-97-0002 "Seismic Design Criteria for Bridges and Other Highway Structures," by C. Rojahn, R. Mayes, D.G. Anderson, J. Clark, J.H. Hom, R.V. Nutt and M.J. O'Rourke, 4/30/97, (PB97-194658, A06, MF-A03).

NCEER-97-0003 “Proceedings of the U.S.-Italian Workshop on Seismic Evaluation and Retrofit,” Edited by D.P. Abrams and G.M. Calvi, 3/19/97, (PB97-194666, A13, MF-A03).

NCEER-97-0004 "Investigation of Seismic Response of Buildings with Linear and Nonlinear Fluid Viscous Dampers," by A.A. Seleemah and M.C. Constantinou, 5/21/97, (PB98-109002, A15, MF-A03).

NCEER-97-0005 "Proceedings of the Workshop on Earthquake Engineering Frontiers in Transportation Facilities," edited by G.C. Lee and I.M. Friedland, 8/29/97, (PB98-128911, A25, MR-A04).

NCEER-97-0006 "Cumulative Seismic Damage of Reinforced Concrete Bridge Piers," by S.K. Kunnath, A. El-Bahy, A. Taylor and W. Stone, 9/2/97, (PB98-108814, A11, MF-A03).

NCEER-97-0007 "Structural Details to Accommodate Seismic Movements of Highway Bridges and Retaining Walls," by R.A. Imbsen, R.A. Schamber, E. Thorkildsen, A. Kartoum, B.T. Martin, T.N. Rosser and J.M. Kulicki, 9/3/97, (PB98-108996, A09, MF-A02).

NCEER-97-0008 "A Method for Earthquake Motion-Damage Relationships with Application to Reinforced Concrete Frames," by A. Singhal and A.S. Kiremidjian, 9/10/97, (PB98-108988, A13, MF-A03).

NCEER-97-0009 "Seismic Analysis and Design of Bridge Abutments Considering Sliding and Rotation," by K. Fishman and R. Richards, Jr., 9/15/97, (PB98-108897, A06, MF-A02).

NCEER-97-0010 "Proceedings of the FHWA/NCEER Workshop on the National Representation of Seismic Ground Motion for New and Existing Highway Facilities," edited by I.M. Friedland, M.S. Power and R.L. Mayes, 9/22/97, (PB98-128903, A21, MF-A04).

NCEER-97-0011 "Seismic Analysis for Design or Retrofit of Gravity Bridge Abutments," by K.L. Fishman, R. Richards, Jr. and R.C. Divito, 10/2/97, (PB98-128937, A08, MF-A02).

NCEER-97-0012 "Evaluation of Simplified Methods of Analysis for Yielding Structures," by P. Tsopelas, M.C. Constantinou, C.A. Kircher and A.S. Whittaker, 10/31/97, (PB98-128929, A10, MF-A03).

NCEER-97-0013 "Seismic Design of Bridge Columns Based on Control and Repairability of Damage," by C-T. Cheng and J.B. Mander, 12/8/97, (PB98-144249, A11, MF-A03).

NCEER-97-0014 "Seismic Resistance of Bridge Piers Based on Damage Avoidance Design," by J.B. Mander and C-T. Cheng, 12/10/97, (PB98-144223, A09, MF-A02).

NCEER-97-0015 “Seismic Response of Nominally Symmetric Systems with Strength Uncertainty,” by S. Balopoulou and M. Grigoriu, 12/23/97, (PB98-153422, A11, MF-A03).

NCEER-97-0016 “Evaluation of Seismic Retrofit Methods for Reinforced Concrete Bridge Columns,” by T.J. Wipf, F.W. Klaiber and F.M. Russo, 12/28/97, (PB98-144215, A12, MF-A03).

NCEER-97-0017 “Seismic Fragility of Existing Conventional Reinforced Concrete Highway Bridges,” by C.L. Mullen and A.S. Cakmak, 12/30/97, (PB98-153406, A08, MF-A02).

NCEER-97-0018 “Loss Asssessment of Memphis Buildings,” edited by D.P. Abrams and M. Shinozuka, 12/31/97, (PB98-144231, A13, MF-A03).

NCEER-97-0019 “Seismic Evaluation of Frames with Infill Walls Using Quasi-static Experiments,” by K.M. Mosalam, R.N. White and P. Gergely, 12/31/97, (PB98-153455, A07, MF-A02).

NCEER-97-0020 “Seismic Evaluation of Frames with Infill Walls Using Pseudo-dynamic Experiments,” by K.M. Mosalam, R.N. White and P. Gergely, 12/31/97, (PB98-153430, A07, MF-A02).

NCEER-97-0021 “Computational Strategies for Frames with Infill Walls: Discrete and Smeared Crack Analyses and Seismic Fragility,” by K.M. Mosalam, R.N. White and P. Gergely, 12/31/97, (PB98-153414, A10, MF-A02).

NCEER-97-0022 "Proceedings of the NCEER Workshop on Evaluation of Liquefaction Resistance of Soils," edited by T.L. Youd and I.M. Idriss, 12/31/97, (PB98-155617, A15, MF-A03).

MCEER-98-0001 "Extraction of Nonlinear Hysteretic Properties of Seismically Isolated Bridges from Quick-Release Field Tests," by Q. Chen, B.M. Douglas, E.M. Maragakis and I.G. Buckle, 5/26/98, (PB99-118838, A06, MF-A01).

MCEER-98-0002 "Methodologies for Evaluating the Importance of Highway Bridges," by A. Thomas, S. Eshenaur and J. Kulicki, 5/29/98, (PB99-118846, A10, MF-A02).

MCEER-98-0003 "Capacity Design of Bridge Piers and the Analysis of Overstrength," by J.B. Mander, A. Dutta and P. Goel, 6/1/98, (PB99-118853, A09, MF-A02).

MCEER-98-0004 "Evaluation of Bridge Damage Data from the Loma Prieta and Northridge, California Earthquakes," by N. Basoz and A. Kiremidjian, 6/2/98, (PB99-118861, A15, MF-A03).

MCEER-98-0005 "Screening Guide for Rapid Assessment of Liquefaction Hazard at Highway Bridge Sites," by T. L. Youd, 6/16/98, (PB99-118879, A06, not available on microfiche).

MCEER-98-0006 "Structural Steel and Steel/Concrete Interface Details for Bridges," by P. Ritchie, N. Kauhl and J. Kulicki, 7/13/98, (PB99-118945, A06, MF-A01).

MCEER-98-0007 "Capacity Design and Fatigue Analysis of Confined Concrete Columns," by A. Dutta and J.B. Mander, 7/14/98, (PB99-118960, A14, MF-A03).

MCEER-98-0008 "Proceedings of the Workshop on Performance Criteria for Telecommunication Services Under Earthquake Conditions," edited by A.J. Schiff, 7/15/98, (PB99-118952, A08, MF-A02).

MCEER-98-0009 "Fatigue Analysis of Unconfined Concrete Columns," by J.B. Mander, A. Dutta and J.H. Kim, 9/12/98, (PB99-123655, A10, MF-A02).

MCEER-98-0010 "Centrifuge Modeling of Cyclic Lateral Response of Pile-Cap Systems and Seat-Type Abutments in Dry Sands," by A.D. Gadre and R. Dobry, 10/2/98, (PB99-123606, A13, MF-A03).

MCEER-98-0011 "IDARC-BRIDGE: A Computational Platform for Seismic Damage Assessment of Bridge Structures," by A.M. Reinhorn, V. Simeonov, G. Mylonakis and Y. Reichman, 10/2/98, (PB99-162919, A15, MF-A03).

MCEER-98-0012 "Experimental Investigation of the Dynamic Response of Two Bridges Before and After Retrofitting with Elastomeric Bearings," by D.A. Wendichansky, S.S. Chen and J.B. Mander, 10/2/98, (PB99-162927, A15, MF-A03).

MCEER-98-0013 "Design Procedures for Hinge Restrainers and Hinge Sear Width for Multiple-Frame Bridges," by R. Des Roches and G.L. Fenves, 11/3/98, (PB99-140477, A13, MF-A03).

MCEER-98-0014 "Response Modification Factors for Seismically Isolated Bridges," by M.C. Constantinou and J.K. Quarshie, 11/3/98, (PB99-140485, A14, MF-A03).

MCEER-98-0015 "Proceedings of the U.S.-Italy Workshop on Seismic Protective Systems for Bridges," edited by I.M. Friedland and M.C. Constantinou, 11/3/98, (PB2000-101711, A22, MF-A04).

MCEER-98-0016 "Appropriate Seismic Reliability for Critical Equipment Systems: Recommendations Based on Regional Analysis of Financial and Life Loss," by K. Porter, C. Scawthorn, C. Taylor and N. Blais, 11/10/98, (PB99-157265, A08, MF-A02).

MCEER-98-0017 "Proceedings of the U.S. Japan Joint Seminar on Civil Infrastructure Systems Research," edited by M. Shinozuka and A. Rose, 11/12/98, (PB99-156713, A16, MF-A03).

MCEER-98-0018 "Modeling of Pile Footings and Drilled Shafts for Seismic Design," by I. PoLam, M. Kapuskar and D. Chaudhuri, 12/21/98, (PB99-157257, A09, MF-A02).

MCEER-99-0001 "Seismic Evaluation of a Masonry Infilled Reinforced Concrete Frame by Pseudodynamic Testing," by S.G. Buonopane and R.N. White, 2/16/99, (PB99-162851, A09, MF-A02).

MCEER-99-0002 "Response History Analysis of Structures with Seismic Isolation and Energy Dissipation Systems: Verification Examples for Program SAP2000," by J. Scheller and M.C. Constantinou, 2/22/99, (PB99-162869, A08, MF-A02).

MCEER-99-0003 "Experimental Study on the Seismic Design and Retrofit of Bridge Columns Including Axial Load Effects," by A. Dutta, T. Kokorina and J.B. Mander, 2/22/99, (PB99-162877, A09, MF-A02).

MCEER-99-0004 "Experimental Study of Bridge Elastomeric and Other Isolation and Energy Dissipation Systems with Emphasis on Uplift Prevention and High Velocity Near-source Seismic Excitation," by A. Kasalanati and M. C. Constantinou, 2/26/99, (PB99-162885, A12, MF-A03).

MCEER-99-0005 "Truss Modeling of Reinforced Concrete Shear-flexure Behavior," by J.H. Kim and J.B. Mander, 3/8/99, (PB99-163693, A12, MF-A03).

MCEER-99-0006 "Experimental Investigation and Computational Modeling of Seismic Response of a 1:4 Scale Model Steel Structure with a Load Balancing Supplemental Damping System," by G. Pekcan, J.B. Mander and S.S. Chen, 4/2/99, (PB99-162893, A11, MF-A03).

MCEER-99-0007 "Effect of Vertical Ground Motions on the Structural Response of Highway Bridges," by M.R. Button, C.J. Cronin and R.L. Mayes, 4/10/99, (PB2000-101411, A10, MF-A03).

MCEER-99-0008 "Seismic Reliability Assessment of Critical Facilities: A Handbook, Supporting Documentation, and Model Code Provisions," by G.S. Johnson, R.E. Sheppard, M.D. Quilici, S.J. Eder and C.R. Scawthorn, 4/12/99, (PB2000-101701, A18, MF-A04).

MCEER-99-0009 "Impact Assessment of Selected MCEER Highway Project Research on the Seismic Design of Highway Structures," by C. Rojahn, R. Mayes, D.G. Anderson, J.H. Clark, D'Appolonia Engineering, S. Gloyd and R.V. Nutt, 4/14/99, (PB99-162901, A10, MF-A02).

MCEER-99-0010 "Site Factors and Site Categories in Seismic Codes," by R. Dobry, R. Ramos and M.S. Power, 7/19/99, (PB2000-101705, A08, MF-A02).

MCEER-99-0011 "Restrainer Design Procedures for Multi-Span Simply-Supported Bridges," by M.J. Randall, M. Saiidi, E. Maragakis and T. Isakovic, 7/20/99, (PB2000-101702, A10, MF-A02).

MCEER-99-0012 "Property Modification Factors for Seismic Isolation Bearings," by M.C. Constantinou, P. Tsopelas, A. Kasalanati and E. Wolff, 7/20/99, (PB2000-103387, A11, MF-A03).

MCEER-99-0013 "Critical Seismic Issues for Existing Steel Bridges," by P. Ritchie, N. Kauhl and J. Kulicki, 7/20/99, (PB2000-101697, A09, MF-A02).

MCEER-99-0014 "Nonstructural Damage Database," by A. Kao, T.T. Soong and A. Vender, 7/24/99, (PB2000-101407, A06, MF-A01).

MCEER-99-0015 "Guide to Remedial Measures for Liquefaction Mitigation at Existing Highway Bridge Sites," by H.G. Cooke and J. K. Mitchell, 7/26/99, (PB2000-101703, A11, MF-A03).

MCEER-99-0016 "Proceedings of the MCEER Workshop on Ground Motion Methodologies for the Eastern United States," edited by N. Abrahamson and A. Becker, 8/11/99, (PB2000-103385, A07, MF-A02).

MCEER-99-0017 "Quindío, Colombia Earthquake of January 25, 1999: Reconnaissance Report," by A.P. Asfura and P.J. Flores, 10/4/99, (PB2000-106893, A06, MF-A01).

MCEER-99-0018 "Hysteretic Models for Cyclic Behavior of Deteriorating Inelastic Structures," by M.V. Sivaselvan and A.M. Reinhorn, 11/5/99, (PB2000-103386, A08, MF-A02).

MCEER-99-0019 "Proceedings of the 7th U.S.- Japan Workshop on Earthquake Resistant Design of Lifeline Facilities and Countermeasures Against Soil Liquefaction," edited by T.D. O'Rourke, J.P. Bardet and M. Hamada, 11/19/99, (PB2000-103354, A99, MF-A06).

MCEER-99-0020 "Development of Measurement Capability for Micro-Vibration Evaluations with Application to Chip Fabrication Facilities," by G.C. Lee, Z. Liang, J.W. Song, J.D. Shen and W.C. Liu, 12/1/99, (PB2000-105993, A08, MF-A02).

MCEER-99-0021 "Design and Retrofit Methodology for Building Structures with Supplemental Energy Dissipating Systems," by G. Pekcan, J.B. Mander and S.S. Chen, 12/31/99, (PB2000-105994, A11, MF-A03).

MCEER-00-0001 "The Marmara, Turkey Earthquake of August 17, 1999: Reconnaissance Report," edited by C. Scawthorn; with major contributions by M. Bruneau, R. Eguchi, T. Holzer, G. Johnson, J. Mander, J. Mitchell, W. Mitchell, A. Papageorgiou, C. Scaethorn, and G. Webb, 3/23/00, (PB2000-106200, A11, MF-A03).

MCEER-00-0002 "Proceedings of the MCEER Workshop for Seismic Hazard Mitigation of Health Care Facilities," edited by G.C. Lee, M. Ettouney, M. Grigoriu, J. Hauer and J. Nigg, 3/29/00, (PB2000-106892, A08, MF-A02).

MCEER-00-0003 "The Chi-Chi, Taiwan Earthquake of September 21, 1999: Reconnaissance Report," edited by G.C. Lee and C.H. Loh, with major contributions by G.C. Lee, M. Bruneau, I.G. Buckle, S.E. Chang, P.J. Flores, T.D. O'Rourke, M. Shinozuka, T.T. Soong, C-H. Loh, K-C. Chang, Z-J. Chen, J-S. Hwang, M-L. Lin, G-Y. Liu, K-C. Tsai, G.C. Yao and C-L. Yen, 4/30/00, (PB2001-100980, A10, MF-A02).

MCEER-00-0004 "Seismic Retrofit of End-Sway Frames of Steel Deck-Truss Bridges with a Supplemental Tendon System: Experimental and Analytical Investigation," by G. Pekcan, J.B. Mander and S.S. Chen, 7/1/00, (PB2001-100982, A10, MF-A02).

MCEER-00-0005 "Sliding Fragility of Unrestrained Equipment in Critical Facilities," by W.H. Chong and T.T. Soong, 7/5/00, (PB2001-100983, A08, MF-A02).

MCEER-00-0006 "Seismic Response of Reinforced Concrete Bridge Pier Walls in the Weak Direction," by N. Abo-Shadi, M. Saiidi and D. Sanders, 7/17/00, (PB2001-100981, A17, MF-A03).

MCEER-00-0007 "Low-Cycle Fatigue Behavior of Longitudinal Reinforcement in Reinforced Concrete Bridge Columns," by J. Brown and S.K. Kunnath, 7/23/00, (PB2001-104392, A08, MF-A02).

MCEER-00-0008 "Soil Structure Interaction of Bridges for Seismic Analysis," I. PoLam and H. Law, 9/25/00, (PB2001-105397, A08, MF-A02).

MCEER-00-0009 "Proceedings of the First MCEER Workshop on Mitigation of Earthquake Disaster by Advanced Technologies (MEDAT-1), edited by M. Shinozuka, D.J. Inman and T.D. O'Rourke, 11/10/00, (PB2001-105399, A14, MF-A03).

MCEER-00-0010 "Development and Evaluation of Simplified Procedures for Analysis and Design of Buildings with Passive Energy Dissipation Systems, Revision 01," by O.M. Ramirez, M.C. Constantinou, C.A. Kircher, A.S. Whittaker, M.W. Johnson, J.D. Gomez and C. Chrysostomou, 11/16/01, (PB2001-105523, A23, MF-A04).

MCEER-00-0011 "Dynamic Soil-Foundation-Structure Interaction Analyses of Large Caissons," by C-Y. Chang, C-M. Mok, Z-L. Wang, R. Settgast, F. Waggoner, M.A. Ketchum, H.M. Gonnermann and C-C. Chin, 12/30/00, (PB2001-104373, A07, MF-A02).

MCEER-00-0012 "Experimental Evaluation of Seismic Performance of Bridge Restrainers," by A.G. Vlassis, E.M. Maragakis and M. Saiid Saiidi, 12/30/00, (PB2001-104354, A09, MF-A02).

MCEER-00-0013 "Effect of Spatial Variation of Ground Motion on Highway Structures," by M. Shinozuka, V. Saxena and G. Deodatis, 12/31/00, (PB2001-108755, A13, MF-A03).

MCEER-00-0014 "A Risk-Based Methodology for Assessing the Seismic Performance of Highway Systems," by S.D. Werner, C.E. Taylor, J.E. Moore, II, J.S. Walton and S. Cho, 12/31/00, (PB2001-108756, A14, MF-A03).

MCEER-01-0001 "Experimental Investigation of P-Delta Effects to Collapse During Earthquakes," by D. Vian and M. Bruneau, 6/25/01, (PB2002-100534, A17, MF-A03).

MCEER-01-0002 "Proceedings of the Second MCEER Workshop on Mitigation of Earthquake Disaster by Advanced Technologies (MEDAT-2)," edited by M. Bruneau and D.J. Inman, 7/23/01, (PB2002-100434, A16, MF-A03).

MCEER-01-0003 "Sensitivity Analysis of Dynamic Systems Subjected to Seismic Loads," by C. Roth and M. Grigoriu, 9/18/01, (PB2003-100884, A12, MF-A03).

MCEER-01-0004 "Overcoming Obstacles to Implementing Earthquake Hazard Mitigation Policies: Stage 1 Report," by D.J. Alesch and W.J. Petak, 12/17/01, (PB2002-107949, A07, MF-A02).

MCEER-01-0005 "Updating Real-Time Earthquake Loss Estimates: Methods, Problems and Insights," by C.E. Taylor, S.E. Chang and R.T. Eguchi, 12/17/01, (PB2002-107948, A05, MF-A01).

MCEER-01-0006 "Experimental Investigation and Retrofit of Steel Pile Foundations and Pile Bents Under Cyclic Lateral Loadings," by A. Shama, J. Mander, B. Blabac and S. Chen, 12/31/01, (PB2002-107950, A13, MF-A03).

MCEER-02-0001 "Assessment of Performance of Bolu Viaduct in the 1999 Duzce Earthquake in Turkey" by P.C. Roussis, M.C. Constantinou, M. Erdik, E. Durukal and M. Dicleli, 5/8/02, (PB2003-100883, A08, MF-A02).

MCEER-02-0002 "Seismic Behavior of Rail Counterweight Systems of Elevators in Buildings," by M.P. Singh, Rildova and L.E. Suarez, 5/27/02. (PB2003-100882, A11, MF-A03).

MCEER-02-0003 "Development of Analysis and Design Procedures for Spread Footings," by G. Mylonakis, G. Gazetas, S. Nikolaou and A. Chauncey, 10/02/02, (PB2004-101636, A13, MF-A03, CD-A13).

MCEER-02-0004 "Bare-Earth Algorithms for Use with SAR and LIDAR Digital Elevation Models," by C.K. Huyck, R.T. Eguchi and B. Houshmand, 10/16/02, (PB2004-101637, A07, CD-A07).

MCEER-02-0005 "Review of Energy Dissipation of Compression Members in Concentrically Braced Frames," by K.Lee and M. Bruneau, 10/18/02, (PB2004-101638, A10, CD-A10).

MCEER-03-0001 "Experimental Investigation of Light-Gauge Steel Plate Shear Walls for the Seismic Retrofit of Buildings" by J. Berman and M. Bruneau, 5/2/03, (PB2004-101622, A10, MF-A03, CD-A10).

MCEER-03-0002 "Statistical Analysis of Fragility Curves," by M. Shinozuka, M.Q. Feng, H. Kim, T. Uzawa and T. Ueda, 6/16/03, (PB2004-101849, A09, CD-A09).

MCEER-03-0003 "Proceedings of the Eighth U.S.-Japan Workshop on Earthquake Resistant Design f Lifeline Facilities and Countermeasures Against Liquefaction," edited by M. Hamada, J.P. Bardet and T.D. O'Rourke, 6/30/03, (PB2004-104386, A99, CD-A99).

MCEER-03-0004 "Proceedings of the PRC-US Workshop on Seismic Analysis and Design of Special Bridges," edited by L.C. Fan and G.C. Lee, 7/15/03, (PB2004-104387, A14, CD-A14).

MCEER-03-0005 "Urban Disaster Recovery: A Framework and Simulation Model," by S.B. Miles and S.E. Chang, 7/25/03, (PB2004-104388, A07, CD-A07).

MCEER-03-0006 "Behavior of Underground Piping Joints Due to Static and Dynamic Loading," by R.D. Meis, M. Maragakis and R. Siddharthan, 11/17/03, (PB2005-102194, A13, MF-A03, CD-A00).

MCEER-04-0001 "Experimental Study of Seismic Isolation Systems with Emphasis on Secondary System Response and Verification of Accuracy of Dynamic Response History Analysis Methods," by E. Wolff and M. Constantinou, 1/16/04 (PB2005-102195, A99, MF-E08, CD-A00).

MCEER-04-0002 "Tension, Compression and Cyclic Testing of Engineered Cementitious Composite Materials," by K. Kesner and S.L. Billington, 3/1/04, (PB2005-102196, A08, CD-A08).

MCEER-04-0003 "Cyclic Testing of Braces Laterally Restrained by Steel Studs to Enhance Performance During Earthquakes," by O.C. Celik, J.W. Berman and M. Bruneau, 3/16/04, (PB2005-102197, A13, MF-A03, CD-A00).

MCEER-04-0004 "Methodologies for Post Earthquake Building Damage Detection Using SAR and Optical Remote Sensing: Application to the August 17, 1999 Marmara, Turkey Earthquake," by C.K. Huyck, B.J. Adams, S. Cho, R.T. Eguchi, B. Mansouri and B. Houshmand, 6/15/04, (PB2005-104888, A10, CD-A00).

MCEER-04-0005 "Nonlinear Structural Analysis Towards Collapse Simulation: A Dynamical Systems Approach," by M.V. Sivaselvan and A.M. Reinhorn, 6/16/04, (PB2005-104889, A11, MF-A03, CD-A00).

MCEER-04-0006 "Proceedings of the Second PRC-US Workshop on Seismic Analysis and Design of Special Bridges," edited by G.C. Lee and L.C. Fan, 6/25/04, (PB2005-104890, A16, CD-A00).

MCEER-04-0007 "Seismic Vulnerability Evaluation of Axially Loaded Steel Built-up Laced Members," by K. Lee and M. Bruneau, 6/30/04, (PB2005-104891, A16, CD-A00).

MCEER-04-0008 "Evaluation of Accuracy of Simplified Methods of Analysis and Design of Buildings with Damping Systems for Near-Fault and for Soft-Soil Seismic Motions," by E.A. Pavlou and M.C. Constantinou, 8/16/04, (PB2005-104892, A08, MF-A02, CD-A00).

MCEER-04-0009 "Assessment of Geotechnical Issues in Acute Care Facilities in California," by M. Lew, T.D. O'Rourke, R. Dobry and M. Koch, 9/15/04, (PB2005-104893, A08, CD-A00).

MCEER-04-0010 "Scissor-Jack-Damper Energy Dissipation System," by A.N. Sigaher-Boyle and M.C. Constantinou, 12/1/04 (PB2005-108221).

MCEER-04-0011 "Seismic Retrofit of Bridge Steel Truss Piers Using a Controlled Rocking Approach," by M. Pollino and M. Bruneau, 12/20/04 (PB2006-105795).

MCEER-05-0001 "Experimental and Analytical Studies of Structures Seismically Isolated with an Uplift-Restraint Isolation System," by P.C. Roussis and M.C. Constantinou, 1/10/05 (PB2005-108222).

MCEER-05-0002 "A Versatile Experimentation Model for Study of Structures Near Collapse Applied to Seismic Evaluation of Irregular Structures," by D. Kusumastuti, A.M. Reinhorn and A. Rutenberg, 3/31/05 (PB2006-101523).

MCEER-05-0003 "Proceedings of the Third PRC-US Workshop on Seismic Analysis and Design of Special Bridges," edited by L.C. Fan and G.C. Lee, 4/20/05, (PB2006-105796).

MCEER-05-0004 "Approaches for the Seismic Retrofit of Braced Steel Bridge Piers and Proof-of-Concept Testing of an Eccentrically Braced Frame with Tubular Link," by J.W. Berman and M. Bruneau, 4/21/05 (PB2006-101524).

MCEER-05-0005 "Simulation of Strong Ground Motions for Seismic Fragility Evaluation of Nonstructural Components in Hospitals," by A. Wanitkorkul and A. Filiatrault, 5/26/05 (PB2006-500027).

MCEER-05-0006 "Seismic Safety in California Hospitals: Assessing an Attempt to Accelerate the Replacement or Seismic Retrofit of Older Hospital Facilities," by D.J. Alesch, L.A. Arendt and W.J. Petak, 6/6/05 (PB2006-105794).

MCEER-05-0007 "Development of Seismic Strengthening and Retrofit Strategies for Critical Facilities Using Engineered Cementitious Composite Materials," by K. Kesner and S.L. Billington, 8/29/05 (PB2006-111701).

MCEER-05-0008 "Experimental and Analytical Studies of Base Isolation Systems for Seismic Protection of Power Transformers," by N. Murota, M.Q. Feng and G-Y. Liu, 9/30/05 (PB2006-111702).

MCEER-05-0009 "3D-BASIS-ME-MB: Computer Program for Nonlinear Dynamic Analysis of Seismically Isolated Structures," by P.C. Tsopelas, P.C. Roussis, M.C. Constantinou, R. Buchanan and A.M. Reinhorn, 10/3/05 (PB2006-111703).

MCEER-05-0010 "Steel Plate Shear Walls for Seismic Design and Retrofit of Building Structures," by D. Vian and M. Bruneau, 12/15/05 (PB2006-111704).

MCEER-05-0011 "The Performance-Based Design Paradigm," by M.J. Astrella and A. Whittaker, 12/15/05 (PB2006-111705).

MCEER-06-0001 "Seismic Fragility of Suspended Ceiling Systems," H. Badillo-Almaraz, A.S. Whittaker, A.M. Reinhorn and G.P. Cimellaro, 2/4/06 (PB2006-111706).

MCEER-06-0002 "Multi-Dimensional Fragility of Structures," by G.P. Cimellaro, A.M. Reinhorn and M. Bruneau, 3/1/06 (PB2007-106974, A09, MF-A02, CD A00).

MCEER-06-0003 "Built-Up Shear Links as Energy Dissipators for Seismic Protection of Bridges," by P. Dusicka, A.M. Itani and I.G. Buckle, 3/15/06 (PB2006-111708).

MCEER-06-0004 "Analytical Investigation of the Structural Fuse Concept," by R.E. Vargas and M. Bruneau, 3/16/06 (PB2006-111709).

MCEER-06-0005 "Experimental Investigation of the Structural Fuse Concept," by R.E. Vargas and M. Bruneau, 3/17/06 (PB2006-111710).

MCEER-06-0006 "Further Development of Tubular Eccentrically Braced Frame Links for the Seismic Retrofit of Braced Steel Truss Bridge Piers," by J.W. Berman and M. Bruneau, 3/27/06 (PB2007-105147).

MCEER-06-0007 "REDARS Validation Report," by S. Cho, C.K. Huyck, S. Ghosh and R.T. Eguchi, 8/8/06 (PB2007-106983).

MCEER-06-0008 "Review of Current NDE Technologies for Post-Earthquake Assessment of Retrofitted Bridge Columns," by J.W. Song, Z. Liang and G.C. Lee, 8/21/06 (PB2007-106984).

MCEER-06-0009 "Liquefaction Remediation in Silty Soils Using Dynamic Compaction and Stone Columns," by S. Thevanayagam, G.R. Martin, R. Nashed, T. Shenthan, T. Kanagalingam and N. Ecemis, 8/28/06 (PB2007-106985).

MCEER-06-0010 "Conceptual Design and Experimental Investigation of Polymer Matrix Composite Infill Panels for Seismic Retrofitting," by W. Jung, M. Chiewanichakorn and A.J. Aref, 9/21/06 (PB2007-106986).

MCEER-06-0011 "A Study of the Coupled Horizontal-Vertical Behavior of Elastomeric and Lead-Rubber Seismic Isolation Bearings," by G.P. Warn and A.S. Whittaker, 9/22/06 (PB2007-108679).

MCEER-06-0012 "Proceedings of the Fourth PRC-US Workshop on Seismic Analysis and Design of Special Bridges: Advancing Bridge Technologies in Research, Design, Construction and Preservation," Edited by L.C. Fan, G.C. Lee and L. Ziang, 10/12/06 (PB2007-109042).

MCEER-06-0013 "Cyclic Response and Low Cycle Fatigue Characteristics of Plate Steels," by P. Dusicka, A.M. Itani and I.G. Buckle, 11/1/06 06 (PB2007-106987).

MCEER-06-0014 "Proceedings of the Second US-Taiwan Bridge Engineering Workshop," edited by W.P. Yen, J. Shen, J-Y. Chen and M. Wang, 11/15/06 (PB2008-500041).

MCEER-06-0015 "User Manual and Technical Documentation for the REDARS^{TM} Import Wizard," by S. Cho, S. Ghosh, C.K. Huyck and S.D. Werner, 11/30/06 (PB2007-114766).

MCEER-06-0016 "Hazard Mitigation Strategy and Monitoring Technologies for Urban and Infrastructure Public Buildings: Proceedings of the China-US Workshops," edited by X.Y. Zhou, A.L. Zhang, G.C. Lee and M. Tong, 12/12/06 (PB2008-500018).

MCEER-07-0001 "Static and Kinetic Coefficients of Friction for Rigid Blocks," by C. Kafali, S. Fathali, M. Grigoriu and A.S. Whittaker, 3/20/07 (PB2007-114767).

MCEER-07-0002 "Hazard Mitigation Investment Decision Making: Organizational Response to Legislative Mandate," by L.A. Arendt, D.J. Alesch and W.J. Petak, 4/9/07 (PB2007-114768).

MCEER-07-0003 "Seismic Behavior of Bidirectional-Resistant Ductile End Diaphragms with Unbonded Braces in Straight or Skewed Steel Bridges," by O. Celik and M. Bruneau, 4/11/07 (PB2008-105141).

MCEER-07-0004 "Modeling Pile Behavior in Large Pile Groups Under Lateral Loading," by A.M. Dodds and G.R. Martin, 4/16/07(PB2008-105142).

MCEER-07-0005 "Experimental Investigation of Blast Performance of Seismically Resistant Concrete-Filled Steel Tube Bridge Piers," by S. Fujikura, M. Bruneau and D. Lopez-Garcia, 4/20/07 (PB2008-105143).

MCEER-07-0006 "Seismic Analysis of Conventional and Isolated Liquefied Natural Gas Tanks Using Mechanical Analogs," by I.P. Christovasilis and A.S. Whittaker, 5/1/07, not available.

MCEER-07-0007 "Experimental Seismic Performance Evaluation of Isolation/Restraint Systems for Mechanical Equipment – Part 1: Heavy Equipment Study," by S. Fathali and A. Filiatrault, 6/6/07 (PB2008-105144).

MCEER-07-0008 "Seismic Vulnerability of Timber Bridges and Timber Substructures," by A.A. Sharma, J.B. Mander, I.M. Friedland and D.R. Allicock, 6/7/07 (PB2008-105145).

MCEER-07-0009 "Experimental and Analytical Study of the XY-Friction Pendulum (XY-FP) Bearing for Bridge Applications," by C.C. Marin-Artieda, A.S. Whittaker and M.C. Constantinou, 6/7/07 (PB2008-105191).

MCEER-07-0010 "Proceedings of the PRC-US Earthquake Engineering Forum for Young Researchers," Edited by G.C. Lee and X.Z. Qi, 6/8/07 (PB2008-500058).

MCEER-07-0011 "Design Recommendations for Perforated Steel Plate Shear Walls," by R. Purba and M. Bruneau, 6/18/07, (PB2008-105192).

MCEER-07-0012 "Performance of Seismic Isolation Hardware Under Service and Seismic Loading," by M.C. Constantinou, A.S. Whittaker, Y. Kalpakidis, D.M. Fenz and G.P. Warn, 8/27/07, (PB2008-105193).

MCEER-07-0013 "Experimental Evaluation of the Seismic Performance of Hospital Piping Subassemblies," by E.R. Goodwin, E. Maragakis and A.M. Itani, 9/4/07, (PB2008-105194).

MCEER-07-0014 "A Simulation Model of Urban Disaster Recovery and Resilience: Implementation for the 1994 Northridge Earthquake," by S. Miles and S.E. Chang, 9/7/07, (PB2008-106426).

MCEER-07-0015 "Statistical and Mechanistic Fragility Analysis of Concrete Bridges," by M. Shinozuka, S. Banerjee and S-H. Kim, 9/10/07, (PB2008-106427).

MCEER-07-0016 "Three-Dimensional Modeling of Inelastic Buckling in Frame Structures," by M. Schachter and AM. Reinhorn, 9/13/07, (PB2008-108125).

MCEER-07-0017 "Modeling of Seismic Wave Scattering on Pile Groups and Caissons," by I. Po Lam, H. Law and C.T. Yang, 9/17/07 (PB2008-108150).

MCEER-07-0018 "Bridge Foundations: Modeling Large Pile Groups and Caissons for Seismic Design," by I. Po Lam, H. Law and G.R. Martin (Coordinating Author), 12/1/07 (PB2008-111190).

MCEER-07-0019 "Principles and Performance of Roller Seismic Isolation Bearings for Highway Bridges," by G.C. Lee, Y.C. Ou, Z. Liang, T.C. Niu and J. Song, 12/10/07 (PB2009-110466).

MCEER-07-0020 "Centrifuge Modeling of Permeability and Pinning Reinforcement Effects on Pile Response to Lateral Spreading," by L.L Gonzalez-Lagos, T. Abdoun and R. Dobry, 12/10/07 (PB2008-111191).

MCEER-07-0021 "Damage to the Highway System from the Pisco, Perú Earthquake of August 15, 2007," by J.S. O'Connor, L. Mesa and M. Nykamp, 12/10/07, (PB2008-108126).

MCEER-07-0022 "Experimental Seismic Performance Evaluation of Isolation/Restraint Systems for Mechanical Equipment – Part 2: Light Equipment Study," by S. Fathali and A. Filiatrault, 12/13/07 (PB2008-111192).

MCEER-07-0023 "Fragility Considerations in Highway Bridge Design," by M. Shinozuka, S. Banerjee and S.H. Kim, 12/14/07 (PB2008-111193).

MCEER-07-0024 "Performance Estimates for Seismically Isolated Bridges," by G.P. Warn and A.S. Whittaker, 12/30/07 (PB2008-112230).

MCEER-08-0001 "Seismic Performance of Steel Girder Bridge Superstructures with Conventional Cross Frames," by L.P. Carden, A.M. Itani and I.G. Buckle, 1/7/08, (PB2008-112231).

MCEER-08-0002 "Seismic Performance of Steel Girder Bridge Superstructures with Ductile End Cross Frames with Seismic Isolators," by L.P. Carden, A.M. Itani and I.G. Buckle, 1/7/08 (PB2008-112232).

MCEER-08-0003 "Analytical and Experimental Investigation of a Controlled Rocking Approach for Seismic Protection of Bridge Steel Truss Piers," by M. Pollino and M. Bruneau, 1/21/08 (PB2008-112233).

MCEER-08-0004 "Linking Lifeline Infrastructure Performance and Community Disaster Resilience: Models and Multi-Stakeholder Processes," by S.E. Chang, C. Pasion, K. Tatebe and R. Ahmad, 3/3/08 (PB2008-112234).

MCEER-08-0005 "Modal Analysis of Generally Damped Linear Structures Subjected to Seismic Excitations," by J. Song, Y-L. Chu, Z. Liang and G.C. Lee, 3/4/08 (PB2009-102311).

MCEER-08-0006 "System Performance Under Multi-Hazard Environments," by C. Kafali and M. Grigoriu, 3/4/08 (PB2008-112235).

MCEER-08-0007 "Mechanical Behavior of Multi-Spherical Sliding Bearings," by D.M. Fenz and M.C. Constantinou, 3/6/08 (PB2008-112236).

MCEER-08-0008 "Post-Earthquake Restoration of the Los Angeles Water Supply System," by T.H.P. Tabucchi and R.A. Davidson, 3/7/08 (PB2008-112237).

MCEER-08-0009 "Fragility Analysis of Water Supply Systems," by A. Jacobson and M. Grigoriu, 3/10/08 (PB2009-105545).

MCEER-08-0010 "Experimental Investigation of Full-Scale Two-Story Steel Plate Shear Walls with Reduced Beam Section Connections," by B. Qu, M. Bruneau, C-H. Lin and K-C. Tsai, 3/17/08 (PB2009-106368).

MCEER-08-0011 "Seismic Evaluation and Rehabilitation of Critical Components of Electrical Power Systems," S. Ersoy, B. Feizi, A. Ashrafi and M. Ala Saadeghvaziri, 3/17/08 (PB2009-105546).

MCEER-08-0012 "Seismic Behavior and Design of Boundary Frame Members of Steel Plate Shear Walls," by B. Qu and M. Bruneau, 4/26/08 . (PB2009-106744).

MCEER-08-0013 "Development and Appraisal of a Numerical Cyclic Loading Protocol for Quantifying Building System Performance," by A. Filiatrault, A. Wanitkorkul and M. Constantinou, 4/27/08 (PB2009-107906).

MCEER-08-0014 "Structural and Nonstructural Earthquake Design: The Challenge of Integrating Specialty Areas in Designing Complex, Critical Facilities," by W.J. Petak and D.J. Alesch, 4/30/08 (PB2009-107907).

MCEER-08-0015 "Seismic Performance Evaluation of Water Systems," by Y. Wang and T.D. O'Rourke, 5/5/08 (PB2009-107908).

MCEER-08-0016 "Seismic Response Modeling of Water Supply Systems," by P. Shi and T.D. O'Rourke, 5/5/08 (PB2009-107910).

MCEER-08-0017 "Numerical and Experimental Studies of Self-Centering Post-Tensioned Steel Frames," by D. Wang and A. Filiatrault, 5/12/08 (PB2009-110479).

MCEER-08-0018 "Development, Implementation and Verification of Dynamic Analysis Models for Multi-Spherical Sliding Bearings," by D.M. Fenz and M.C. Constantinou, 8/15/08 (PB2009-107911).

MCEER-08-0019 "Performance Assessment of Conventional and Base Isolated Nuclear Power Plants for Earthquake Blast Loadings," by Y.N. Huang, A.S. Whittaker and N. Luco, 10/28/08 (PB2009-107912).

MCEER-08-0020 "Remote Sensing for Resilient Multi-Hazard Disaster Response – Volume I: Introduction to Damage Assessment Methodologies," by B.J. Adams and R.T. Eguchi, 11/17/08 (PB2010-102695).

MCEER-08-0021 "Remote Sensing for Resilient Multi-Hazard Disaster Response – Volume II: Counting the Number of Collapsed Buildings Using an Object-Oriented Analysis: Case Study of the 2003 Bam Earthquake," by L. Gusella, C.K. Huyck and B.J. Adams, 11/17/08 (PB2010-100925).

MCEER-08-0022 "Remote Sensing for Resilient Multi-Hazard Disaster Response – Volume III: Multi-Sensor Image Fusion Techniques for Robust Neighborhood-Scale Urban Damage Assessment," by B.J. Adams and A. McMillan, 11/17/08 (PB2010-100926).

MCEER-08-0023 "Remote Sensing for Resilient Multi-Hazard Disaster Response – Volume IV: A Study of Multi-Temporal and Multi-Resolution SAR Imagery for Post-Katrina Flood Monitoring in New Orleans," by A. McMillan, J.G. Morley, B.J. Adams and S. Chesworth, 11/17/08 (PB2010-100927).

MCEER-08-0024 "Remote Sensing for Resilient Multi-Hazard Disaster Response – Volume V: Integration of Remote Sensing Imagery and VIEWS^{TM} Field Data for Post-Hurricane Charley Building Damage Assessment," by J.A. Womble, K. Mehta and B.J. Adams, 11/17/08 (PB2009-115532).

MCEER-08-0025 "Building Inventory Compilation for Disaster Management: Application of Remote Sensing and Statistical Modeling," by P. Sarabandi, A.S. Kiremidjian, R.T. Eguchi and B. J. Adams, 11/20/08 (PB2009-110484).

MCEER-08-0026 "New Experimental Capabilities and Loading Protocols for Seismic Qualification and Fragility Assessment of Nonstructural Systems," by R. Retamales, G. Mosqueda, A. Filiatrault and A. Reinhorn, 11/24/08 (PB2009-110485).

MCEER-08-0027 "Effects of Heating and Load History on the Behavior of Lead-Rubber Bearings," by I.V. Kalpakidis and M.C. Constantinou, 12/1/08 (PB2009-115533).

MCEER-08-0028 "Experimental and Analytical Investigation of Blast Performance of Seismically Resistant Bridge Piers," by S.Fujikura and M. Bruneau, 12/8/08 (PB2009-115534).

MCEER-08-0029 "Evolutionary Methodology for Aseismic Decision Support," by Y. Hu and G. Dargush, 12/15/08.

MCEER-08-0030 "Development of a Steel Plate Shear Wall Bridge Pier System Conceived from a Multi-Hazard Perspective," by D. Keller and M. Bruneau, 12/19/08 (PB2010-102696).

MCEER-09-0001 "Modal Analysis of Arbitrarily Damped Three-Dimensional Linear Structures Subjected to Seismic Excitations," by Y.L. Chu, J. Song and G.C. Lee, 1/31/09 (PB2010-100922).

MCEER-09-0002 "Air-Blast Effects on Structural Shapes," by G. Ballantyne, A.S. Whittaker, A.J. Aref and G.F. Dargush, 2/2/09 (PB2010-102697).

MCEER-09-0003 "Water Supply Performance During Earthquakes and Extreme Events," by A.L. Bonneau and T.D. O'Rourke, 2/16/09 (PB2010-100923).

MCEER-09-0004 "Generalized Linear (Mixed) Models of Post-Earthquake Ignitions," by R.A. Davidson, 7/20/09 (PB2010-102698).

MCEER-09-0005 "Seismic Testing of a Full-Scale Two-Story Light-Frame Wood Building: NEESWood Benchmark Test," by I.P. Christovasilis, A. Filiatrault and A. Wanitkorkul, 7/22/09 (PB2012-102401).

MCEER-09-0006 "IDARC2D Version 7.0: A Program for the Inelastic Damage Analysis of Structures," by A.M. Reinhorn, H. Roh, M. Sivaselvan, S.K. Kunnath, R.E. Valles, A. Madan, C. Li, R. Lobo and Y.J. Park, 7/28/09 (PB2010-103199).

MCEER-09-0007 "Enhancements to Hospital Resiliency: Improving Emergency Planning for and Response to Hurricanes," by D.B. Hess and L.A. Arendt, 7/30/09 (PB2010-100924).

MCEER-09-0008 "Assessment of Base-Isolated Nuclear Structures for Design and Beyond-Design Basis Earthquake Shaking," by Y.N. Huang, A.S. Whittaker, R.P. Kennedy and R.L. Mayes, 8/20/09 (PB2010-102699).

MCEER-09-0009 "Quantification of Disaster Resilience of Health Care Facilities," by G.P. Cimellaro, C. Fumo, A.M Reinhorn and M. Bruneau, 9/14/09 (PB2010-105384).

MCEER-09-0010 "Performance-Based Assessment and Design of Squat Reinforced Concrete Shear Walls," by C.K. Gulec and A.S. Whittaker, 9/15/09 (PB2010-102700).

MCEER-09-0011 "Proceedings of the Fourth US-Taiwan Bridge Engineering Workshop," edited by W.P. Yen, J.J. Shen, T.M. Lee and R.B. Zheng, 10/27/09 (PB2010-500009).

MCEER-09-0012 "Proceedings of the Special International Workshop on Seismic Connection Details for Segmental Bridge Construction," edited by W. Phillip Yen and George C. Lee, 12/21/09 (PB2012-102402).

MCEER-10-0001 "Direct Displacement Procedure for Performance-Based Seismic Design of Multistory Woodframe Structures," by W. Pang and D. Rosowsky, 4/26/10 (PB2012-102403).

MCEER-10-0002 "Simplified Direct Displacement Design of Six-Story NEESWood Capstone Building and Pre-Test Seismic Performance Assessment," by W. Pang, D. Rosowsky, J. van de Lindt and S. Pei, 5/28/10 (PB2012-102404).

MCEER-10-0003 "Integration of Seismic Protection Systems in Performance-Based Seismic Design of Woodframed Structures," by J.K. Shinde and M.D. Symans, 6/18/10 (PB2012-102405).

MCEER-10-0004 "Modeling and Seismic Evaluation of Nonstructural Components: Testing Frame for Experimental Evaluation of Suspended Ceiling Systems," by A.M. Reinhorn, K.P. Ryu and G. Maddaloni, 6/30/10 (PB2012-102406).

MCEER-10-0005 "Analytical Development and Experimental Validation of a Structural-Fuse Bridge Pier Concept," by S. El-Bahey and M. Bruneau, 10/1/10 (PB2012-102407).

MCEER-10-0006 "A Framework for Defining and Measuring Resilience at the Community Scale: The PEOPLES Resilience Framework," by C.S. Renschler, A.E. Frazier, L.A. Arendt, G.P. Cimellaro, A.M. Reinhorn and M. Bruneau, 10/8/10 (PB2012-102408).

MCEER-10-0007 "Impact of Horizontal Boundary Elements Design on Seismic Behavior of Steel Plate Shear Walls," by R. Purba and M. Bruneau, 11/14/10 (PB2012-102409).

MCEER-10-0008 "Seismic Testing of a Full-Scale Mid-Rise Building: The NEESWood Capstone Test," by S. Pei, J.W. van de Lindt, S.E. Pryor, H. Shimizu, H. Isoda and D.R. Rammer, 12/1/10 (PB2012-102410).

MCEER-10-0009 "Modeling the Effects of Detonations of High Explosives to Inform Blast-Resistant Design," by P. Sherkar, A.S. Whittaker and A.J. Aref, 12/1/10 (PB2012-102411).

MCEER-10-0010 "L'Aquila Earthquake of April 6, 2009 in Italy: Rebuilding a Resilient City to Withstand Multiple Hazards," by G.P. Cimellaro, I.P. Christovasilis, A.M. Reinhorn, A. De Stefano and T. Kirova, 12/29/10.

MCEER-11-0001 "Numerical and Experimental Investigation of the Seismic Response of Light-Frame Wood Structures," by I.P. Christovasilis and A. Filiatrault, 8/8/11 (PB2012-102412).

MCEER-11-0002 "Seismic Design and Analysis of a Precast Segmental Concrete Bridge Model," by M. Anagnostopoulou, A. Filiatrault and A. Aref, 9/15/11.

MCEER-11-0003 'Proceedings of the Workshop on Improving Earthquake Response of Substation Equipment," Edited by A.M. Reinhorn, 9/19/11 (PB2012-102413).

MCEER-11-0004 "LRFD-Based Analysis and Design Procedures for Bridge Bearings and Seismic Isolators," by M.C. Constantinou, I. Kalpakidis, A. Filiatrault and R.A. Ecker Lay, 9/26/11.

MCEER-11-0005 "Experimental Seismic Evaluation, Model Parameterization, and Effects of Cold-Formed Steel-Framed Gypsum Partition Walls on the Seismic Performance of an Essential Facility," by R. Davies, R. Retamales, G. Mosqueda and A. Filiatrault, 10/12/11.

MCEER-11-0006 "Modeling and Seismic Performance Evaluation of High Voltage Transformers and Bushings," by A.M. Reinhorn, K. Oikonomou, H. Roh, A. Schiff and L. Kempner, Jr., 10/3/11.

MCEER-11-0007 "Extreme Load Combinations: A Survey of State Bridge Engineers," by G.C. Lee, Z. Liang, J.J. Shen and J.S. O'Connor, 10/14/11.

MCEER-12-0001 "Simplified Analysis Procedures in Support of Performance Based Seismic Design," by Y.N. Huang and A.S. Whittaker.

MCEER-12-0002 "Seismic Protection of Electrical Transformer Bushing Systems by Stiffening Techniques," by M. Koliou, A. Filiatrault, A.M. Reinhorn and N. Oliveto, 6/1/12.

MCEER-12-0003 "Post-Earthquake Bridge Inspection Guidelines," by J.S. O'Connor and S. Alampalli, 6/8/12.

MCEER-12-0004 "Integrated Design Methodology for Isolated Floor Systems in Single-Degree-of-Freedom Structural Fuse Systems," by S. Cui, M. Bruneau and M.C. Constantinou, 6/13/12.

MCEER-12-0005 "Characterizing the Rotational Components of Earthquake Ground Motion," by D. Basu, A.S. Whittaker and M.C. Constantinou, 6/15/12.

MCEER-12-0006 "Bayesian Fragility for Nonstructural Systems," by C.H. Lee and M.D. Grigoriu, 9/12/12.

MCEER-12-0007 "A Numerical Model for Capturing the In-Plane Seismic Response of Interior Metal Stud Partition Walls," by R.L. Wood and T.C. Hutchinson, 9/12/12.

MCEER-12-0008 "Assessment of Floor Accelerations in Yielding Buildings," by J.D. Wieser, G. Pekcan, A.E. Zaghi, A.M. Itani and E. Maragakis, 10/5/12.

MCEER-13-0001 "Experimental Seismic Study of Pressurized Fire Sprinkler Piping Systems," by Y. Tian, A. Filiatrault and G. Mosqueda, 4/8/13.

MCEER-13-0002 "Enhancing Resource Coordination for Multi-Modal Evacuation Planning," by D.B. Hess, B.W. Conley and C.M. Farrell, 2/8/13.

MCEER-13-0003 "Seismic Response of Base Isolated Buildings Considering Pounding to Moat Walls," by A. Masroor and G. Mosqueda, 2/26/13.

MCEER-13-0004 "Seismic Response Control of Structures Using a Novel Adaptive Passive Negative Stiffness Device," by D.T.R. Pasala, A.A. Sarlis, S. Nagarajaiah, A.M. Reinhorn, M.C. Constantinou and D.P. Taylor, 6/10/13.

MCEER-13-0005 "Negative Stiffness Device for Seismic Protection of Structures," by A.A. Sarlis, D.T.R. Pasala, M.C. Constantinou, A.M. Reinhorn, S. Nagarajaiah and D.P. Taylor, 6/12/13.

MCEER-13-0006 "Emilia Earthquake of May 20, 2012 in Northern Italy: Rebuilding a Resilient Community to Withstand Multiple Hazards," by G.P. Cimellaro, M. Chiriatti, A.M. Reinhorn and L. Tirca, June 30, 2013.

MCEER-13-0007 "Precast Concrete Segmental Components and Systems for Accelerated Bridge Construction in Seismic Regions," by A.J. Aref, G.C. Lee, Y.C. Ou and P. Sideris, with contributions from K.C. Chang, S. Chen, A. Filiatrault and Y. Zhou, June 13, 2013.

MCEER-13-0008 "A Study of U.S. Bridge Failures (1980-2012)," by G.C. Lee, S.B. Mohan, C. Huang and B.N. Fard, June 15, 2013.

MCEER-13-0009 "Development of a Database Framework for Modeling Damaged Bridges," by G.C. Lee, J.C. Qi and C. Huang, June 16, 2013.

MCEER-13-0010 "Model of Triple Friction Pendulum Bearing for General Geometric and Frictional Parameters and for Uplift Conditions," by A.A. Sarlis and M.C. Constantinou, July 1, 2013.

MCEER-13-0011 "Shake Table Testing of Triple Friction Pendulum Isolators under Extreme Conditions," by A.A. Sarlis, M.C. Constantinou and A.M. Reinhorn, July 2, 2013.

MCEER-13-0012 "Theoretical Framework for the Development of MH-LRFD," by G.C. Lee (coordinating author), H.A Capers, Jr., C. Huang, J.M. Kulicki, Z. Liang, T. Murphy, J.J.D. Shen, M. Shinozuka and P.W.H. Yen, July 31, 2013.

MCEER-13-0013 "Seismic Protection of Highway Bridges with Negative Stiffness Devices," by N.K.A. Attary, M.D. Symans, S. Nagarajaiah, A.M. Reinhorn, M.C. Constantinou, A.A. Sarlis, D.T.R. Pasala, and D.P. Taylor, September 3, 2014.

MCEER-14-0001 "Simplified Seismic Collapse Capacity-Based Evaluation and Design of Frame Buildings with and without Supplemental Damping Systems," by M. Hamidia, A. Filiatrault, and A. Aref, May 19, 2014.

MCEER-14-0002 "Comprehensive Analytical Seismic Fragility of Fire Sprinkler Piping Systems," by Siavash Soroushian, Emmanuel "Manos" Maragakis, Arash E. Zaghi, Alicia Echevarria, Yuan Tian and Andre Filiatrault, August 26, 2014.

MCEER-14-0003 "Hybrid Simulation of the Seismic Response of a Steel Moment Frame Building Structure through Collapse," by M. Del Carpio Ramos, G. Mosqueda and D.G. Lignos, October 30, 2014.

MCEER-14-0004 "Blast and Seismic Resistant Concrete-Filled Double Skin Tubes and Modified Steel Jacketed Bridge Columns," by P.P. Fouche and M. Bruneau, June 30, 2015.

MCEER-14-0005 "Seismic Performance of Steel Plate Shear Walls Considering Various Design Approaches," by R. Purba and M. Bruneau, October 31, 2014.

MCEER-14-0006 "Air-Blast Effects on Civil Structures," by Jinwon Shin, Andrew S. Whittaker, Amjad J. Aref and David Cormie, October 30, 2014.

MCEER-14-0007 "Seismic Performance Evaluation of Precast Girders with Field-Cast Ultra High Performance Concrete (UHPC) Connections," by G.C. Lee, C. Huang, J. Song, and J. S. O'Connor, July 31, 2014.

MCEER-14-0008 "Post-Earthquake Fire Resistance of Ductile Concrete-Filled Double-Skin Tube Columns," by Reza Imani, Gilberto Mosqueda and Michel Bruneau, December 1, 2014.

MCEER-14-0009 "Cyclic Inelastic Behavior of Concrete Filled Sandwich Panel Walls Subjected to In-Plane Flexure," by Y. Alzeni and M. Bruneau, December 19, 2014.

MCEER-14-0010 "Analytical and Experimental Investigation of Self-Centering Steel Plate Shear Walls," by D.M. Dowden and M. Bruneau, December 19, 2014.

MCEER-15-0001 "Seismic Analysis of Multi-story Unreinforced Masonry Buildings with Flexible Diaphragms," by J. Aleman, G. Mosqueda and A.S. Whittaker, June 12, 2015.

MCEER-15-0002 "Site Response, Soil-Structure Interaction and Structure-Soil-Structure Interaction for Performance Assessment of Buildings and Nuclear Structures," by C. Bolisetti and A.S. Whittaker, June 15, 2015.

MCEER-15-0003 "Stress Wave Attenuation in Solids for Mitigating Impulsive Loadings," by R. Rafiee-Dehkharghani, A.J. Aref and G. Dargush, August 15, 2015.

MCEER-15-0004 "Computational, Analytical, and Experimental Modeling of Masonry Structures," by K.M. Dolatshahi and A.J. Aref, November 16, 2015.

MCEER-15-0005 "Property Modification Factors for Seismic Isolators: Design Guidance for Buildings," by W.J. McVitty and M.C. Constantinou, June 30, 2015.

MCEER-15-0006 "Seismic Isolation of Nuclear Power Plants using Sliding Bearings," by Manish Kumar, Andrew S. Whittaker and Michael C. Constantinou, December 27, 2015.

MCEER-15-0007 "Quintuple Friction Pendulum Isolator Behavior, Modeling and Validation," by Donghun Lee and Michael C. Constantinou, December 28, 2015.

MCEER-15-0008 "Seismic Isolation of Nuclear Power Plants using Elastomeric Bearings," by Manish Kumar, Andrew S. Whittaker and Michael C. Constantinou, December 29, 2015.

MCEER-16-0001 "Experimental, Numerical and Analytical Studies on the Seismic Response of Steel-Plate Concrete (SC) Composite Shear Walls," by Siamak Epackachi and Andrew S. Whittaker, June 15, 2016.

MCEER-16-0002 "Seismic Demand in Columns of Steel Frames," by Lisa Shrestha and Michel Bruneau, June 17, 2016.

MCEER-16-0003 "Development and Evaluation of Procedures for Analysis and Design of Buildings with Fluidic Self-Centering Systems" by Shoma Kitayama and Michael C. Constantinou, July 21, 2016.

MCEER-16-0004 "Real Time Control of Shake Tables for Nonlinear Hysteretic Systems," by Ki Pung Ryu and Andrei M. Reinhorn, October 22, 2016.

MCEER-16-0006 "Seismic Isolation of High Voltage Electrical Power Transformers," by Kostis Oikonomou, Michael C. Constantinou, Andrei M. Reinhorn and Leon Kemper, Jr., November 2, 2016.

MCEER-16-0007 "Open Space Damping System Theory and Experimental Validation," by Erkan Polat and Michael C. Constantinou, December 13, 2016.

MCEER-16-0008 "Seismic Response of Low Aspect Ratio Reinforced Concrete Walls for Buildings and Safety-Related Nuclear Applications," by Bismarck N. Luna and Andrew S. Whittaker.

MCEER-16-0009 "Buckling Restrained Braces Applications for Superstructure and Substructure Protection in Bridges," by Xiaone Wei and Michel Bruneau, December 28, 2016.

MCEER-16-0010 "Procedures and Results of Assessment of Seismic Performance of Seismically Isolated Electrical Transformers with Due Consideration for Vertical Isolation and Vertical Ground Motion Effects," by Shoma Kitayama, Michael C. Constantinou and Donghun Lee, December 31, 2016.

MCEER-17-0001 "Diagonal Tension Field Inclination Angle in Steel Plate Shear Walls," by Yushan Fu, Fangbo Wang and Michel Bruneau, February 10, 2017.

MCEER-17-0002 "Behavior of Steel Plate Shear Walls Subjected to Long Duration Earthquakes," by Ramla Qureshi and Michel Bruneau, September 1, 2017.

MCEER-17-0003 "Response of Steel-plate Concrete (SC) Wall Piers to Combined In-plane and Out-of-plane Seismic Loadings," by Brian Terranova, Andrew S. Whittaker, Siamak Epackachi and Nebojsa Orbovic, July 17, 2017.

ISSN 1520-295X